THE PREDICTION AND EXPERIMENTAL MEASUREMENT OF TORSIONAL VIBRATIONS IN VARIABLE FREQUENCY DRIVE CONTROLLED INDUCTION MOTOR MACHINERY

A Thesis

by

LUCAS HAMPTON PERKINS

Submitted to the Office of Graduate and Professional Studies of
Texas A&M University
in partial fulfillment of the requirements for the degree of

MASTER OF SCIENCE

Chair of Committee,	Alan Palazzolo
Committee Members,	Adolfo Delgado
	Hamid Toliyat
Head of Department,	Andreas Polycarpou

August 2021

Major Subject: Mechanical Engineering

ABSTRACT

The performance of detailed, mechanical system analyses of rotating machinery is an important step in avoiding potential failure due to excitations on the system. Excitations such as compressors, pump, turbines and motors and can generate both steady-state and transient vibrations leading to fatigue failure. With the growing use of motors as a means to drive machinery, the popularity of Variable Frequency Drives (VFDs) to control motor speed has also increased. These speed controllers present many useful benefits to the industry, however, an increasing number of system failures caused by VFDs have been recorded in the literature. These failures are due to undesirable torque harmonics caused by the interaction of both the switching frequency and carrier frequency of the VFD. When close to a natural frequency of the mechanical system, these unwanted torque frequencies can cause large vibration amplitudes leading to fatigue failure.

For this research, an in-house "VFD Software" which numerically analyzes the coupled electrical and mechanical side of a rotordynamic system to output the system response and predicted fatigue life is further developed. The accuracy of the fatigue life prediction is improved by allowing for a strain life approach to be performed over the more conservative and less accurate stress life method. This method incorporates the material ductility and strain into the life prediction and treats the life degrading factors of surface finish, size, stress concentration, and notch sensitivity as functions of life instead of constants. Furthermore, the transient analysis of the software is also improved by allowing the users to manually input a drive torque as a series

of torque frequencies, amplitudes, and phase angles in the case that the electrical system harmonics are previously known.

To further study the presence and accurate prediction of torque harmonics and vibrations in rotating machinery, a VFD test rig has also been designed and fabricated. The test rig incorporates the use of a VFD controlled, 2-pole induction motor to drive a shaft supported by two ball bearings and a tilting pad bearing. A torque transducer, torsional vibration geared sleeve, and 4 Bently probes are used to measure the dynamic torques and torsional vibrations along with other system responses. Initial experimental results show the presence of a torque harmonic spectrum which interacts with the software predicted natural frequency of the system. This spectrum can be correlated to integer harmonics of the running speed and values predicted by the VFD Software. The rig also proves to be able to measure small vibration amplitudes that are predicted by the software from known torque frequencies and amplitudes.

DEDICATION

This thesis is dedicated to my parents, Rob and Sandra Perkins,

and my fiancé, Claire

You have been a constant source of love and support.

Finally, to God, who has blessed me and provided for me

during all seasons.

ACKNOWLEDGEMENTS

Thank you to Dr. Alan Palazzolo for your immense support and mentorship throughout my research. You helped me grow in an academic and technical way through work that I discovered a love for.

To my committee members Dr. Delgado and Dr. Toliyat, thank you for your support and most importantly for your passion in your respective fields. Your abilities to teach were the cornerstone to my interest in the work I was able to accomplish.

To Tom and Willy, your wisdom and experiences in electrical systems cannot be taken for granted. Without you both, my test rig would not have come together like it did and I would be without many of the practical skills I have today.

Finally, to all the members of the lab who never hesitated to lend a hand or share their individual expertise. You made research fun and opened my eyes to so many interesting topics.

CONTRIBUTORS AND FUNDING SOURCES

Contributors

This work was due in large part to my committee chair Dr. Alan Palazzolo and committee members Dr. Adolfo Delgado of the Department of Mechanical Engineering and Dr. Hamid Toliyat of the Department of Electrical and Computer Engineering. Preliminary work on the VFD Software was completed by Dr. Xu Han, Dr. Yashu Li, and Sahil Mishra.

Funding Sources

The further development of the project outlined by this thesis was due to the financial support of the Turbomachinery Research Consortium (TRC) and is gratefully appreciated.

TABLE OF CONTENTS

LIST OF FIGURES

LIST OF TABLES

1. INTRODUCTION

1.1. Problem Statement

The performance of detailed, mechanical system analyses of rotating machinery is an important step in avoiding potential failure due to excitations on the system. Excitations such as compressors, pump, turbines and motors and can generate both steady-state and transient vibrations leading to fatigue failure. With the growing use of motors as a means to drive machinery, the popularity of Variable Frequency Drives (VFDs) to control motor speed has also increased. These speed controllers present many useful benefits to the industry, however, an increasing number of system failures caused by VFDs have been recorded in the literature. These failures are due to undesirable torque harmonics caused by the interaction of both the switching frequency and carrier frequency of the VFD. When close to a natural frequency of the mechanical system, these unwanted torque frequencies can cause large vibration amplitudes leading to fatigue failure.

In this thesis, an in-house "VFD Software" which numerically analyzes the coupled electrical and mechanical side of a rotordynamic system to output the system response and predicted fatigue life is further developed. The accuracy of the fatigue life prediction is improved by allowing for a strain life approach to be performed over the more conservative and less accurate stress life method. This method incorporates the material ductility and strain into the life prediction and treats the life degrading factors of surface finish, size, stress concentration, and notch sensitivity as functions of life instead of constants. Furthermore, the transient analysis of the software is also improved by allowing the users to manually input a drive torque as a series

of torque frequencies, amplitudes, and phase angles in the case that the electrical system harmonics are previously known.

To further study the presence and accurate prediction of torque harmonics and vibrations in rotating machinery, a VFD test rig has also been designed and fabricated. The test rig incorporates the use of a VFD controlled, 2-pole induction motor to drive a shaft supported by two ball bearings and a tilting pad bearing. A torque transducer, torsional vibration geared sleeve, and 4 Bently probes are used to measure the dynamic torques and torsional vibrations along with other system responses. Initial experimental results show the presence of a torque harmonic spectrum which interacts with the software predicted natural frequency of the system. This spectrum can be correlated to integer harmonics of the running speed and values predicted by the VFD Software. The rig also proves to be able to measure small vibration amplitudes that are predicted by the software from known torque frequencies and amplitudes.

1.2. VFD Software

The VFD Software is a software package that has been in development for the Turbomachinery Research Consortium (TRC) for several years. The software has the ability to simultaneously solve both the electrical and mechanical model of a VFD controlled system. For the electrical model, the user specifies the motor type (induction or synchronous), the motor parameters (inductances and resistances), and the VFD control method (V/hz, field oriented, or vector). The mechanical system is modeled by inputting shaft dimensions, coupling and bearing parameters, gear ratios, load torques, added inertias, etc. The system life prediction can be performed using either a stress-based or strain-based method to predict how long each element in the model will last before failure.

1.3. VFD Test Rig

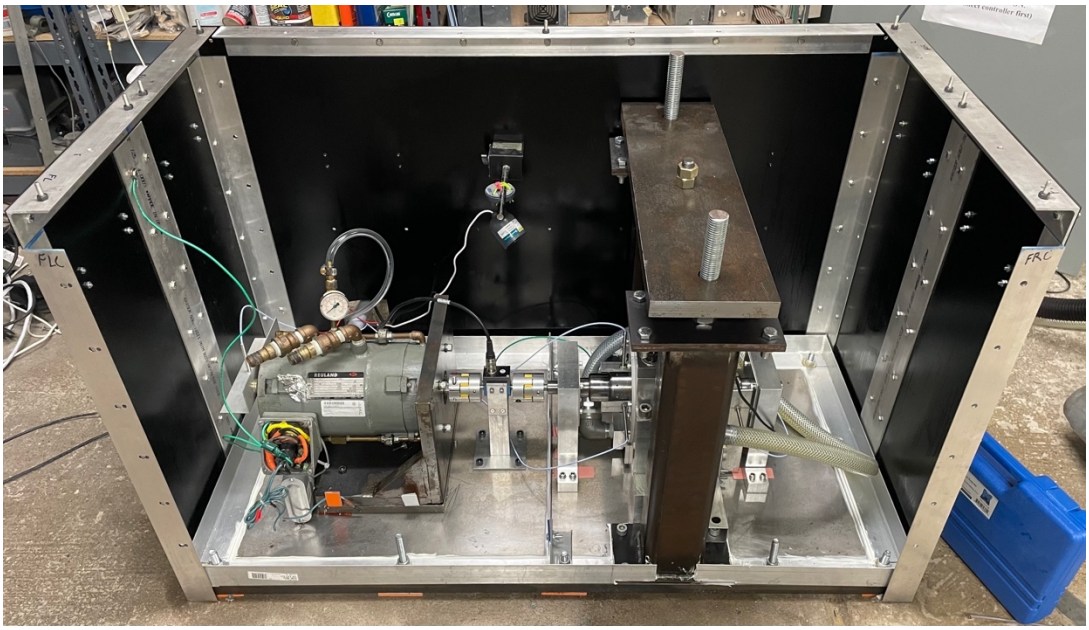

Figure 1: VFD Test Rig

The VFD test rig shown in Figure 1 is developed to correlate real world experimental results to the VFD Software along with Song's torque harmonics predicted in [1]. The VFD test rig allows for the measurement of torque harmonics by a torque transducer and torsional vibration frequencies and amplitudes using Bessel functions and the FFT of the signal of a Bently probe placed above a gear-like sleeve. The design of the test rig also allows for a range of other experiments including VFD setting optimization, tilting pad bearing drag and load studies, and other future work.

The electrical system of the VFD test rig includes a 25 HP, 2 phase, Reuland induction motor controlled by an Automation Direct VFD utilizing an open loop V/Hz control scheme. The mechanical system of the rig consists of the motor shaft connected to the torque transducer via an elastomer damped coupling. A similar coupling then connects the other side of the torque

transducer to a larger steel shaft that is supported by two ball bearings at either end and a tilting pad bearing in the center. The tilting pad bearing housing allows for vertical motion so an induced vertical load can be applied to increase the viscous drag on the shaft.

1.4. Key Contributions and Novel Work

1.4.1. Strain-Based Life Prediction

The implementation of a strain-based approach for life prediction was created through the development of new MATLAB codes and new additions to the VFD Software Excel GUI. The new approach gives the user an addition method of life prediction with the following features,

- Improved accuracy in predicting system life to allow for more complex rotor dynamic designs
- The ability for users to define individual materials for the life prediction method with an increased number of commonly available material properties to improve the life prediction model
- The generation and display of strain-based S-N curves within the Excel UI

The results of the strain life prediction method are compared to manual calculations as well as a strain life analysis to illustrate the occasional over conservative nature of the stress life prediction. The equivalent S-N curves of the two methods are also compared to further illustrate the differences between them.

1.4.2. Transient Torque Analysis with Defined Torque Frequencies and Amplitudes

The system transient analysis was improved for the user defined torque option within the software. This allows the user to skip the solving of the electrical system and instead define the driving torque as a series of torque frequencies, amplitudes and phase shifts. The user can also add a sigmoid ramp up to a mean torque value in a defined rise time. This addition to the code is useful in instances where the user already knows what torque frequencies and amplitudes are expected within the system. This feature is utilized to predict torsional vibration amplitudes within the experimental test rig.

1.4.3. Experimental VFD Test Rig

The complete VFD Test Rig was designed and fabricated to perform the many defined experiments explained in 1.3. The main accomplishments of the work related to the test rig include,

- Design, fabrication and installation of the mechanical systems of the rig (main shaft, bearing housings, torsional vibration sleeve, tilting pad bearing (TPB) side load system and housing, sensor mounts, safety enclosure, etc.)
- Identification and installation of major electrical components (VFD, line filter/noise and EMI reduction, safety systems)
- Data acquisition system installation including 4 Bently probes (once around, x & y sensors, and torsional vibration), load cell, and torque transducer. LabView VI's were also created for collecting the data and MATLAB was used for real time data processing during experimentation.

- Shaft alignment between motor shaft and main shaft.
- Harmonic torque and torsional vibration measurements to correlate to predicted values from the VFD software and to identify interactions between the mechanical and electrical system of the test rig.

1.4.4. Further Software Development

Other improvements to the software were added to improve the user experience including,

- The ability to save the results within the Excel file to eliminate the need to rerun upon closing the software.
- General bug fixes and user input error checking improvements

2. LITERATURE REVIEW

The literature contains several papers that describe the necessary considerations that must be made when implementing VFD control of electric motors. In [2], the need to consider different excitations on the interference diagram due to VFD implementation is outlined. This illustrates the presence of steady state torque harmonics due to various characteristics of VFDs such as PWM switching and the line frequency.

Real world issues related to VFD generated torques have also been documented in the literature such as in [3], [4], [5], and [6]. The main consideration taken into account when designing rotating machinery is to avoid inducing a mechanical resonance. Resonance occurs when there is an interaction between the excitation frequencies (i.e. torque harmonics created by a VFD) and the natural frequency of the system. While simply trying to avoid introducing excitations at these frequencies is a good starting point, [7] illustrates the short comings of this due to damping and other factors. It expresses the improved practice of "predicting damage and life based on the simulated torsional stress response to VFD motor induced mean and alternating stresses."

The harmonic torques produced by a VFD controlled motor occur at a range of frequencies shown by Song's formulas in [1]. Song derives these equations by using a rotating d-q reference frame where the induction motor's electromagnetic torque is a product of the stator and rotor currents. The method for the d-q analysis is clearly shown in [8]. In the case of a VFD using open-loop V/Hz control, the stator currents are generated directly by a PWM inverter. Therefore, the harmonics from the PWM will consequently generate a related harmonic torque.

Other sources of VFD generated torque harmonics shown in the literature include the number of inverter levels along with the control scheme of the VFD. Reference [7] illustrates these points and the presence of higher harmonic torque amplitudes in higher level inverters using open-loop Volts-Hertz control.

While the harmonic torque frequencies and amplitudes can be experimentally measured by a commercially available, high precision, in-line transducer, the measurement of the torsional vibration frequencies and amplitudes rely on a proximity probe mounted above a gear-like portion of the shaft and Bessel functions as shown in [9].

The stress-based life prediction is commonly used in torsional fatigue life analysis and is clearly outlined in [10]. In some systems, the stress-based life prediction proves to be overly conservative, and the life prediction can be more accurately found using the strain-based method outlined in [11]. This source also outlines the advantages present in this method. The strain-based life prediction does require more information on the properties of the material and mechanical system; however, these values are either presented in [11] or can be found in [12] or [13].

3. THEORY

3.1. Strain-Based Life Prediction

The Strain Theory Life Prediction Model outlined by [11] is considered to be a more accurate method for performing a life prediction analysis while still remaining conservative. The method differs from the stress model because it includes the ductility effects and assumes the life of an element is dependent on the acting strain instead of the stress.

The Strain Theory Life Prediction Model centers around the Coffin-Manson equation which relates the cyclic strain amplitude, ε, to the number of cycles to failure, N. This equation is defined as,

$$\varepsilon(N) = \frac{\sigma_f'}{E} * N^b + \varepsilon_f' * N^c \tag{1}$$

Where,

$E = Elastic\ Modulus$

$\sigma_f' = true\ stress\ at\ fracture$

$\varepsilon_f' = true\ strain\ at\ fracture$

$N = cycles\ to\ failure\ (life)$

$b = elastic\ strain\ exponent\ (slope\ of\ elastic\ strain\ line)$

$c = plastic\ strain\ exponent\ (slope\ of\ plastic\ strain\ line)$

To determine the true stress and strain at fracture, the reduction of area, RA, is used in the equations,

$$\sigma_f' = \frac{\sigma_u}{1-RA} \tag{2}$$

$$\varepsilon_f' = \ln\left(\frac{1}{1-RA}\right) \tag{3}$$

The justification in [11] also outlines that the strain life equation of $\varepsilon(N)$ can be transformed into the familiar form of a SN Curve simply by multiplying the equation by the Elastic Modulus. From this assumption we get the equation,

$$\sigma(N) = \sigma_f' * N^b + E * \varepsilon_f' * N^c \tag{4}$$

This assumption maintains the benefits and accuracy of the previously defined method while allowing for the stress to be used, which is easy to calculate without the use of FEA.

The final step in the strain theory life prediction is to convert the previously discussed equation of tensile stress, $\sigma(N)$, into an equation of shear stress, $\tau(N)$. This involves multiplying (4) by the shear factor and delimiting factors. The resulting shear stress equation is,

$$\tau(N) = \sigma(N) * F_{sh} * k_a * \frac{k_b}{k_f * SF} \tag{5}$$

Where,

$F_{sh} = Shear\ Factor$

$k_a = Surface\ finish\ factor$

$k_b = Size\ factor$

$k_f = Effective\ stress\ concentration\ factor$

$SF = Safety\ Factor$

In the strain life method, the values of k_a, k_b, and k_f are all assumed to be a function dependent on the number of cycles, N. This implementation further improves the accuracy these factors have generally been assumed to remain constant.

To determine the surface factor as a function of life the following equations are used,

$$k_a(N) = \frac{10^b}{N^m} \tag{6}$$

$$m = \frac{\log\left(\frac{k_a(1000)}{k_a(10^6)}\right)}{3.0} \tag{7}$$

$$b = \log\left(\frac{k_a(1000)^2}{k_a(10^6)}\right) \tag{8}$$

The surface finish factor at 1000 and 1e6 cycles are defined as,

$$k_a(1000) = 1.00$$

$$k_a(10^6) = nominal\ surface\ finish\ factor$$

The nominal surface finish factor is found from various sources, but most commonly from section 6-9 of Shigley's book. In [10], the nominal surface finish factor is calculated as a function of the minimum tensile strength, S_{ut}, using the equation,

$$k_a = a * S_{ut}^b \tag{9}$$

The constants a and b are also defined in [10] for different surface finishes ranging from "ground" to "as forged".

The size factor as a factor of life is found by,

$$k_b(N) = \frac{10^b}{N^m} \tag{9}$$

$$m = \frac{\log\left(\frac{k_b(1000)}{k_b(10^6)}\right)}{3.0} \tag{10}$$

$$b = \log\left(\frac{k_b(1000)^2}{k_b(10^6)}\right) \tag{11}$$

The size factor at 1000 and 1e6 cycles are defined as,

$$k_b(1000) = 1.00$$

$$k_b(10^6) = nominal\ size\ factor$$

In this case the nominal size factor is also defined in section 6 of [10]. As suggested by the name, the size factor is a function of the diameter of the rotating element and can be found by the piecewise functions,

$$0.879d^{-0.107} \quad .11 < d < 2\ in$$

$$0.91d^{-0.157} \quad 2 < d < 10\ in$$

$$1.24d^{-0.107} \quad 2.79 < d < 51\ mm$$

$$1.51d^{-0.157} \quad 51 < d < 254\ mm$$

The fatigue stress concentration factor as a function of cycles is,

$$k_f(N) = \frac{10^b}{N^m} \tag{12}$$

$$m = \frac{\log\left(\frac{k_f(1000)}{k_f(10^6)}\right)}{3.0} \tag{13}$$

$$b = \log\left(\frac{k_f(1000)^2}{k_f(10^6)}\right) \tag{14}$$

Where,

$$k_f(1000) = \sqrt{k_f(10^6)}$$

$$k_f(10^6) = 1 + q * (K_t - 1)$$

$$q = notch\ factor$$

$$K_t = nominal\ geometric\ stress\ concentration\ factor$$

The nominal geometric stress concentration factor can be calculated using FEA or by the extensive reference made by Peterson in [12].

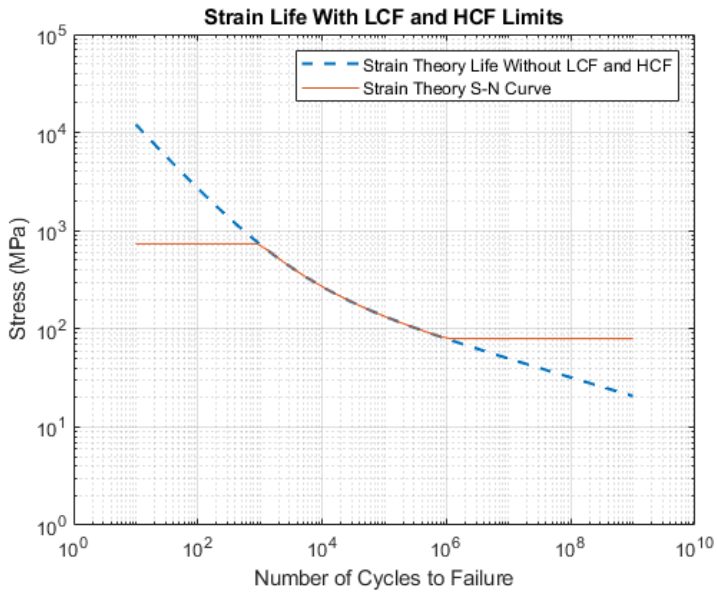

Figure 2: High Cycle and Low Cycle Fatigue Limit

Once the sheer stress versus number of cycles is plotted from Equation 5, the low cycle and high cycle fatigue limits are set at 10^3 and 10^6 cycles respectively. This is illustrated clearly in Figure *2*.

3.1.1. Pure Torsional Criteria

For pure torsional loading [14] states that:

"Experimental results tend to show that the value of the mean shear stress has no influence on the fatigue life of a ductile structural component subjected to cyclic torsional loading as long as the maximum stress is less than the yield strength of the material. Shigley and Mitchell stated 'up to a certain point, torsional mean stress has no effect on the torsional endurance limit τ_e*'.*

Hence, the plot of the alternating shear stress τ_a *versus the mean shear stress* τ_m *is bounded by a horizontal line with* $\tau_a = \tau_e$ *and a 45 degree yield line."*

This criterion is shown in,

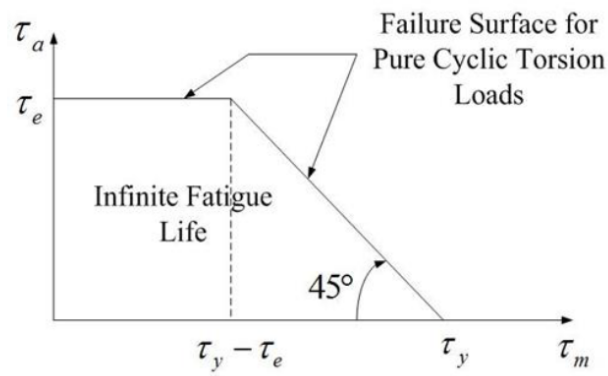

Figure 3 Pure Torsional Criteria [14]

Where, τ_y denotes the torsional yield strength of the material. Thus, we have the following two cases:

Case 1: If $\tau_m < \tau_y - \tau_e$ and $\tau_a > \tau_e$

Then $\tau_{eff} = \tau_a$

Mean shear stress has no influence on effective shear stress (15)

Case 2: If $\tau_m > \tau_y - \tau_e$ and $\tau_a > \tau_y - \tau_m$

Then $\tau_{eff} = \dfrac{\tau_a \tau_e}{\tau_y - \tau_m}$

Mean shear stress has influence on effective shear stress (16)

Miner's rule states that if there are k different stress levels (with linear damage hypothesis) and the average number of cycles to failure at the i^{th}stress S_i, is N_i, then the damage, D is

$$D = \sum_{i=1}^{k} \frac{n_i}{N_i} \qquad (17)$$

Where, n_i denotes the number of stress cycles accumulated at stress S_i.

The final number of cycles to failure N is given by,

$$N = \frac{1}{D} \tag{18}$$

3.2. Torsional Vibration Measurement

The torsional vibration analysis outlined in [9] functions by placing a proximity probe above a gear-like element on a rotating shaft. The signal from the probe is a frequency modulated wave. The simplest form of a frequency modulated signal is defined as,

$$V(t) = V_0\, cos(2\pi f_c t + \beta sin 2\pi f_m t) \tag{19}$$

where f_c is the carrier signal frequency, f_m is the modulation frequency (in this case the torsional vibration frequency), and β is proportional to the torsional vibration amplitude. When the carrier signal is generated by a gear-like element with N_t teeth running at a mean shaft rotational speed of N rpm, and with an angular displacement given by,

$$\theta(t) = \theta_0 \cos(\omega t) \tag{20}$$

Then,

$$f_c = \frac{N_t N}{60} \tag{19}$$

$$f_m = \frac{\omega}{2\pi} \tag{20}$$

And,

$$\beta = N_t \theta_0 \tag{21}$$

The equation for the frequency modulated signal can be expanded into the Bessel function series to get,

$$V(t) = V_0(J_0(N_t\theta_0)cos2\pi f_c t + J_1(N_t\theta_0)cos2\pi(f_c + f_m)t - J_1(N_t\theta_0)cos2\pi(f_c - 2f_m) + J_2(N_t\theta_0)cos2\pi(f_c + 2f_m)t + \cdots \quad (22)$$

The value of $\beta = N_t\theta_0$ is considered the modulation index of $J_i(N_t\theta_0)$ which are Bessel functions of ith order, $i = 1, 2, 3, \ldots$. The numerical values of Bessel functions are available from the built in Bessel MATLAB function or in published handbooks to calculate the torsional vibration amplitude from the FFT of the proximity probe data.

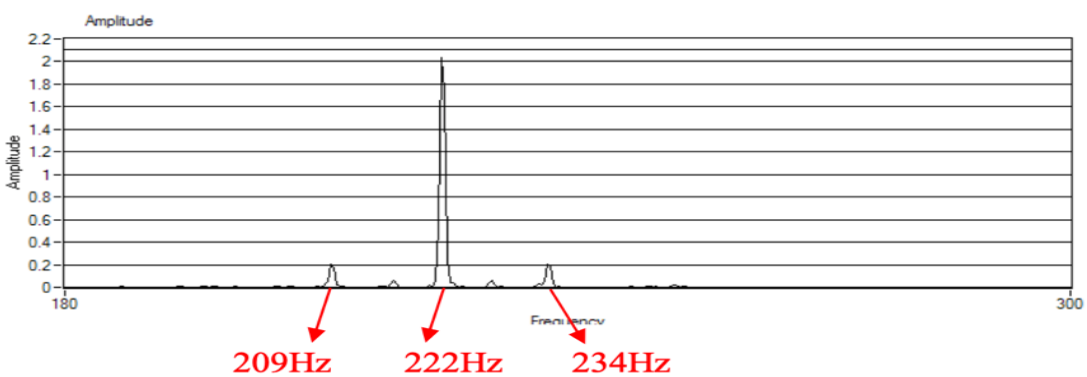

Figure 4 FFT of Sensor Data

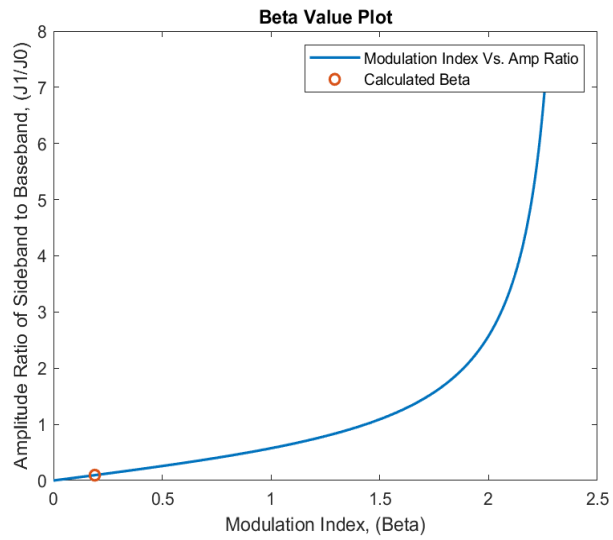

Figure 5 Beta Value Plot

The FFT of the square wave signal from the probe is taken similar to the one shown in Figure 4. The frequency of the torsional vibration is calculated by taking the difference between the baseband frequency and one of the symmetric side bands. In this case the torsional frequency is averaged to be 12.5 Hz.

To determine the amplitude of the torsion, the amplitude of the baseband frequency, J0, and the side band amplitude, J1, are recorded.

For the example, the ratio of these amplitudes is found to be

$$\frac{J_1(\beta)}{J_0(\beta)} = \frac{0.21}{2.2} = 0.09545 \qquad (23)$$

The modulation index, β, is then found by comparing this ratio to the ratio of J1 and J0 from a table of Bessel Values or the plot shown in Figure 5. In this case,

$$\beta = 0.190$$

Where β equals the product of the torsional vibration amplitude, θ, and the number of teeth, N. In this case where N= 40 teeth,

$$\theta = 0.00475\, rad$$

3.3. Song's Formulas

The equations outlined in [1] are referred to as Song's formulas and identify the torque harmonic frequencies that can be induced by a motor under VFD V/Hz control. The electromagnetic torque of an induction motor is a function of the stator and rotor currents in a q-d reference frame. PWM is used by the VFD to achieve target stater voltage amplitudes and frequencies and the modulation of this voltage can cause the potentially damaging torque harmonics. The harmonic frequencies are therefore affected by both the PWM frequency and the line frequency of the VFD.

The torque frequencies outlined by Song are defined as,

$$f_T = |m \cdot f_{PWM} \pm n \cdot f_e|$$

Where,

$$f_{PWM} = PWM\ Frequency$$

$$f_e = line\ (electrical)\ frequency$$

The values of m and n differ for different types of torque harmonics and are defined by,

Baseband Harmonics

$$\begin{cases} m = 0 \\ n = 6j, \end{cases} \qquad \forall j = 0,1,2,3 \ldots$$

Sideband Harmonics Around Even Multiples of the Carrier Frequency

$$\begin{cases} m = 2i, & \forall i = 1,2,3, \ldots \\ y = 3 \cdot (2j) & \forall j = 0,1,2, \ldots \end{cases}$$

Sideband Harmonics Around Odd Multiples of the Carrier Frequency

$$\begin{cases} m = 2i + 1 & \forall i = 0,1,2, \ldots \\ n = 3 \cdot (2j + 1) & \forall j = 0,1,2, \ldots \end{cases}$$

4. STRAIN BASED LIFE PREDICTION

4.1. Example 1: Strain Theory Life Prediction of Simple ungeared compressor train

4.1.1. Assumptions

The example described in this section focuses on a compressor model that is driven by a motor. This motor is assumed to be connected directly to the compressor and does not use a gearbox. The direct connection of the motor to the shaft also avoids the use of any couplings and therefore does not require any coupling stiffness or damping characteristics to be defined.

4.1.2. Model

The model of the compressor train is shown in Figure *6*. The system is kept simple and is assumed to have only two nodes with one at the motor and the other at the compressor. The shaft element connecting the two nodes acts as a simple torsional spring. All parameters for the system are shown in Table *1*.

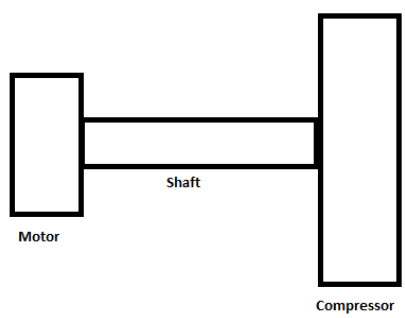

Figure 6 Single Element Motor-Compressor Train

Table 1 Mechanical System Properties

Description	Value
Motor Inertia I_m	2.6 kgm^2
Compressor Inertia I_c	2.5 kgm^2
Shaft Outer Diameter D_o	40 mm
Shaft Inner Diameter D_i	20 mm
Shaft Length L	1 m
Modulus of Rigidity of Steel G	82.7 GPa
Density of Steel ρ	7850 kg/m^3
Operating Torque T	2.5 kNm
Dynamic Torque T_d	100 Nm
Frequency of Dynamic Torque f	20 Hz

In this system, the static torque from the motor balances the load provided by the compressor while the dynamic torque from the motor has the form,

$$T = T_d \cos(2\pi f t)$$

4.1.3. Natural Frequency

The system has 2 degrees of freedom defined as θ_1 and θ_2. Let the vector of the degrees of freedom vector be defined as,

$$\bar{\theta} = \begin{bmatrix} \theta_1 \\ \theta_2 \end{bmatrix}$$

The calculated mass of the shaft is,

$$m = \rho\pi\left(\frac{{D_o}^2 - {D_i}^2}{4}\right)L = 7850\pi\left(\frac{0.04^2 - 0.02^2}{4}\right) = 7.398\ kg$$

The calculated shaft inertia is,

$$I_s = m\left(\frac{{D_o}^2 + {D_i}^2}{8}\right) = 7.398\left(\frac{0.04^2 + 0.02^2}{8}\right) = 1.8496\ \times 10^{-3}\ kgm^2$$

The inertia matrix is,

$$I = \begin{bmatrix} I_m + \frac{I_s}{2} & 0 \\ 0 & I_c + \frac{I_s}{2} \end{bmatrix} = \begin{bmatrix} 2.600925 & 0 \\ 0 & 2.500925 \end{bmatrix}$$

The shafts polar moment of inertia is,

$$J = \pi\left(\frac{{D_o}^4 - {D_i}^4}{32}\right) = \pi\left(\frac{0.04^4 - 0.02^4}{32}\right) = 2.3562 \times 10^{-7}\ m^4$$

The shaft stiffness is,

$$k = \frac{GJ}{L} = \frac{82.7 \times 10^9 \times 2.3562 \times 10^{-7}}{1} = 1.9486 \times 10^4\ Nm/rad$$

The complete shaft stiffness matrix is therefore,

$$K = \begin{bmatrix} k & -k \\ -k & k \end{bmatrix} = 1.9486 \times 10^4 \begin{bmatrix} 1 & -1 \\ -1 & 1 \end{bmatrix}$$

Consider the homogenous form of the equation of motion,

$$I\ddot{\bar{\theta}} + K\bar{\theta} = 0$$

The assumed harmonic solution is of the form,

$$\bar{\theta} = \bar{\theta}e^{i\omega t}$$

Substituting the assumed solution into the homogenous form,

$$(K - \omega^2 I)\bar{\theta} = 0$$

The trivial solutions of the previous equation are ignored and therefore,

$$det(K - \omega^2 I) = 0$$

$$\therefore \quad \begin{vmatrix} k - \omega^2\left(I_m + \frac{I_s}{2}\right) & -k \\ -k & k - \omega^2\left(I_c + \frac{I_s}{2}\right) \end{vmatrix} = 0$$

$$\therefore \quad k^2 - \omega^2 k(I_m + I_c + I_s) + \omega^4\left(I_m + \frac{I_s}{2}\right)\left(I_c + \frac{I_s}{2}\right) - k^2 = 0$$

$$\therefore \quad \omega = 0 \;\; or \;\; \omega = \sqrt{\frac{k(I_m + I_c + I_s)}{\left(I_m + \frac{I_s}{2}\right)\left(I_c + \frac{I_s}{2}\right)}} = \sqrt{\frac{1.9486 \times 10^4 \, (2.6 + 2.5 + 1.8496 \times 10^{-3})}{(2.600925)(2.500925)}}$$

$$\therefore \quad \omega = 0 \;\; or \; \omega = 123.63 \, rad/s$$

Thus, the system's natural frequency is,

$$\omega_n = 123.63 \frac{rad}{s} \, or \; f_n = \frac{\omega_n}{2\pi} = \frac{123.63}{2\pi} = 19.676 \, Hz$$

4.1.4. Dynamic Shear Stress

The equation of motion of the simple motor compressor system is,

$$I\ddot{\bar{\theta}} + K\bar{\theta} = \bar{F}$$

The compressor is assumed to generate a constant load to the system so that the only excitation is from the dynamic motor torque. Therefore,

$$\bar{F} = \begin{bmatrix} T_d \cos(2\pi f t) \\ 0 \end{bmatrix}$$

The forcing frequency is represented as,

$$\omega = 2\pi f = \; 40\pi \, rad/s$$

The force vector can be converted to the complex form as,

$$\bar{F} = Real(\tilde{F} e^{i\omega t})$$

Where,

$$\tilde{F} = \begin{bmatrix} T_d \\ 0 \end{bmatrix} = \begin{bmatrix} 100 \\ 0 \end{bmatrix}$$

Assume the complex form of the solution as,

$$\bar{\theta} = Real(\tilde{\theta} e^{i\omega t})$$

Substituting the assumed solution in the equation of motion for steady state vibration we get,

$$\tilde{\theta} = [K - \omega^2 I]^{-1}\tilde{F}$$

$$\therefore \quad \tilde{\theta} = \begin{bmatrix} k - \omega^2\left(I_m + \frac{I_s}{2}\right) & -k \\ -k & k - \omega^2\left(I_c + \frac{I_s}{2}\right) \end{bmatrix}^{-1} \tilde{F}$$

$$\therefore \quad \tilde{\theta} = \begin{bmatrix} 19486 - (40\pi)^2(2.600925) & -19486 \\ -19486 & 19486 - (40\pi)^2(2.500925) \end{bmatrix}^{-1} \begin{bmatrix} 100 \\ 0 \end{bmatrix}$$

$$\therefore \quad \tilde{\theta} = \begin{bmatrix} -3.835 \times 10^{-4} & -3.735 \times 10^{-4} \\ -3.735 \times 10^{-4} & -4.138 \times 10^{-4} \end{bmatrix} \begin{bmatrix} 100 \\ 0 \end{bmatrix} = \begin{bmatrix} -0.03835 \\ 0.03735 \end{bmatrix}$$

Therefore, the angular position of either node can be defined as the functions of time,

$$\theta_1(t) = -0.03835\cos(40\pi t)$$

$$\theta_2(t) = 0.03735\cos(40\pi t)$$

The shaft twist as a function of time is,

$$\emptyset = \theta_1(t) - \theta_2(t) = -0.0757\cos(40\pi t) = 0.0757\cos(40\pi t + \pi)$$

Thus, amplitude and phase of twist is,

$$\emptyset_A = 0.0757\, rad \text{ And } \emptyset_{phase} = \pi\, rad$$

The torque amplitude due to twist is,

$$T_A = \emptyset_A \frac{GJ}{L} = 0.0757 \frac{82.7 \times 10^9 \times 2.3562 \times 10^{-7}}{1} = 1475.1\, Nm$$

The shear stress amplitude due to twist is,

$$\tau_A = \frac{T_A D_o}{2J} = \frac{1475.1 \times 0.04}{2 \times 2.3562 \times 10^{-7}} = 125.16\, MPa$$

4.1.5. Mean Shear Stress

The mean shear stress in the shaft can be determined by the constant torque of system,

$$\tau_A = \frac{TD_o}{2J} = \frac{2.5 \times 10^3 \times 0.04}{2 \times 2.3562 \ \times 10^{-7}} = 212.21\ MPa$$

4.1.6. Strain Theory S-N Curve

The material properties of the steel are defined for this system as,

$$Geometrical\ Stress\ Concentration\ Factor, K_t = 1.55$$
$$Ultimate\ Tensile\ Strength, \sigma_u = 860\ MPa$$
$$Ratio\ of\ Ultimate\ Shear\ Strength, \tau_u, to\ Ultimate\ Tensile\ Strength\ \sigma_u = \ 0.8$$
$$Shear\ Factor, F_{sh} = 0.577$$
$$Surface\ Finish\ Factor, k_a = \ 0.9$$
$$Size\ Effect\ Factor, k_b = 0.667$$
$$Safety\ Factor, SF = 1.35$$
$$Reduction\ of\ Area\ in\ Tensile\ Test, RA = \ 0.4$$
$$Elastic\ Modulus, E = 1.95e5\ MPa$$
$$Fatigue\ Strength\ Exponent, b = \ -0.085$$
$$Fatigue\ Ductility\ Exponent\ , c = \ -0.6$$
$$Notch\ Sensitivity, q = 0.91$$
$$Yield\ Strength,\ \ \sigma_y = 460\ MPa$$

To determine the surface factor as a function of life the following equations are used,

$$k_a(N) = \frac{10^b}{N^m}$$

$$m = \frac{\log\left(\frac{k_a(1000)}{k_a(10^6)}\right)}{3.0}$$

$$b = \log\left(\frac{k_a(1000)^2}{k_a(10^6)}\right)$$

The surface finish factor at 1000 and 1e6 cycles are defined as,

$$k_a(1000) = 1.00$$

$$k_a(10^6) = surface\ finish\ from\ material\ properties\ list = 0.9$$

Therefore,

$$m = \frac{\log\left(\frac{1}{.9}\right)}{3.0} = 0.01525$$

$$b = \log\left(\frac{1^2}{.9}\right) = 0.04576$$

$$k_a(N) = \frac{10^{0.04576}}{N^{0.01525}}$$

The size factor as a function of life is found by,

$$k_b(N) = \frac{10^b}{N^m}$$

$$m = \frac{\log\left(\frac{k_b(1000)}{k_b(10^6)}\right)}{3.0}$$

$$b = \log\left(\frac{k_b(1000)^2}{k_b(10^6)}\right)$$

The size factor at 1000 and 1e6 cycles are defined as,

$$k_b(1000) = 1.00$$

$$k_b(10^6) = size\ factor\ from\ material\ properties\ list = 0.667$$

Therefore,

$$m = \frac{\log\left(\frac{1}{0.667}\right)}{3.0} = 0.05862$$

$$b = \log\left(\frac{1^2}{0.667}\right) = 0.17587$$

$$k_b(N) = \frac{10^{0.17587}}{N^{0.05862}}$$

The fatigue stress concentration factor, k_f, is found by,

$$k_f = 1 + q(k_t - 1)$$

$$k_f = 1 + 0.91(1.55 - 1) = 1.5005$$

The effective stress concentration factor as a function of cycles is,

$$k_f(N) = \frac{10^b}{N^m}$$

$$m = \frac{\log\left(\frac{k_f(1000)}{k_f(10^6)}\right)}{3.0}$$

$$b = \log\left(\frac{k_f(1000)^2}{k_f(10^6)}\right)$$

Where,

$$k_f(1000) = \sqrt{k_f(10^6)}$$

$$= \sqrt{1.5005} = 1.2249$$

Therefore,

$$m = \frac{\log\left(\frac{1.2249}{1.5005}\right)}{3.0} = -0.02937$$

$$b = \log\left(\frac{1.2249^2}{1.5005}\right) = 0$$

$$k_f(N) = \frac{1}{N^{-0.02937}}$$

The true stress and strain at fracture,

$$\sigma_f' = \frac{\sigma_u}{1 - RA} = \frac{860e6}{1 - 0.4} = 1433\ MPa$$

$$\varepsilon_f' = \ln\left(\frac{1}{1 - RA}\right) = 0.5108$$

Using the Coffin-Manson equation, the relation of the strain to the number of cycles to failure is,

$$\varepsilon(N) = \frac{\sigma_f'}{E} * N^b + \varepsilon_f' * N^c$$

Therefore,

$$\varepsilon(N) = \frac{1.433e3}{1.95e5} * N^{-0.085} + .5108 * N^{-0.6}$$

From the justification in 3.1, the strain versus cycles can be converted to stress versus cycles simply by multiplying the equation by the elastic modulus. Therefore,

$$\sigma(N) = \varepsilon(N) * E$$

$$\sigma(N) = \left(\frac{\sigma_f'}{E} * N^b + \varepsilon_f' * N^c\right) * E$$

$$\sigma(N) = \sigma_f' * N^b + \varepsilon_f' * E * N^c$$

$$\sigma(N) = 1433e6 * N^{-0.085} + 8.122e10 * N^{-0.6}$$

The previous equation outlines the tensile stress versus life equation. This must then be converted into the equation for shear stress versus life using the equation,

$$\tau(N) = \sigma(N) * F_{sh} * k_a * \frac{k_b}{k_f * SF}$$

The values of $\sigma(N)$, k_a, k_b, and k_f are all functions of N as previously discussed while F_{sh} and SF are constants. Solving for $\tau(N)$ and plotting the results gives the plot (blue) shown in Figure *7*.

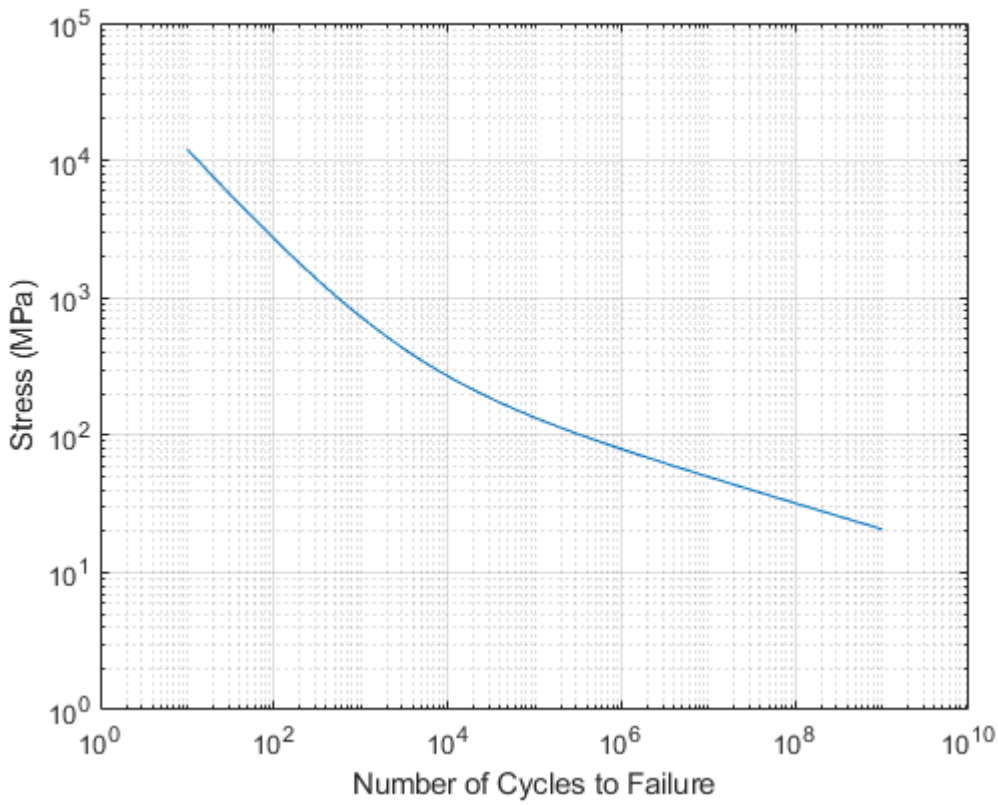

Figure 7: Strain Theory Life Prediction Without Low and High Cycle Limits

The low cycle fatigue (LCF) and high cycle fatigue (HCF) are specified to occur at 10^3 and 10^6 cycles respectively. Therefore, from Figure *7*,

$$\tau(10^3) = 734.55\ MPa$$

$$\tau(10^6) = 79.58\ MPa$$

The LCF and HCF limits are added to the plot of $\sigma(N)$ and the complete strain life theory S-N curve is shown in Figure *8*.

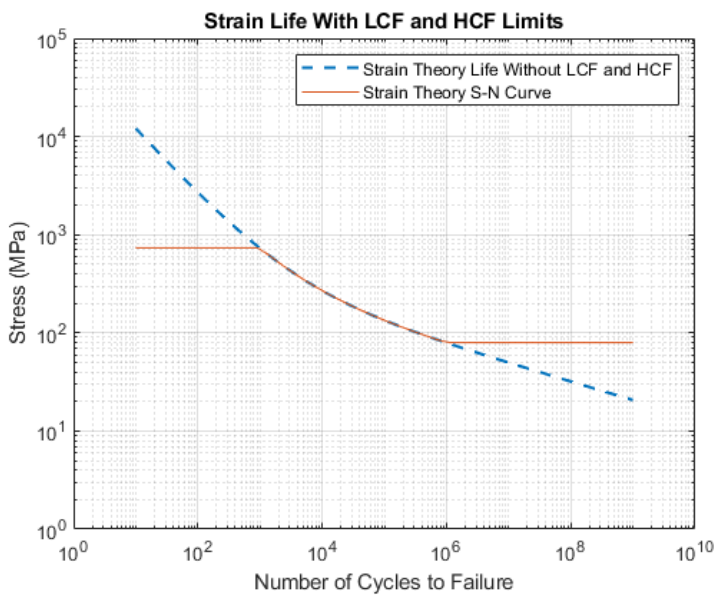

Figure 8: Strain Theory S-N Curve

The previously determined mean and amplitude shear stresses were calculated to be,

$$\tau_m = 212.21\ MPa$$

$$\tau_a = 125.16\ MPa$$

The torsional yield stress, τ_y, is calculated by the equation,

$$\tau_y = \sigma_y * F_{sh}$$

$$\tau_y = 460 * 0.577 = 265.42\ MPa$$

The endurance limit, τ_e, is defined as the high cycle fatigue limit in the strain theory model and therefore,

$$\tau_e = 79.58\ MPa$$

In 3.1.1, it is shown that if,

$$\tau_m > \tau_y - \tau_e\ and\ \tau_a > \tau_y - \tau_m$$

Then, mean shear stress has influence on effective shear stress and the effective shear is,

$$\tau_{eff} = \frac{\tau_a}{\frac{\tau_y - \tau_m}{\tau_e}}$$

For this example,

$$\tau_m > \tau_y - \tau_e\ and\ \tau_a > \tau_y - \tau_m$$

$$212.21\ MPa > 185.84\ and\ 125.16\ MPa > 53.21\ MPa$$

And the effective shear stress is,

$$\tau_{eff} = \frac{125.16}{\frac{53.21}{79.58}} = 187.19\ MPa$$

From the S-N curve in Figure *8*, we can interpolate that the number of cycles to failure due to an effective amplitude shear stress of $\tau_{eff} = 187.19\ MPa$ is,

$$N = \ 35307\ cycles$$

The damage per cycle is,

$$D = \frac{1}{N} = \ 2.8323e(-5)$$

Using the frequency of the dynamic torque of 20 Hz, the time of one cycle is,

$$t = \frac{1}{20} = \ 0.05\ s$$

Finally, the time to failure is calculated by,

$$t_{failure} = 35307 * 0.05 * \left(\frac{1\ min}{60\ sec}\right) * \left(\frac{1\ hr}{60\ min}\right) * \left(\frac{1\ day}{24\ hr}\right) = \ .02\ Days$$

4.1.7. VFD Software Results

To perform the analysis with the TRC Code, the options sheet must be set up to run a torsional model with a user defined torque, SI units, and strain-based life prediction.

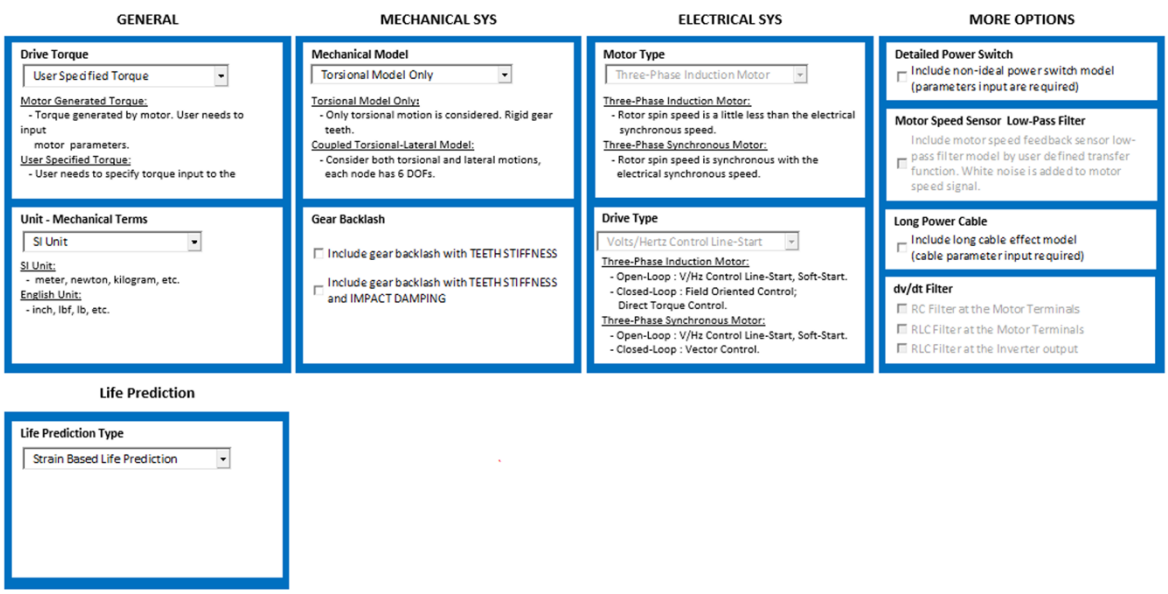

Figure 9: System Options

On the “Mech-Torsional Only” sheet, the parameters should be input as shown in Figure *10*. All other fields should be left blank. The save button must then be clicked to set up the system model.

SHAFT

Shaft	Element	Left Node	Right Node	Outer Radius	Inner Radius	Length	Shear Modulus	Density	Damping
#	#	#	#	m	m	m	N/m^2	Kg/m^3	N.m.s/rad
1	1	1	2	0.02	0.01	1	8.27E+10	7850	0

ADDED INERTIA

Node	Inertia	Bearing Damping
#	Kg.m^2	N.m.s/rad
1	2.6	0
2	2.5	0

Figure 10: System Parameters

The user defined toque is then input as shown in Figure *11* and the “Save” button is then selected. This example uses a SSHR analysis with a torque amplitude of 100 N-m and a mean torque of 2500 N-m.

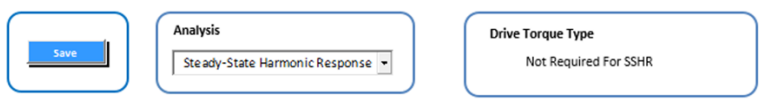

DYNAMIC TORQUE

Applied Node	Frequency	Amplitude	Angle
#	Hz	N.m	deg
1	20	100	0
1	0	2500	0
2	0	-2500	0

Figure 11: User Defined Torque

To run the simulation, the inputs in Figure *12* are put into the “SSHR Simulation” sheet and the run button is selected. Once the simulation is complete the “Show Output” button must also be selected to get the results shown in Figure *13*.

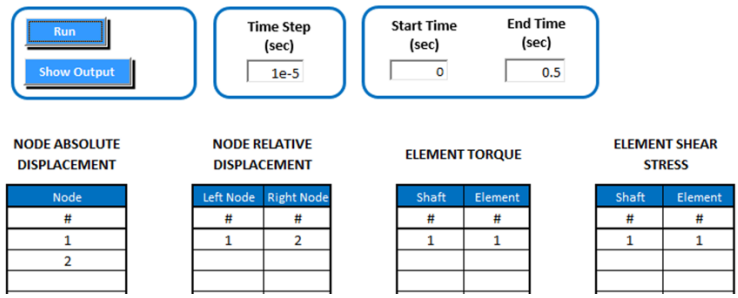

Figure 12: SSHR Settings

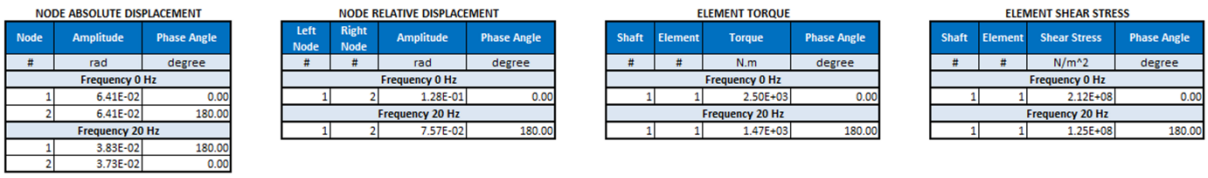

NODE ABSOLUTE DISPLACEMENT

Node	Amplitude	Phase Angle
#	rad	degree
Frequency 0 Hz		
1	6.41E-02	0.00
2	6.41E-02	180.00
Frequency 20 Hz		
1	3.83E-02	180.00
2	3.73E-02	0.00

NODE RELATIVE DISPLACEMENT

Left Node	Right Node	Amplitude	Phase Angle
#	#	rad	degree
Frequency 0 Hz			
1	2	1.28E-01	0.00
Frequency 20 Hz			
1	2	7.57E-02	180.00

ELEMENT TORQUE

Shaft	Element	Torque	Phase Angle
#	#	N.m	degree
Frequency 0 Hz			
1	1	2.50E+03	0.00
Frequency 20 Hz			
1	1	1.47E+03	180.00

ELEMENT SHEAR STRESS

Shaft	Element	Shear Stress	Phase Angle
#	#	N/m^2	degree
Frequency 0 Hz			
1	1	2.12E+08	0.00
Frequency 20 Hz			
1	1	1.25E+08	180.00

Figure 13: SSHR Results

The results show a mean shear stress (seen by the 0 Hz Frequency) of,

$$\tau_m = 2.12e8 \frac{N}{m^2} = 212\ MPa$$

And an amplitude shear stress (seen by the 20 Hz Frequency) of,

$$\tau_a = 1.25e8 \frac{N}{m^2} = 125\ MPa$$

Finally, the strain theory life prediction is run by setting up the "Material Properties" and "Specified Elements for Fatigue Analysis" sections of the "Strain Based Life" sheet as shown in Figure *14* and Figure *15*. Once completed, the "Run" button is pressed.

Run

Material Properties

Material	Material	Geometrical Stress Concentration Factor,	Ultimate Tensile Strength, σ_u	Ratio of Ultimate Shear Strength, τ_u, to Ultimate Tensile Strength σ_u	Ratio of Shear Stress to Normal Stress (Shear Factor), Fsh	Surface Finish Factor, ka	Size Effect Factor, kb	Safety Factor, SF	Reduction of Area in Tensile Test, RA	Elastic Modulus, E	Fatigue Strength Exponent, b	Fatigue Ductility Exponent, c	Notch Sensitivity, q	Yield Strength
(Name)	#	#	MPa	#	#	#	#	#	#	MPa	#	#	#	MPa
4340 BHN 243	1	1.55	860	0.8	0.577	0.9	0.667	1.35	0.4	1.95E+05	-0.085	-0.6	0.91	460

Figure 14: Material Properties

Specified Elements for Fatigue Analysis

Description	Unit	Life Prediction Data											
Shaft	#	1											
Element	#	1											
Material	#	1											
Time Step for Stress Signal Gen	sec	0.00001											
Start Time for Rainflow Analysis	sec	0											
End Time for Rainflow Analysis	sec	0.05											

Figure 15: Specified Elements for Fatigue Analysis

Once the strain life analysis is complete, the results section will populate with the solution to the analysis. The results for this example are shown in Figure *16*.

Results

Description	Unit	Life Prediction Results								
Shaft	#	1								
Element	#	1								
Damage	-	0.000029								
Number of Cyles to Failure	#	34705.784								
Rainflow Cycles counted by alg	#	1								
Fatigue Life	days	0.020084								

Figure 16: Strain Life Results

The VFD Software results table shows the predicted number of cycles to failure to be 34706 cycles compared to the 35307 cycles calculated by the manual calculations. The fatigue life from the software is also found to be 0.02 days which is also similar to the manual calculations. All deviations in values are the result of rounding error.

4.2. Example 2: Comparison of Strain life to stress life prediction on a system

To illustrate the differences between the strain-based and stress-based life prediction models and their effects on a system analysis, a comparison was done on the system in Example 1 of Section 6 of the user guide. The complete system will be defined in this example.

4.2.1. System Set Up

To perform the analysis, the mechanical parameters in Figure *17* are set up in the Mech-Torsional Only sheet in the VFD Software.

SHAFT

Shaft	Element	Left Node	Right Node	Outer Radius	Inner Radius	Length	Shear Modulus	Density	Damping
#	#	#	#	m	m	m	N/m^2	Kg/m^3	N.m.s/rad
1	1	1	2	0.04	0.03	0.5	8.00E+10	8000	0
1	2	2	3	0.05	0.04	0.5	8.00E+10	8000	0
1	3	3	4	0.01	0	0.5	8.00E+10	8000	0
2	1	5	6	0.02	0.01	0.5	8.00E+10	8000	0
2	2	6	7	0.02	0.01	0.5	8.00E+10	8000	0
3	1	8	9	0.01	0.005	0.5	8.00E+10	8000	0

ADDED INERTIA

Node	Inertia	Bearing Damping
#	Kg.m^2	N.m.s/rad
1	2.6	0
2	1	0
3	1	0
4	1	0
5	1	0
6	1	0
7	1	0
8	1	0
9	2.5	0

GEARS

Driver Node	Follower Node	Gear Ratio
#	#	-
4	5	2

COUPLING FLANGE

Left Node	Right Node	Stiffness	Damping
#	#	N.m/rad	N.m.s/rad
7	8	1000	0

PROPORTIONAL DAMPING

f	ξ
Hz	%
3	5
40	3
92.5	3

Figure 17: Mechanical Parameters

The “Save” button is then selected to begin the system modeling and calculations of mode shapes and natural frequencies. Next, the motor parameters are input for the induction motor under the Induction Motor sheet as shown in Figure *18* and the Save button is selected.

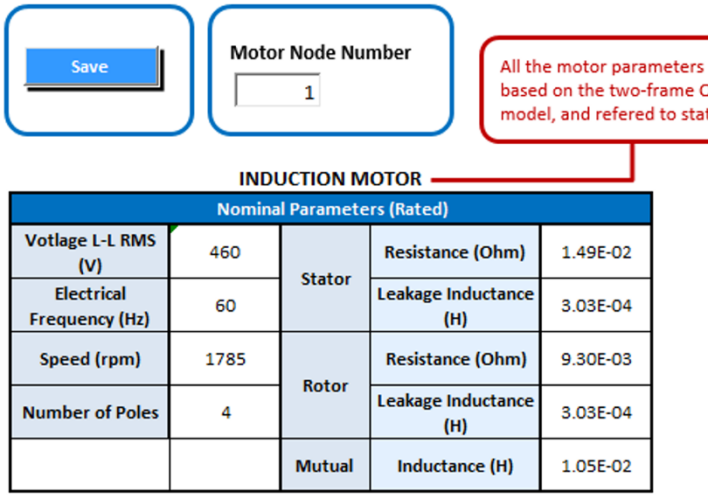

Figure 18: Motor Parameters

The motor is controlled using the Volts/Hertz control method with the parameters shown in Figure *19* and the accompanying “Save” button is also selected.

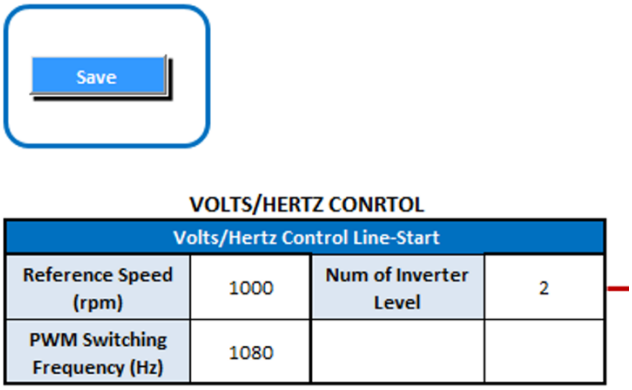

Figure 19: Control Settings

The final step before running the simulation is to add a load torque of 1 Nm/(rad/s) as shown in Figure *20*.

LOAD TORQUE

Node	a_0	a_1	a_2	a_3
#	N.m	N.m/(rad/s)	N.m/(rad/s)^2	N.m/(rad/s)^3
9	0	1	0	0

Figure 20: Load Torque

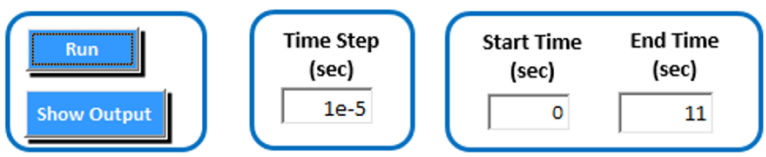

Figure 21: Simulation Settings

The simulation sheet can be left blank except for the inputs specified in Figure *21*. Once these values are input, the Run button will perform the transient analysis of the electrical and mechanical system to get the data necessary for the life prediction.

Description	Unit	Life Prediction Data								
Shaft	#	1	1	1	2	2	3			
Element	#	1	2	3	1	2	1			
Time Step for Stress Signal Generat	sec	1.00E-05	1.00E-05	1.00E-05	1.00E-05	1.00E-05	1.00E-05			
Start Time for Rainflow Analysis	sec	0	0	0	0	0	0			
End Time for Rainflow Analysis	sec	10	10	10	10	10	10			
Ultimate Tensile Strength (σ_{ut})	MPa	830	830	830	830	830	830			
Tensile Yield Strength (σ_{yt})	MPa	475	475	475	475	475	475			
Tensile Endurance Limit (σ_e)	MPa	200	200	200	200	200	200			
Low Cycle Fatigue Cycles (N_{LCF})	#	1.00E+03	1.00E+03	1.00E+03	1.00E+03	1.00E+03	1.00E+03			
Infinite Fatigue Life Cycles (N_{INF})	#	1.00E+06	1.00E+06	1.00E+06	1.00E+06	1.00E+06	1.00E+06			
Ratio of Ultimate Shear Strength (τ_{xu}) to Ultimate Tensile Strength (σ_{ut})	-	0.8	0.8	0.8	0.8	0.8	0.8			
Ratio of Low Cycle Fatigue Shear Strength (τ_{LCF}) to Ultimate Shear	-	0.9	0.9	0.9	0.9	0.9	0.9			
Ratio of Shear Yield Strength (τ_{xy}) to Tensile Yield Strength (σ_{yt})	-	0.577	0.577	0.577	0.577	0.577	0.577			
Theoretical Stress Concentration F	-	3	3	3	3	3	3			
Notch Sensitivity Factor (q)	-	1	1	1	1	1	1			
Surface Finish Factor (k_a)	-	1	1	1	1	1	1			
Size Factor (k_b)	-	0.734	0.734	0.734	0.734	0.734	0.734			
Load Factor (k_c)	-	0.57	0.57	0.57	0.57	0.57	0.57			
Temperature Factor (k_d)	-	1	1	1	1	1	1			
Reliability Factor (k_e)	-	0.753	0.753	0.753	0.753	0.753	0.753			
Miscellaneous Factor (k_f)	-	1	1	1	1	1	1			

Figure 22: Stress Life Prediction Parameters

4.2.2. Results

Description	Unit	Life Prediction Results								
Shaft	#	1	1	1	2	2	3			
Element	#	1	2	3	1	2	1			
Damage	-	0	0	Inf	0.000003	0.000002	Inf			
Number of Cyles to Failure	#	Inf	Inf	0	295251.8	471257.2	0			
Rainflow Cycles counted by algorith	#	3639	639	91	106	90	19			
Fatigue Life	days	Inf	Inf	0	34.17266	54.54366	0			

Figure 23: Stress Based Life Results

As a baseline, the stress analysis is run first with the material properties shown in Figure *22*. The stress-based life prediction is run to get the results shown in Figure *23*. From the results it is seen that the system fails instantly at 2 of the elements and fails after a few days for the elements located in shaft 2.

The analysis type for the life prediction is then changed to the strain-based life prediction in the Options sheet. The material properties and specified elements are then input for the same material as shown below in Figure *24* before running the strain-based life analysis.

Run

Material Properties

Material	Material	Geometrical Stress Concentration Factor, Kt	Ultimate Tensile Strength, σu	Ratio of Ultimate Shear Strength, τu, to Ultimate Tensile Strength σu	Ratio of Shear Stress to Normal Stress (Shear Factor), Fsh	Surface Finish Factor, ka	Size Effect Factor, kb	Safety Factor, SF	Reduction of Area in Tensile Test, RA	Elastic Modulus, E	Fatigue Strength Exponent, b	Fatigue Ductility Exponent , c	Notch Sensitivity, q	Yield Strength
(Name)	#	#	MPa	#	#	#	#	#	#	MPa	#	#	#	MPa
4340 BHN 243	1	3	830	0.8	0.57	1	0.734	1.35	0.4	1.95E+05	-0.085	-0.6	1	475

Specified Elements for Fatigue Analysis

Description	Unit	Life Prediction Data											
Shaft	#	1	1	1	2	2	3						
Element	#	1	2	3	1	2	1						
Material	#	1	1	1	1	1	1						
Time Step for Stress Signal Generation	sec	0.00001	0.00001	0.00001	0.00001	0.00001	0.00001						
Start Time for Rainflow Analysis	sec	0	0	0	0	0	0						
End Time for Rainflow Analysis	sec	10	10	10	10	10	10						

Figure 24: Strain Life Prediction Parameters

After performing the strain life prediction analysis, the results in Figure *25* are output.

Description	Unit	Life Prediction Results								
Shaft	#	1	1	1	2	2	3			
Element	#	1	2	3	1	2	1			
Damage	-	0	0	Inf	0	0	0.000058			
Number of Cyles to Failure	#	Inf	Inf	0	Inf	Inf	17190.04			
Rainflow Cycles counted by algorithm	#	3639	639	91	106	90	19			
Fatigue Life	days	Inf	Inf	0	Inf	Inf	1.989588			

Figure 25: Strain Life Prediction Results

By comparing the results of the strain and stress-based life methods for this example, several interesting conclusions can be drawn. While both of the life prediction methods predict instant failure at element 3 of shaft 1, the strain-based method determines that the elements on

shaft 2 exhibit infinite life as opposed to the eventual failure shown by the stress-based method. This illustrates the over conservativeness that is sometimes seen when utilizing the stress-based method as outlined in [11]. Finally, the element in shaft three is shown to not fail instantly but instead after one day of running according to the more accurate strain-based life prediction method.

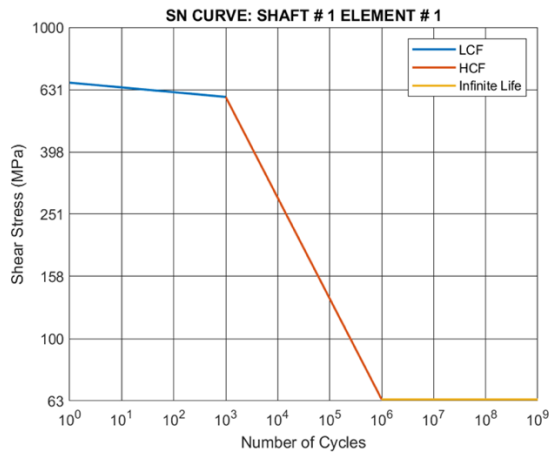

Figure 26: Stress Life SN Curve

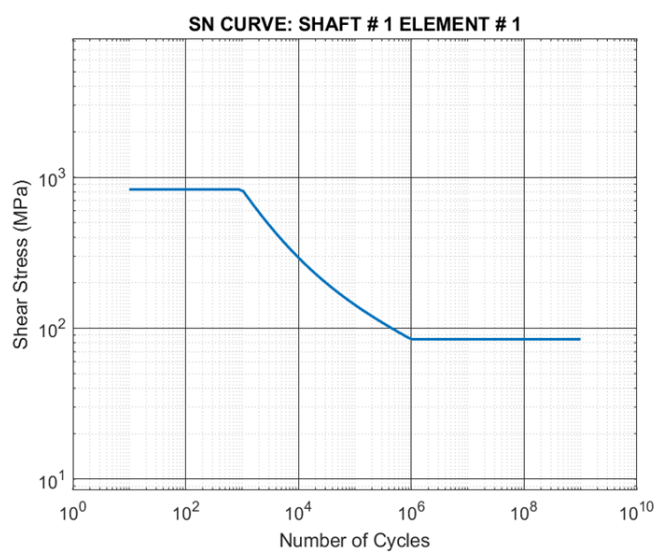

Figure 27: Strain Life SN Curve

The S-N curves for both the stress life prediction and strain life prediction are output in the Excel UI. The S-N curves for shaft 1, element 1 are shown in Figure *26* and Figure *27*. The strain life S-N curve is shifted up compared to the strain life S-N curve, indicating a longer life prediction for an equivalent shear stress. The high cycle fatigue region also shows a nonlinear behavior on the log-log plot due to the life degrading factors being treated as functions of life.

5. TRANSIENT ANALYSIS WITH TIME BASED FUNCTION OF TORQUE AND OPTIONAL RAMP UP

The Transient Analysis and Time-Based Function of Torque Option can be selected for cases where a user wishes to input a torque excitation with known frequencies, amplitudes, and phase shifts. This is particularly useful when a torque spectrum analysis was previously run i.e., in the case of a VFD controlled motor.

The Time-Based Function of Torque requires the user to input an applied node similar to the time-table based torque input. The user can then input the desired frequencies, amplitudes, and phase angles of the torque. The user must also specify if a torque ramp up is desired along with a mean torque value. If a torque ramp up was desired, the ramp up time must also be specified. Once all the user specified values are input, the "Save" button must be clicked.

It is important to note that the motor ramp up follows a sigmoid curve from zero to the mean drive torque. Also, the dynamic torques do not begin until after the ramp up is completed.

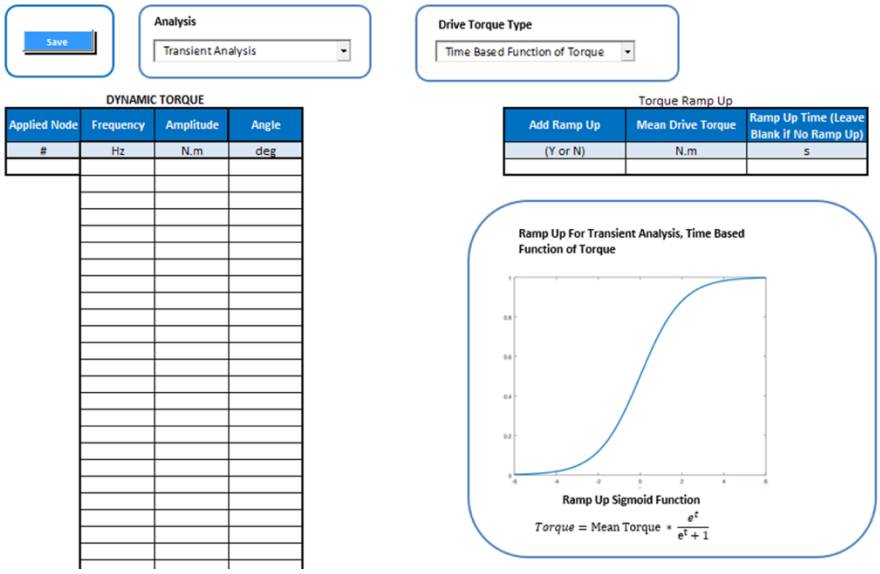

Figure 28: Transient Analysis Time Based Function of Torque

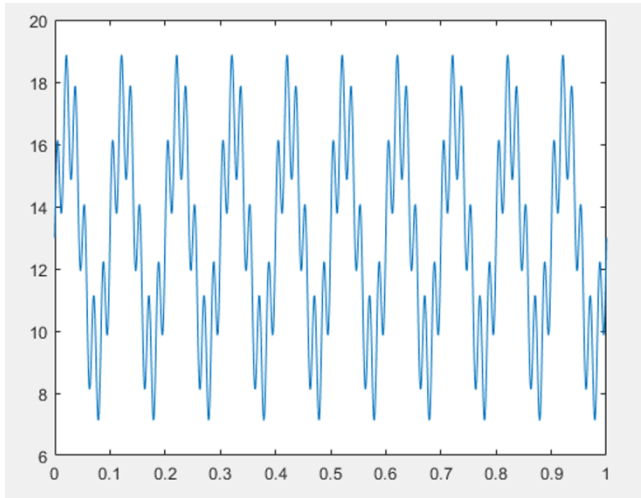

Figure 29: Time Signal No Ramp Up

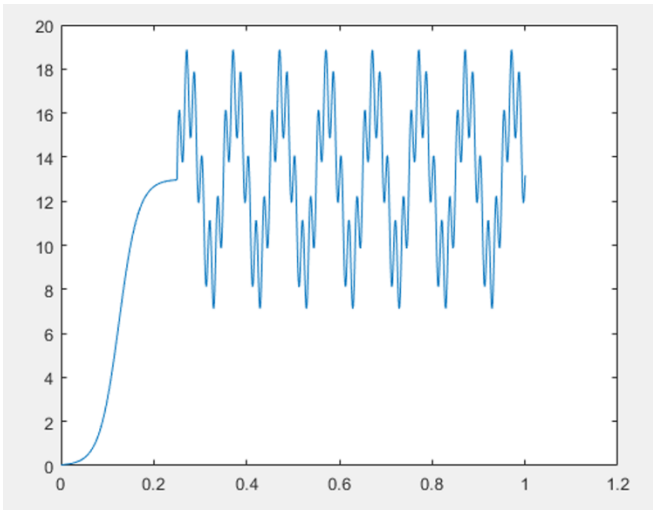

Figure 30: Time Signal of Torque With 0.2s Ramp Up

The newly implemented option in the Excel UI is shown in Figure *28*. Examples of the user defined torque with and without a ramp up is shown in Figure *29* and Figure *30*.

6. EXPERIMENTAL VFD TEST RIG

6.1. Design Overview

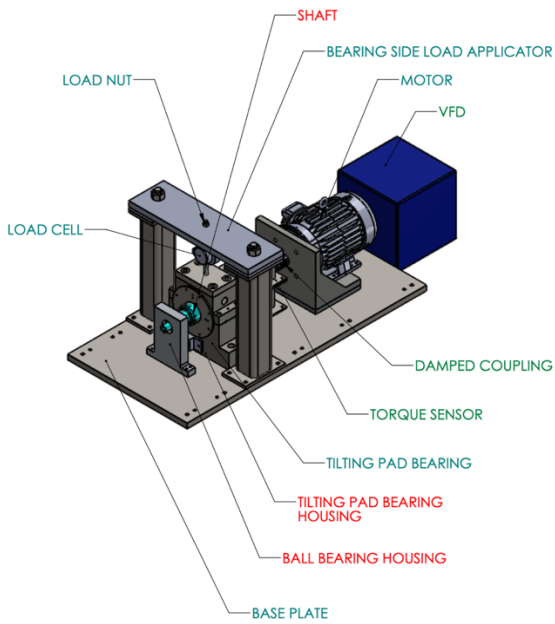

Figure 31 Test Rig Isometric View

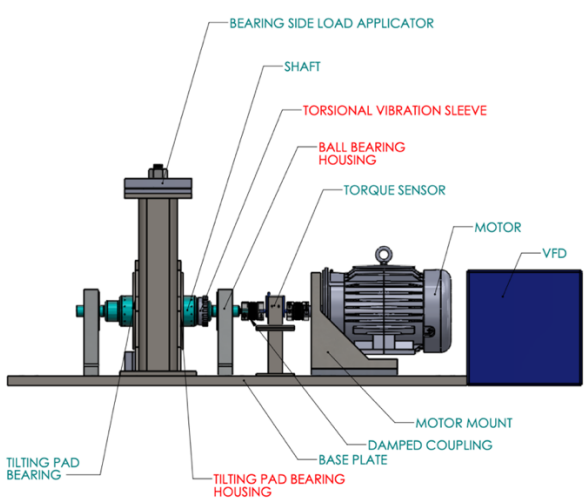

Figure 32 Test Rig Side View

The design of the VFD test rig is shown in Figure *31* and Figure *32*. The test rig is composed up of several main elements discussed in this section.

The test rig motor is a Reuland motor controlled by a Dura Pulse VFD and is connected to the torque sensor by an elastomer damped coupling. The torque sensor is an Interface T4 torque transducer that measures the dynamic torques generated by the motor and VFD system. The other side of the torque sensor is attached to a steel shaft via a similar damped coupling. The shaft is supported by two ball bearings and a tilting pad bearing. The shaft adds an inertial load to the system while also containing the torsional vibration sleeve that is used to measure the torsional vibration amplitude and frequency. Finally, the tilting pad bearing housing is connected to a bearing side load applicator via the load cell to allow for specific side loads to be applied to the TPB. This allows for the viscous drag on the shaft to be increased.

6.2. Variable Frequency Drive (VFD)

Dynamic torque generated by variable frequency drives are a result of both the VFD topology and the modulation strategy. The topology consists of a variety of different options but the most common are topologies of a varying number of levels. Figure *33* shows an example of a three level and 5 level voltage inverters. Alternatively, the modulation strategy involves different methods such as PWM, space vector methods, pre-calculated methods, etc.

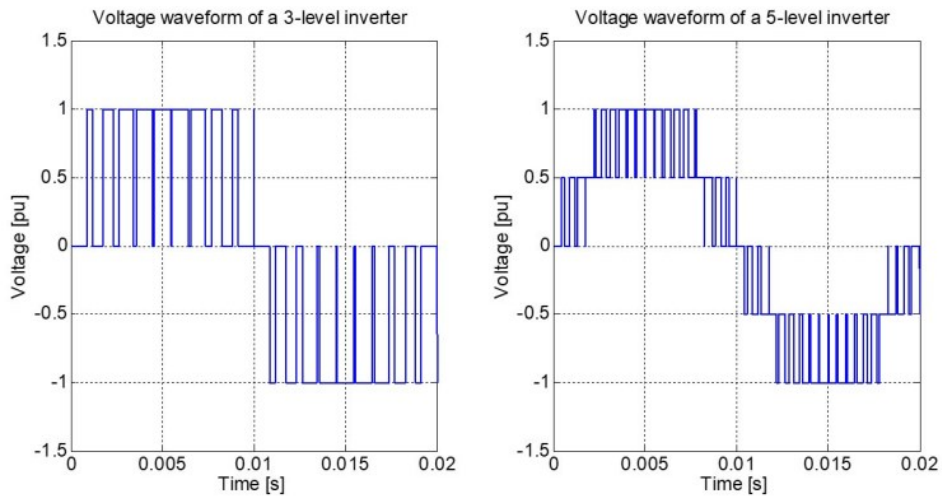

Figure 33 Different Level Topologies

Figure 34 Dura Pulse VFD

To meet the needs of the test rig and offer a wide variety of control to influence the generation of dynamic torques, the Dura Pulse GS3-4025 variable frequency drive is used to control the induction motor. The VFD operates with an output frequency between .1 and 400 Hz with a resolution of .1 Hz. The speed can therefore be adjusted to run the motor at a speed ranging from 6 to 24,000 RPM with a step size of 6 RPM.

For the test rig's 25 HP motor, the recommended carrier frequency of the PWM is 9 kHz. This can be set to a user specified value and has an impact on the torque harmonics that the VFD creates.

6.3. Motor

Figure 35 Reuland Induction Motor

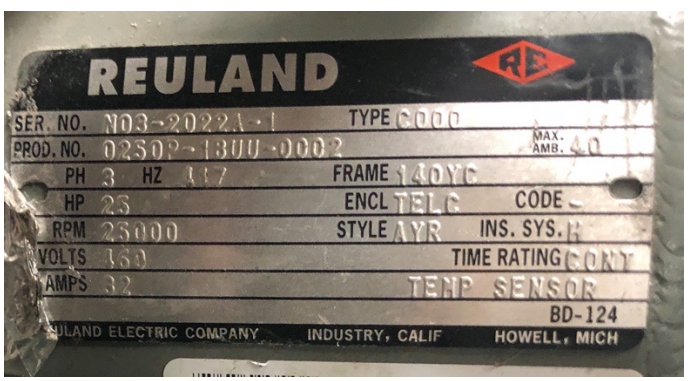

Figure 36 Reuland Motor Name Plate

The VFD test rig uses the 2 pole, Reuland induction motor shown in Figure *35*. The 25 HP motor is rated for a speed of 25000 RPM and voltage of 460 V as shown by the name plate

data in Figure *36*. The motor requires an oil mist during operation and can be water cooled in high load situations. For the rig the water-cooling feature is not used.

	Equivalent Circuit Data		Rev 0	Rev Date 11-16-20
Reference Number:	Product Number: 0250P-1BUU-0002	Document Number:	EQ-145R0265-01	
Prepared By:	Reuland Engineering	Page:	1 of 1	
Motor Description:	25 HP, 25,000 rpm, 145TC Frame			

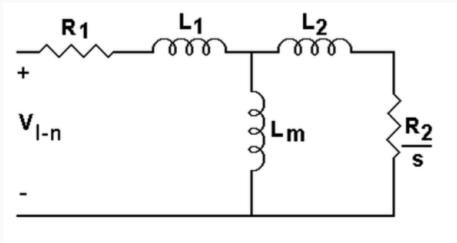

Y-BASED EQUIVALENT CIRCUIT

CIRCUIT PARAMETERS	
R1 (ohms)	0.0765
R2 (ohms)	0.0715
L1 (uH)	461.83
L2 (uH)	343.91
Lm (mH)	14.73

BASE HP =	25
BASE FREQUENCY (HZ) =	416.67
BASE VOLTS (V_{L-L}) =	460
BASE SPEED (RPM) =	25000
F.L AMPS (A) =	28.8
MAGNETIZING AMPS (A) =	6.9
SLIP FREQUENCY (HZ) =	3.7942

NOTE: SLIP FREQUENCY MUST BE ADDED TO BASE FREQUENCY IN ORDER TO ACHIEVE BASE SPEED

Figure 37: Reuland Motor Parameters

The motor parameters were able to be obtained directly from the manufacturer in the document shown in Figure *37*. This includes all resistances and inductances needed by the VFD code to generate the equivalent circuit.

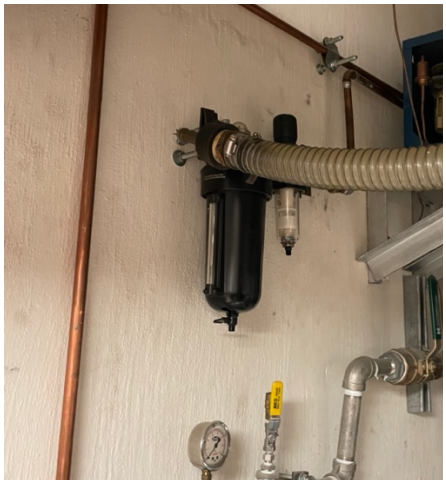

Figure 38: Oil Mist System

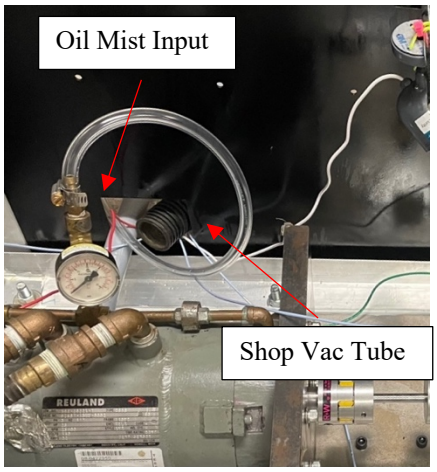

Figure 39: Oil Mist Input and Vacuum Filter

To lubricate the bearings inside the motor, the oil mist system in Figure *38* is connected to the top of the motor by the clear tube shown in Figure *39*. During motor operation, the compressed air line to the oil mist system is opened and the regulator feeding into the oil mist system is adjusted to 10 PSI to regulate the flow of the mist into the motor.

To ensure that the oil mist fumes are not released into the room and inhaled by the users, several air filters were installed on the inside of a shop vac and the shop vac hose was fed into the test rig enclosure as shown in Figure *39*. After several tests, this solution proved to be very successful at eliminating any oil mist from the developed test rig.

6.4. Shaft and Bearings

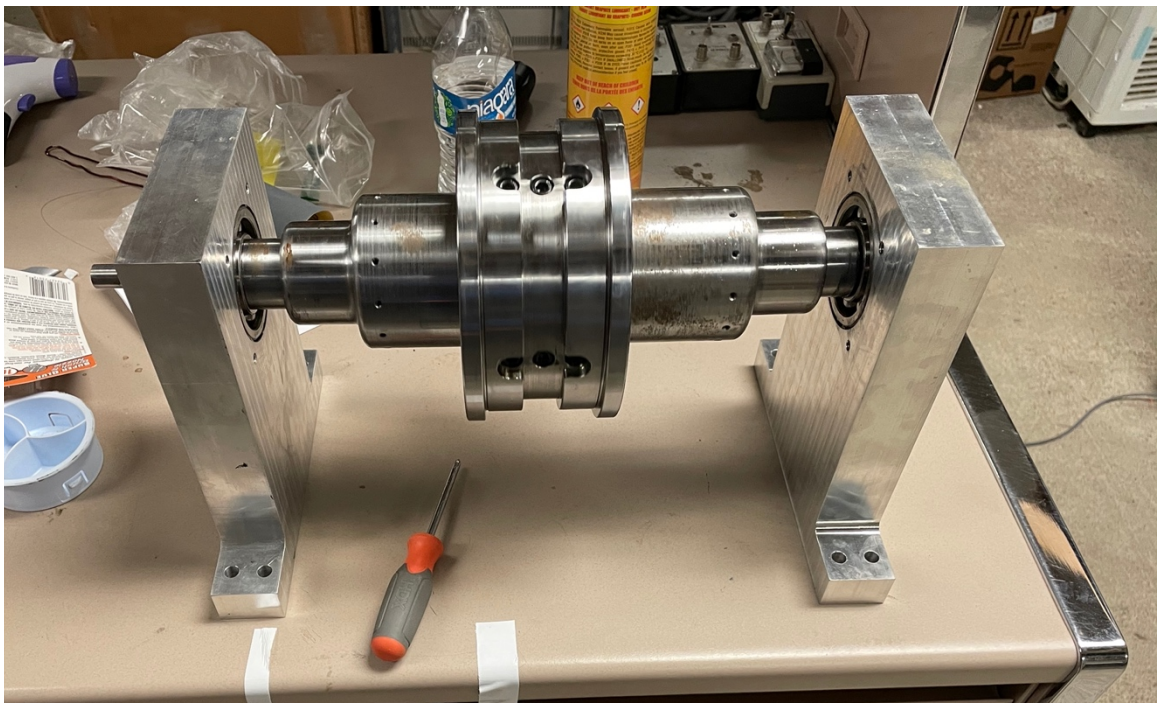

Figure 40: Main Shaft with Installed Bearings

The main shaft is made of 4340 Steel and is supported by 2 SKF RMS 9 ball bearings and a tilting pad bearing (TPB) as pictured in Figure *40*. The shaft allows for a TPB clearance between 3 and 4 mils and has 2 balancing planes located on either end of the large OD section. Both of the ball bearings are rated to support the maximum, 10 kN, load the side load system can

apply. They are mounted with a temperature press fit that was achieved by heating the bearings up to 450 degrees in an oven before quickly pressing them onto the room temperature shaft.

6.5. Ball Bearing Housing

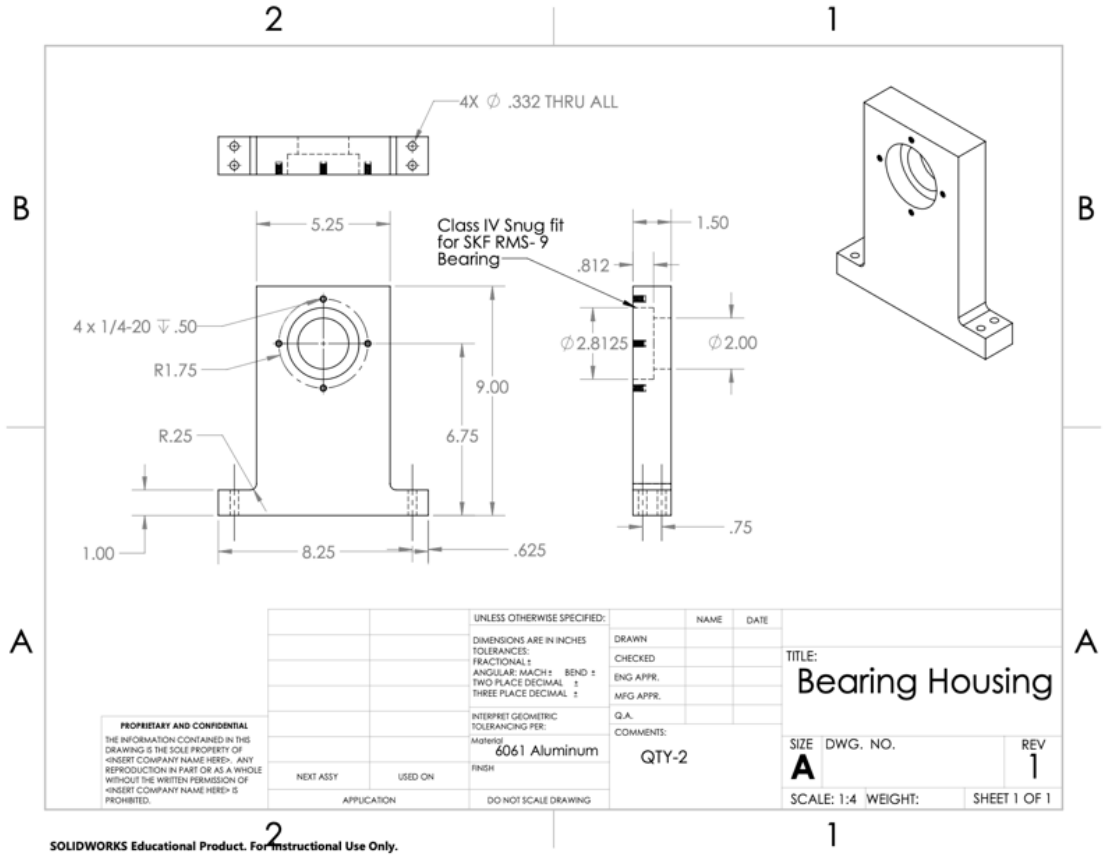

Figure 41 Ball Bearing Housing Drawing

The ball bearing housings are designed to house a SKF RMS-9 ball bearing with a Class IV fit. The housings are also designed to support the maximum side load of 10 kN from the side load applicator with a factor of safety of 5.8.

6.6. TPB Bearing Housing

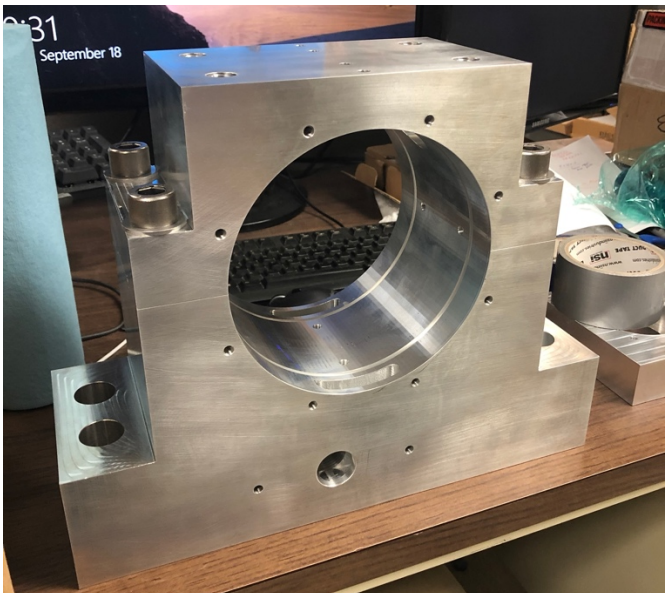

Figure 42: Tilting Pad Bearing Housing

The Tilting Pad Bearing (TPB) housing in Figure *42* was designed to support the 5 pad TPB used by the test rig. The housing also allows for oil to be fed into the bearing from the top rig side and drained out from the hole in the bottom. The bearing housing comes apart into 2 pieces to allow for the bearing install and also has 2 groves cut into the inner surface to allow for o-rings that stabilize the bearing and direct the oil to the bearing pads.

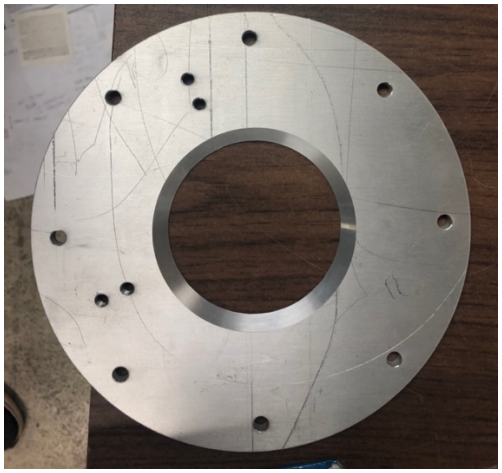

Figure 43: TPB Seal Plate

The seal plate in Figure *43* was designed with a 10 mil radial clearance to contain the oil and also act as a mounting point for the x and y Bentley probe brackets.

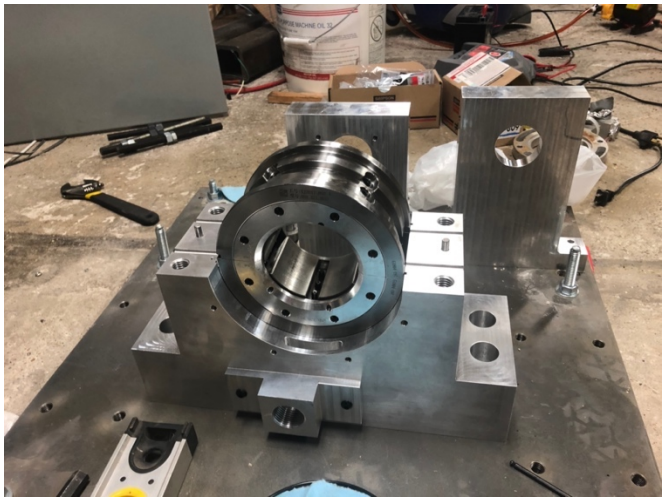

Figure 44: Housing with Bearing

Figure *44* shows the installation of the TPB into the housing and the oil out flange with 1” NPT threading located on the bottom half of the housing. Vertical guide pins are located on the

bottom half of the housing to ensure proper alignment of the two halves. On the bottom left and right side of the housing, 1” thru holes are also seen which allow for linear bearings to be used to enable linear motion of the housing. The linear motion allows for the side load to be applied to the housing.

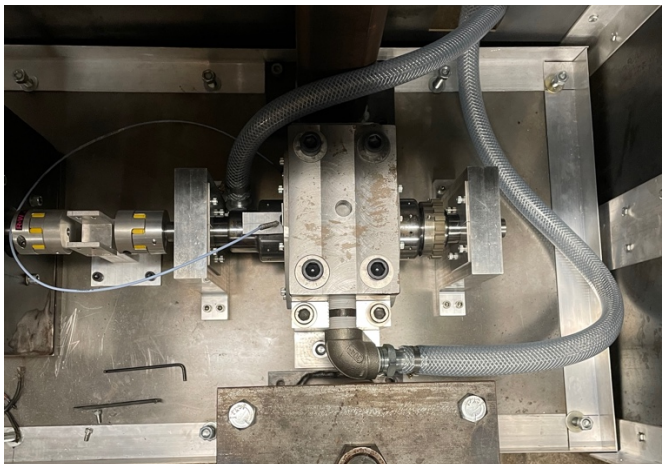

Figure 45: TPB Housing with Oil Connections

The image in Figure *45* shows the installed bearing housing with the oil in connection attached at the side of the bearing housing and the oil out line installed on the housing front, below the shaft. During operation, 2 gpm of oil are delivered to the housing to create the fluid film.

6.7. Base Plate and Oil Retention

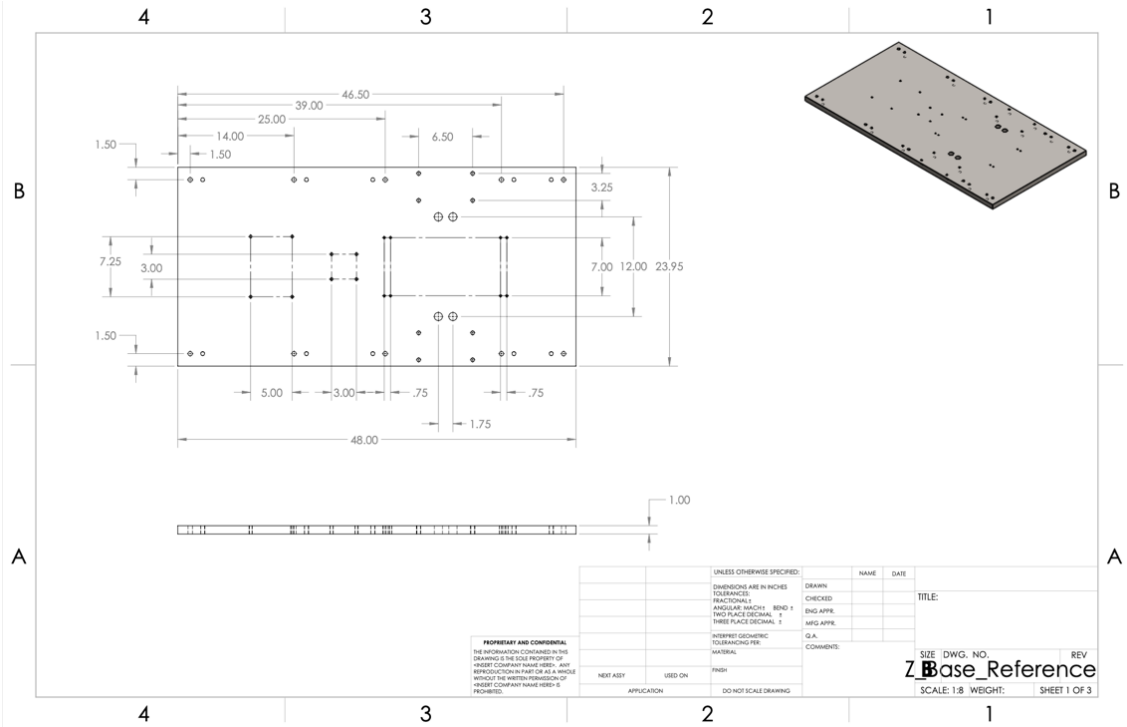

Figure 46 Base Plate Drawing Page 1

The mounting holes for all components were added to the base plate. Also added were 10 sets of 2 holes along the border to allow the test rig to be securely mounted to the ground with anchor bolts. For each pair of holes, one hole is threaded while the other is a through hole for a 1/2” bolt. To level the plate, threaded feet were attached to the threaded holes and adjusted until a level condition was created. To secure the plate, anchor bolts were then inserted and fastened to the unthreaded holes.

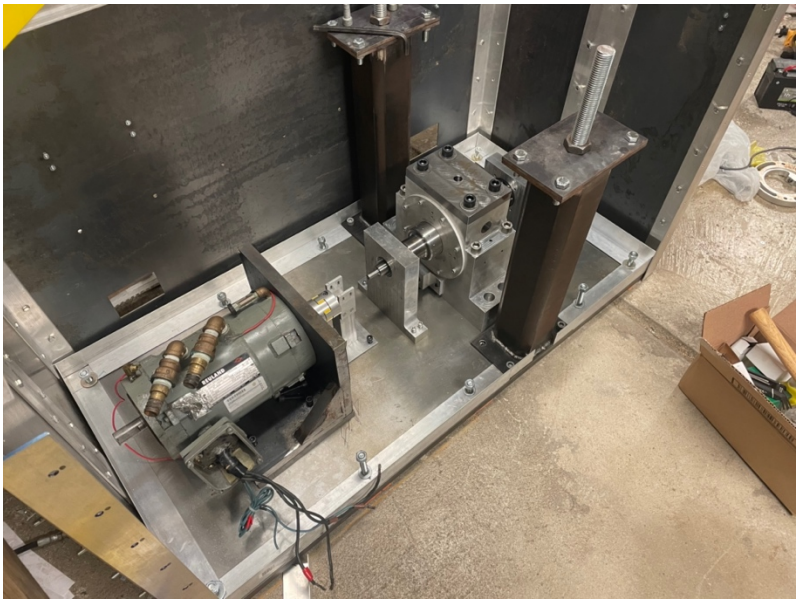

Figure 47: Oil Retention Barrier

To keep any oil that leaks out of the TPB from spilling onto the floor, an oil retainment barrier was created using aluminum angles and the anchor bolts that hold the rig to the floor as shown by Figure *47*. All edges were then sealed with a silicone caulk. Upon initial test runs of the rig, high leakage from the TPB was experienced due to an unintentional high oil flow rate into the bearing. The oil barrier successfully contained all oil and allowed for easy clean up using a small 12 V pump.

6.8. Couplings

The couplings for the test rig were purchased from RW Couplings after using the VFD software to analyze the system and determine the best couplings to meet our requirements. Since a wide range of torque harmonics will be generated by the rig, it was predicted that the couplings would need to provide adequate damping to the system to protect the expensive torque

transducer from high torques and failure. After considering several couplings, the EKL-60-C coupling determined to be a good option. The coupling contains an elastomer insert to provide damping against torsional vibration.

To validate the EKL-60-C coupling as a good choice, the damping was first calculated to be 3.09 lbf-in-s/rad at 60 Hz and 2.47 lbf-in-s/rad at 75 Hz from the information provided in the data sheet (see Appendix 2). This value of damping was then put into the VFD Software model, and the following analysis was run.

6.9. System excitation at the natural frequency

The first simulation that was performed was the analysis of exciting the system with a 20 lbf-in torque at the system natural frequency of 75 Hz. The 20 lbf-in torque was selected because it is above the upper limit of the typical torque amplitudes found in previous test rig simulations. To run the simulation the mechanical model was set up as shown in Figure *48*.

SHAFT

Shaft	Element	Left Node	Right Node	Outer Radius	Inner Radius	Length	Shear Modulus	Density	Damping
#	#	#	#	in	in	in	psi	lb/in^3	lbf.in.s/rad
1	1	1	2	0.5	0	5.5	1.18E+07	0	0
1	2	2	3	1.655	0	4	1.18E+07	0	0
1	3	3	4	0.5	0	6.5	1.18E+07	0	0
1	4	4	5	1.1024	0.23622	2.2835	1.81E+04	0	2.47
1	5	5	6	0.19685	0	3.3465	1.18E+07	0.283	0
1	6	6	7	1.1024	0.23622	2.2835	1.81E+04	0	2.47
1	7	7	8	0.25	0	1	1.18E+07	0.283	0
1	8	8	9	0.565	0	3	1.18E+07	0.283	0
1	9	9	10	1.065	0	1.5	1.18E+07	0.283	0
1	10	10	11	1.565	0	2.79	1.18E+07	0.283	0
1	11	11	12	1.565	0	1.335	1.18E+07	0.283	0
1	12	12	13	1.565	0	1.335	1.18E+07	0.283	0
1	13	13	14	1.565	0	2.54	1.18E+07	0.283	0
1	14	14	15	1.065	0	1.5	1.18E+07	0.283	0
1	15	15	16	0.565	0	2	1.18E+07	0.283	0

ADDED INERTIA

Node	Inertia	Bearing Damping
#	lb.in^2	lbf.in.s/rad
1	2.4577	0
2	2.4577	0
3	2.4577	0
4	2.59439	0
5	0.13669	0
6	0.13669	0
7	0.13669	0
12	0	0.053

Figure 48: VFD Rig Mechanical Model

The user defined torque was set up for a transient analysis with a time-based function of torque as shown in Figure *49*.

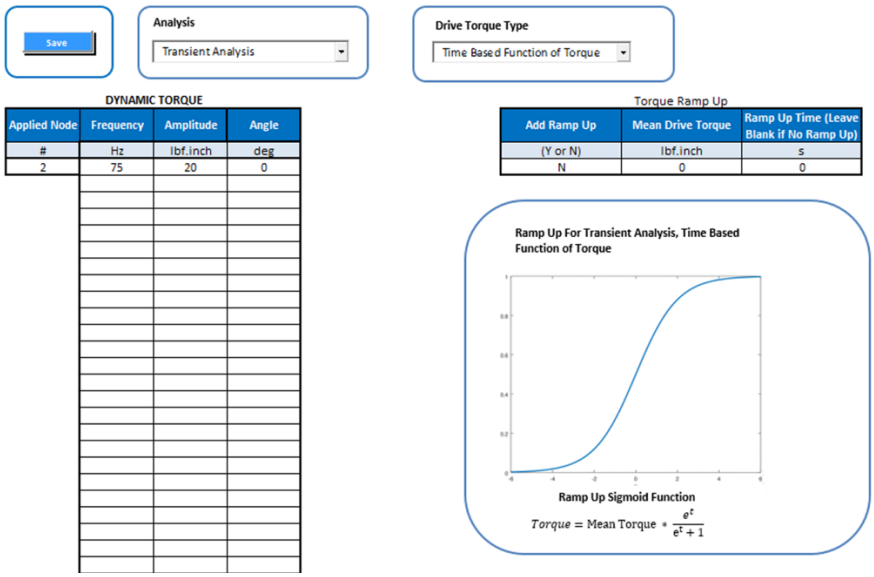

Figure 49: User Defined Torque

The simulation was run for a time of 1 second and the relative position at each end of the torque sensor was output as shown in Figure *50*. The plot shows that the damping provided by the couplings allows for a stable system.

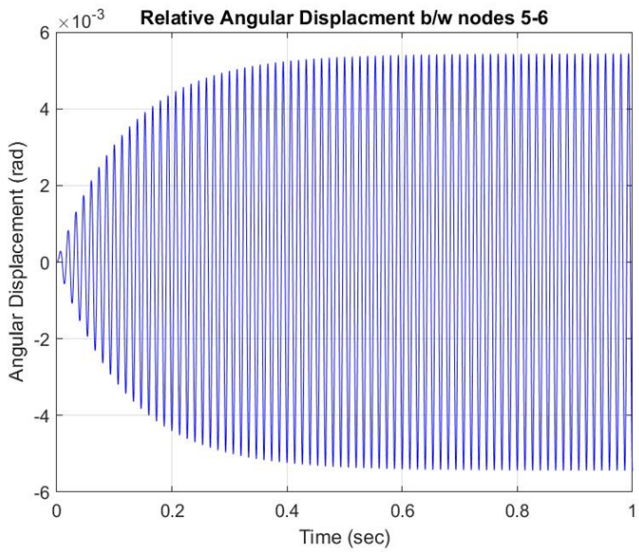

Figure 50: Angular Displacement of Torque Sensor Ends

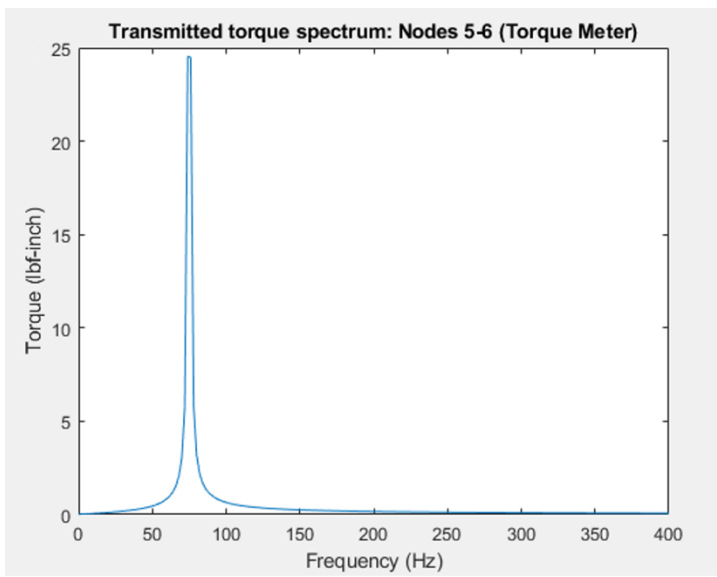

Figure 51: Torque Sensor Torque Response

Furthermore, the calculated torque that the torque transducer experiences is shown to peak at under 25 lbf-in by Figure *51*. The results of this simulation show that the elastomer couplings

provide good damping to safely run the torque sensor while still allowing for measurable torques to be experienced.

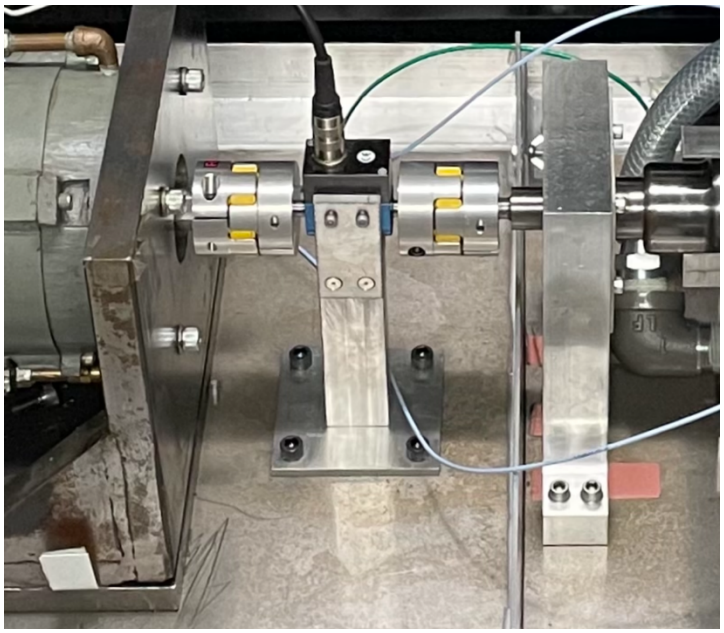

Figure 52: Installed Couplings and Torque Transducer

The installed EKL couplings and torque transducer are shown in Figure *52*. The yellow elastomer insert is placed between the two coupling halves to provide the damping to the system.

6.10. Dynamic Torque Measurement

The main functionality of the test rig is to measure the dynamic torques that are produced by the VFD control of the induction motor.

Figure 53 Interface T4 Torque Sensor

To measure the dynamic torques, the Interface T4 torque transducer (Figure 53) is mounted between the motor and the shaft as shown by Figure 52. The specs of the transducer are,

- 15 Nm capacity
- $\pm$ 10V DC output
- 1kHz bandwidth
- Max speed rated to 10,000 RPM

6.11. Torsional Vibration Sleeve

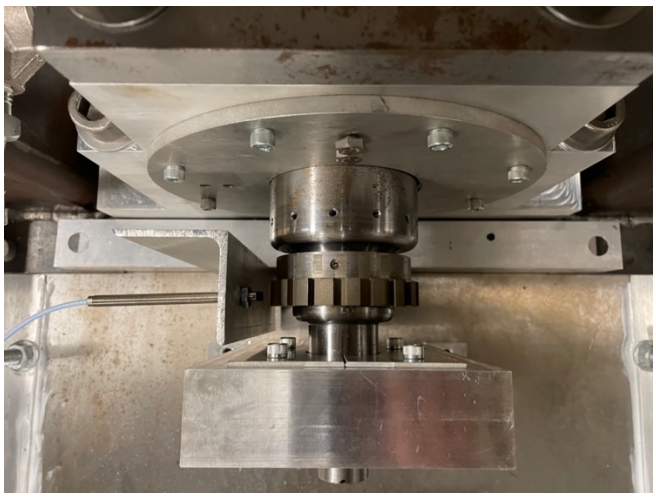

Figure 54 Torsional Vibration Sleeve with Probe

The torsional vibration for the test rig is measured by placing the torsional vibration sleeve on the shaft with a Bently probe above the teeth as shown in Figure *54*. As the shaft rotates, a square wave is generated from the relative position of the teeth and the probe. When the shaft is rotating at a constant angular velocity with no torsional vibration, the duty cycle of each square wave remains constant. However, when torsional vibration is present, the vibration creates a cyclical slowing down and speeding up of the shaft which modulates the square wave. When the shaft speeds up, the resulting pulse of the spare wave is shorter while the pulse is longer when the shaft slows down. To get the measurement of the torsional vibration amplitude and frequency from this modulated wave, a Bessel analysis is performed as described in 3.2.

6.11.1. Optimal Number of Teeth – Ideal Conditions

A discussion on the effect which the number of teeth has on the accuracy of the torsional vibration measurement was unable to be found in literature. To get a better insight into the appropriate number of teeth for the test rig, a simulation was created in MATLAB. The first function creates the modulated square wave of a shaft based on the number of teeth, shaft speed, torsional vibration amplitude, and torsional vibration frequency. Another script then performs the FFT of the square wave and extracts the peak locations of the main bands and side bands. This study was run with the assumption that the sleeve was perfectly machined.

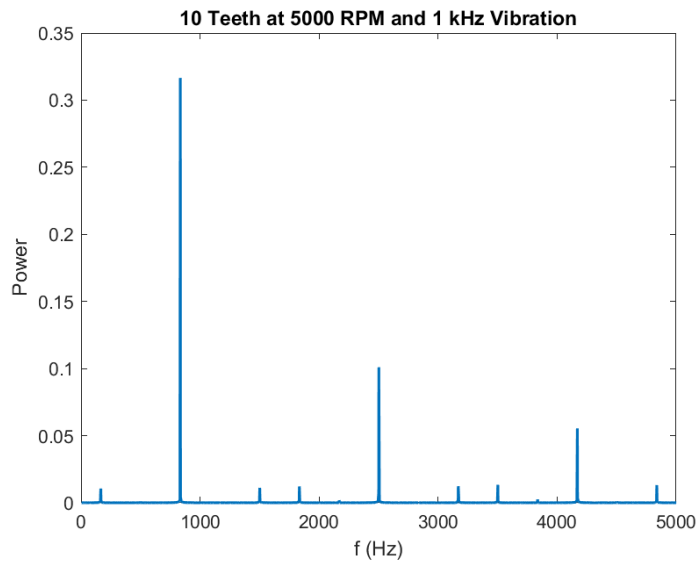

Figure 55 10 Teeth at 5000 RPM and 1 kHz Vibration

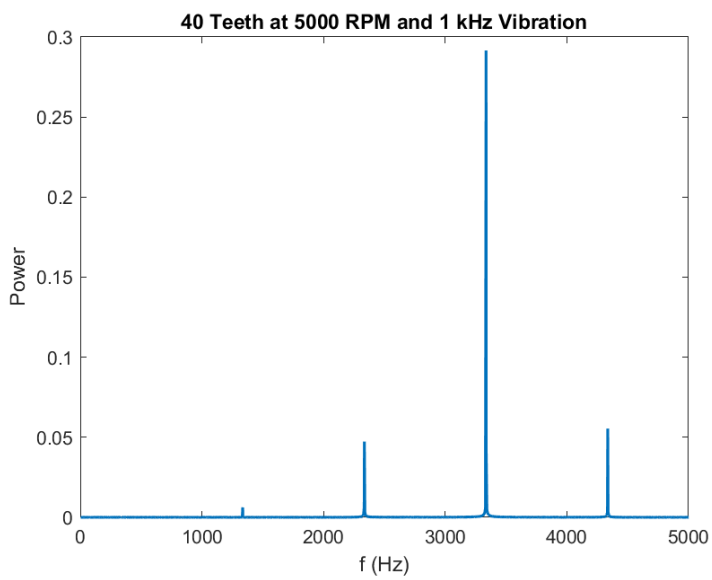

Figure 56 40 Teeth at 5000 RPM and 1 kHz Vibration

A main limiting factor for the minimum number of teeth is due to the square wave pulse frequency and the maximum torsional vibration frequency to be measured. The number of teeth

must result in a pulse frequency that is high enough that the left side band still appears in the FFT. Figure *55* illustrates the problem that having two low of teeth can have. In this case, a shaft is rotating at 5000 RPM with 10 teeth. This creates a main band pulse frequency at 833 Hz. Upon initial inspection, the torsional vibration sideband appears to occur at 1500 Hz. However, this would lead to a calculated vibration frequency of,

$$f_{vib} = 1500\ Hz - 833\ Hz = 667\ Hz$$

Instead, the second side band must be used to get an accurate calculation of the vibration frequency of 1000 Hz.

Table 2 MATLAB Simulation Data

Number of Teeth	Shaft Speed (RPM)	Torsional Vibration Amplitude (Radians)	Torsional Vibration Frequency (Hz)	Calculated Vibration Amplitude (Radians)	Calculated Vibration Frequency (Hz)	Error
20	5000	5.00E-03	200	4.97E-03	200	0.0066
30	5000	5.00E-03	200	4.97E-03	200	0.0065
40	5000	5.00E-03	200	4.97E-03	200	0.0062
40	5000	5.00E-02	200	4.99E-02	200	0.0023
40	5000	5.00E-04	200	5.22E-04	200	0.0433
30	5000	5.00E-04	200	5.22E-04	200	0.0432
30	5000	5.00E-02	200	5.06E-02	200	0.0122

A wide range of conditions were tested using the MATLAB code. Table *2* shows the calculated error in measuring a torsional vibration at 200 Hz, or the upper bound of where most destructive vibrations typically occur. While the 40 teeth sleeve proved to result in the lowest error, a 20 teeth vibration sleeve also proved to maintain acceptably low error values as well. With a lower number of teeth, a lower sampling rate for the probe is required to measure torsional vibration.

6.11.2. Torsional Vibration Sampling Rate

The torsional vibration measurement requires the highest sampling rate of any measurement on the test rig. This is because the Bently probe above the vibration sleeve must be able to

accurately generate the square wave of the passing teeth with the presence of small torsional vibration signal modulation. To estimate the required sampling rate needed for accurate measurements, the previously discussed MATLAB script was run with a vibration amplitude of 5e-3 radians at 1000 Hz. The shaft was simulated to be running at the max speed of 10,000 RPM and the FFT of the square signal was taken.

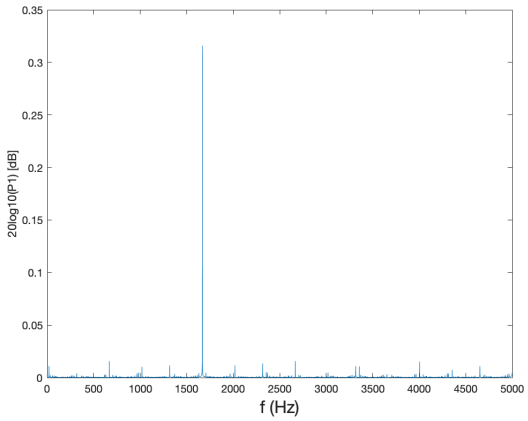

Figure 57: Torsional Vibration FFT - 24kHz Sampling Rate

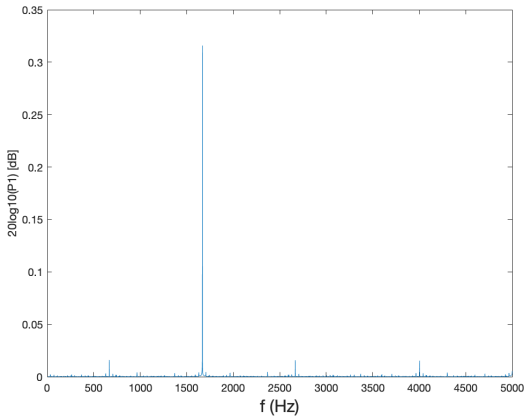

Figure 58: Torsional Vibration FFT - 48kHz Sampling Rate

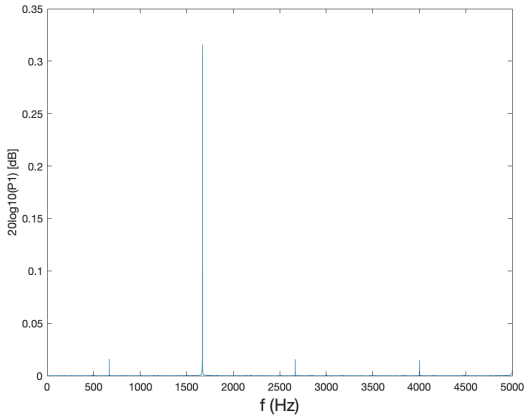

Figure 59: Torsional Vibration FFT - 240kHz Sampling Rate

Table 3: Torsional Vibration Sampling Rate and Error

Sampling Rate	Measured Vibration Amplitude	Meaured Vibration Frequency	Error (%)
24 kHz	0.004962	1000	0.76
48 kHz	0.004996	1000	0.08
240 kHz	0.004997	1000	0.06

The results shown in Figure *57*, Figure *58*, and Figure *59* show that by increasing the sampling rate of the torsional vibration probe, the presence of unwanted side bands decreases. This allows for an easier determination of which sidebands are indicative of torsional vibrations within the system. From the data in Table *3*, the error remains low for all 3 sampling frequencies, however, 48 kHz shows the greatest improvement and can easily be achieved with affordable DAQ systems.

6.12. Side Load Applicator

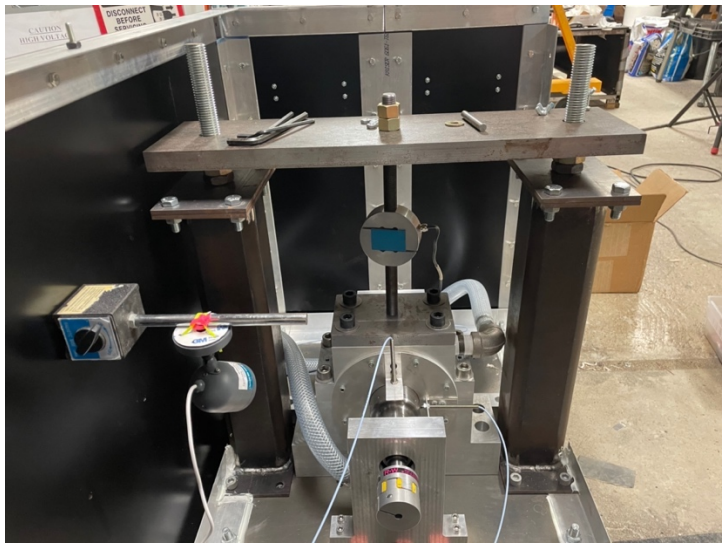

Figure 60: Side Load Applicator

The side load applicator can be used to increase the load that the tilting pad bearing experiences. This is achieved by inducing a large upwards force on the tilting pad bearing through the jack bolts in Figure *60*. The tilting pad bearing housing is held in place via dowel linear bearings to allow for vertical motion of the housing. This allows the force to be transferred from the jack bolts and mounting frame to the tilting pad bearing housing via a load cell to allow the applied force to be accurately controlled. The design allows for forces up to 10,000 N.

The purpose of the side load applicator is to apply a load and drag torque to the shaft by the TPB.

6.13. Data Acquisition System

To meet the necessary sampling rate of all the test rig probes, two DAQ cards are used for the VFD Test rig. The test rig currently uses a 250kHz USB6221 and a 20kHz USB6001 DAQ. The following measurements are made by each DAQ,

USB6221

- Torque Transducer – 150kHz (Ch 0)
- Torsional Vibration Bently Probe – 150kHz (Ch 1)

USB6001

- Once Around Bently Probe – 5 kHz (Ch 0)
- X Bently Probe – 5kHz (Ch1)
- Y Bently Probe – 5kHz (Ch2)
- Load Cell – 5kHz (Ch3)

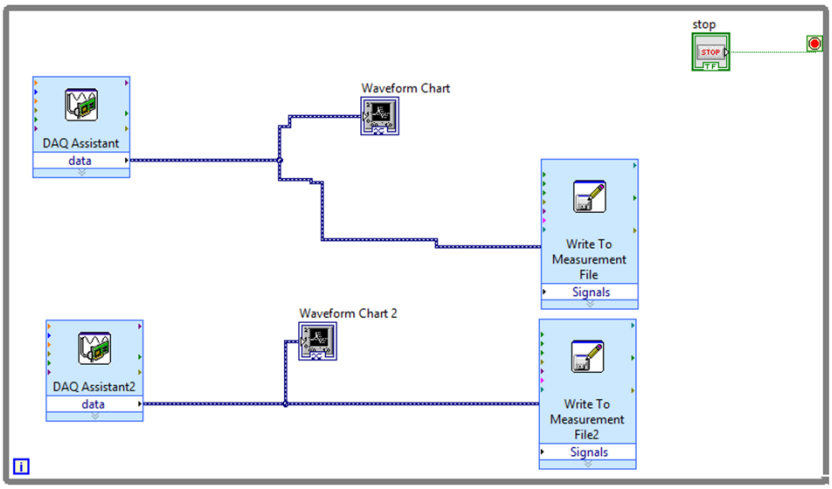

Figure 61: LabView Code

All data is recorded using a LabView VI as shown by Figure *61*. The data is collected at the specified sampling rates and output into one .lvm file per DAQ. The files are placed within a folder for as specified by the VI.

While the test rig is running, the matlab script RealTimeData.m is run to process the measured data in real time and the information is displayed on a simple GUI.

6.13.1. RPM Measurement

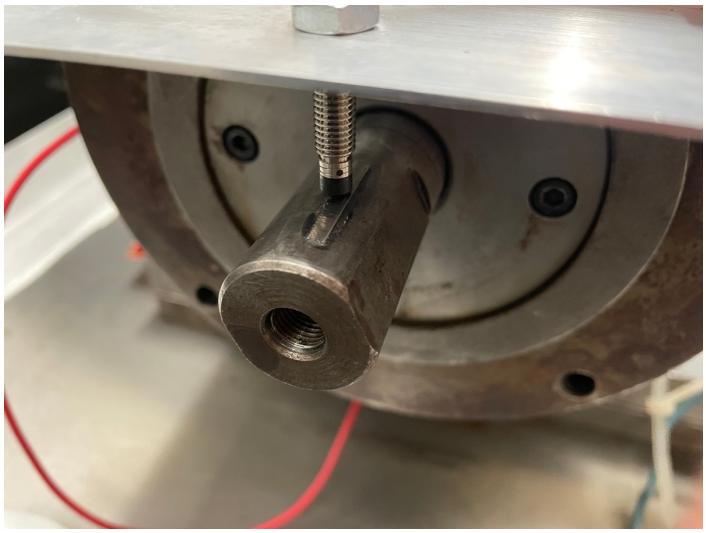

Figure 62: Once Around

The RPM is calculated by first having the user specify a voltage threshold in MATLAB that indicates the voltage output by the Bently probe as it passes over the once around in Figure *62*. The voltage data is then converted into binary with 1's indicating when once around is below the probe. The average time between pulses experienced in 1 second of data is then converted into the RPM output.

6.13.2. Torque Frequency Spectrum Analysis

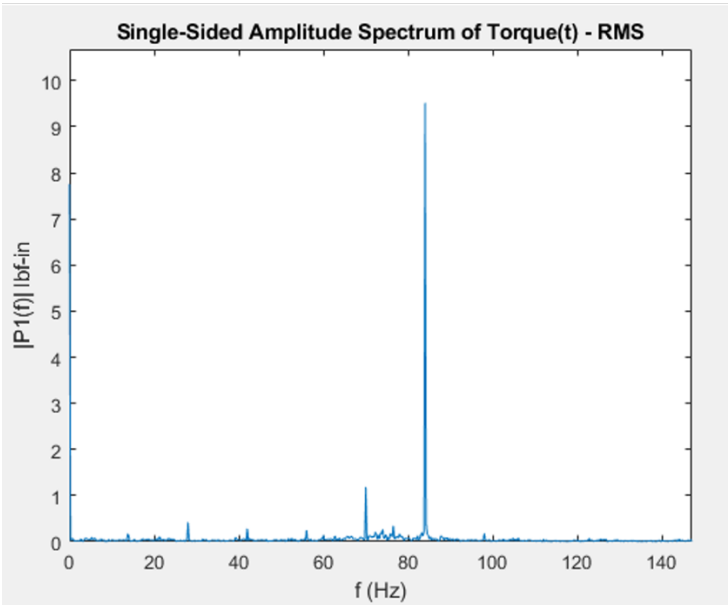

Figure 63: Harmonic Torque MATLAB Analysis

The harmonic torque spectrum recorded from the torque transducer can be analyzed using an FFT as shown in Figure 60. The MATLAB script, torqueAnalysis.m, was written to allow for the torque spectrum for the test rig data to be easily calculated. To use the code, the user specifies the time interval of the recorded data to analyze along with the sampling rate. MATLAB then generates the associated FFT.

6.13.3. Lateral Vibration Measurement

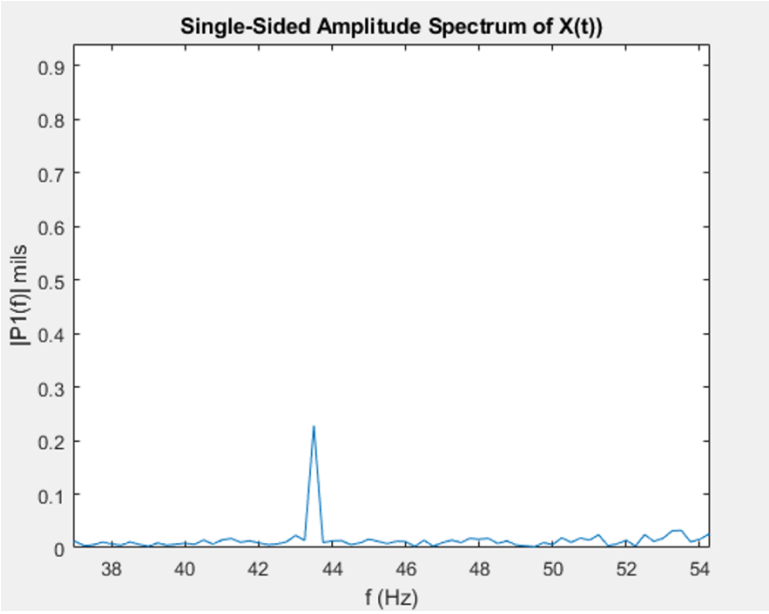

Figure 64: Lateral Vibration in the X Direction

The lateral vibration of the shaft relative to the tilting pad bearing can be determined in both the X and Y direction using the MATLAB script, XandYAnalysis.m as shown in Figure 61. Similar to the torque analysis script, the user specifies the time interval to perform the analysis and the code generates the plot. For the case of the VFD line frequency of 44 Hz, the vibration amplitude of 0.22 mils at 43.5 Hz is found from Figure 61. The frequency is slightly offset from the 44 Hz frequency due to the slip of the motor shaft. The peak lines up with the rotational frequency of the shaft as calculated by the once around.

6.13.4. Waterfall Plots

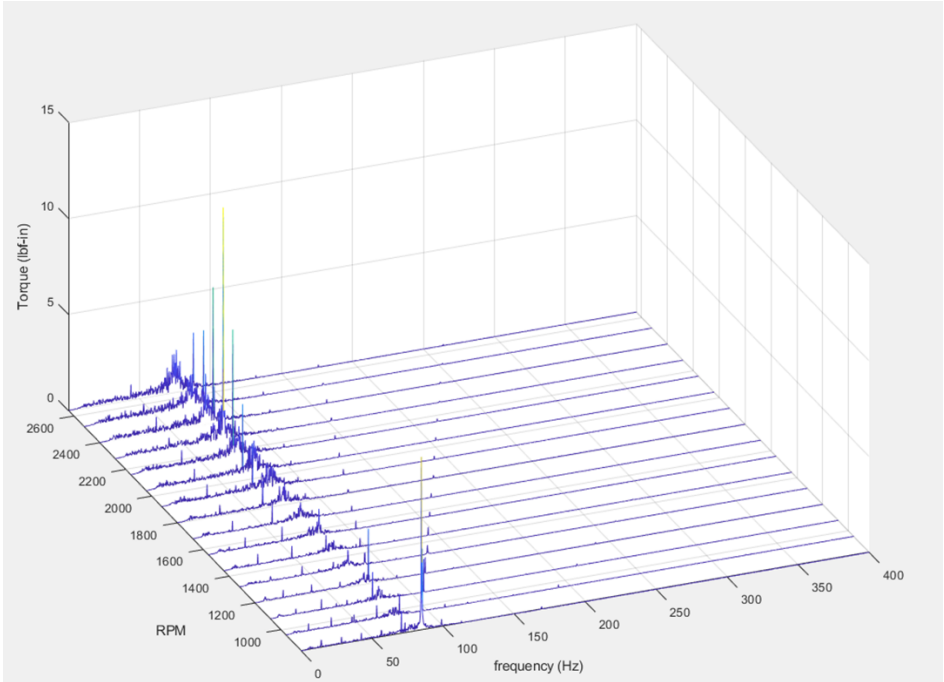

Figure 65: Waterfall Plot 7kHz PWM Switching

Name	Date modified	Type	Size
6221Data_001	5/28/2021 10:23 AM	LVM File	2,338 KB
6221Data_002	5/28/2021 10:23 AM	LVM File	2,339 KB
6221Data_003	5/28/2021 10:23 AM	LVM File	2,337 KB
6221Data_004	5/28/2021 10:23 AM	LVM File	2,341 KB
6221Data_005	5/28/2021 10:23 AM	LVM File	2,321 KB
6221Data_006	5/28/2021 10:23 AM	LVM File	2,321 KB
6221Data_007	5/28/2021 10:23 AM	LVM File	2,321 KB
6221Data_008	5/28/2021 10:23 AM	LVM File	2,321 KB
6221Data_009	5/28/2021 10:23 AM	LVM File	2,321 KB
6221Data_010	5/28/2021 10:23 AM	LVM File	2,321 KB
6221Data_011	5/28/2021 10:23 AM	LVM File	2,321 KB
6221Data_012	5/28/2021 10:23 AM	LVM File	2,320 KB
6221Data_013	5/28/2021 10:24 AM	LVM File	2,320 KB
6221Data_014	5/28/2021 10:24 AM	LVM File	2,320 KB
6221Data_015	5/28/2021 10:24 AM	LVM File	2,320 KB

Figure 66: LabView Data Files

The ability to perform waterfall plots from the test rig similar to the one shown in Figure 65 is very important in analyzing the harmonic torque spectrum. To perform a waterfall analysis with the test rig, the user must collect several seconds of data for each running speed of the

motor. The LabView code makes it easy to collect data in a way similar to Figure 66. In this case, every data file is one second of data and every 4 files are a different running speed. For example, files “001”, “002”, “003”, and “004” are for a running speed of 14Hz (840 RPM) while files “005”, “006”, “007”, and “008” are for 16Hz (960 RPM) etc.

To make the processing of the data into a waterfall plot simple, a MATLAB script fftwaterfall.m was created. The user must specify the frequency range of the data in Hz, the number of files per speed, the sampling rate, and the folder that the files are located in. Once run, the desired waterfall plot is created.

6.13.5. Shaft Alignment

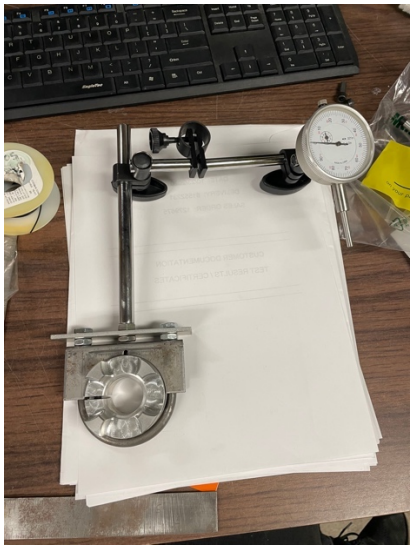

Figure 67: Dial Indicator and Clamp

Figure 68: Dial Indicators on Rig

The shaft alignment process was performed using the reverse dial indicator method shown in [15]. The shaft alignment was done by treating the bearing housings and main shaft as the fixed reference and the motor as the movable reference. The first step in the process was to set up the appropriate reference. This was set by looking at the main shaft from the perspective of the motor to determine the 3, 6, 9, and 12 o'clock positions.

Two of the dial indicator mounts were made as shown in Figure 67 and they were installed onto the couplings of the rig with the dial indicators touching opposite sides of the shafts as shown in Figure 68.

To simplify the procedure, the equations outlined in [15] were put into a MATLAB code to allow for the dial indicator measurements at all 4 positions to be input. The code then outputs the necessary shims to be placed under the motor feet and the necessary distance that the motor must be shifted parallel to the base plate.

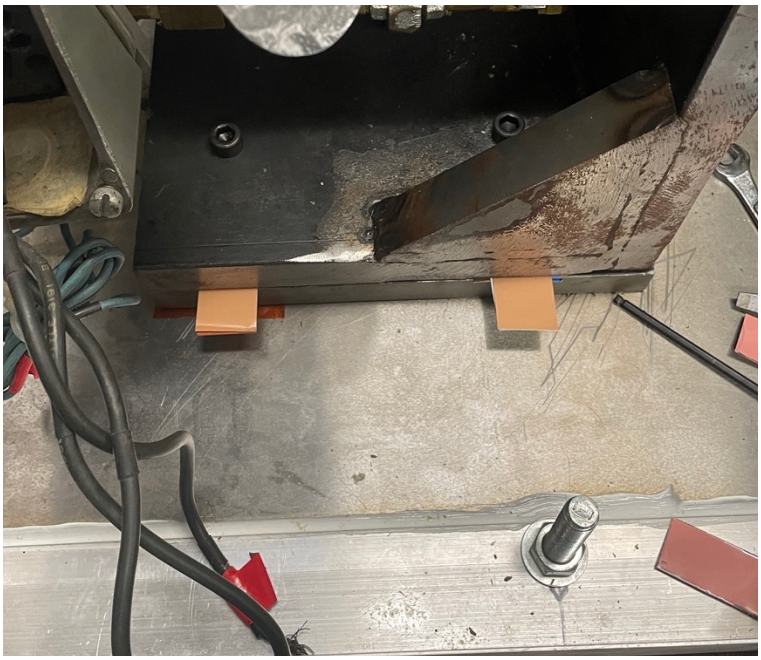

Figure 69: Shims Used for Shaft Alignment

To adjust the vertical height of the motor as needed, aluminum shims were used on the motor base as shown by Figure 69. To move the motor parallel to the plate, a rubber mallet was used to slightly shift the motor base plate.

The process was repeated until there were no further improvements between trials. This was around the point where the necessary shims and shifting of the motor base was around 5 to 10 mils.

6.14. Completed Test Rig

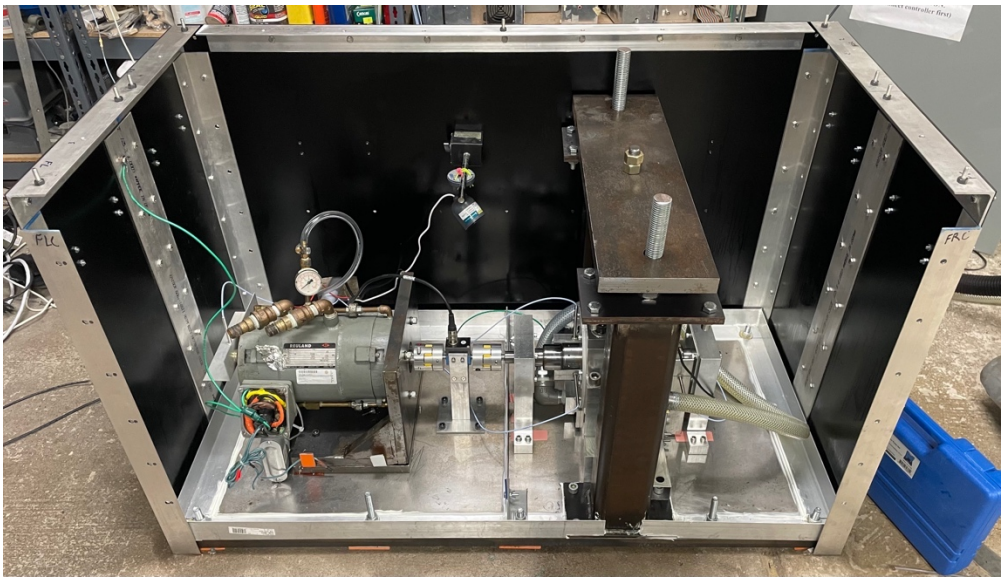

Figure 70: Completed Test Rig

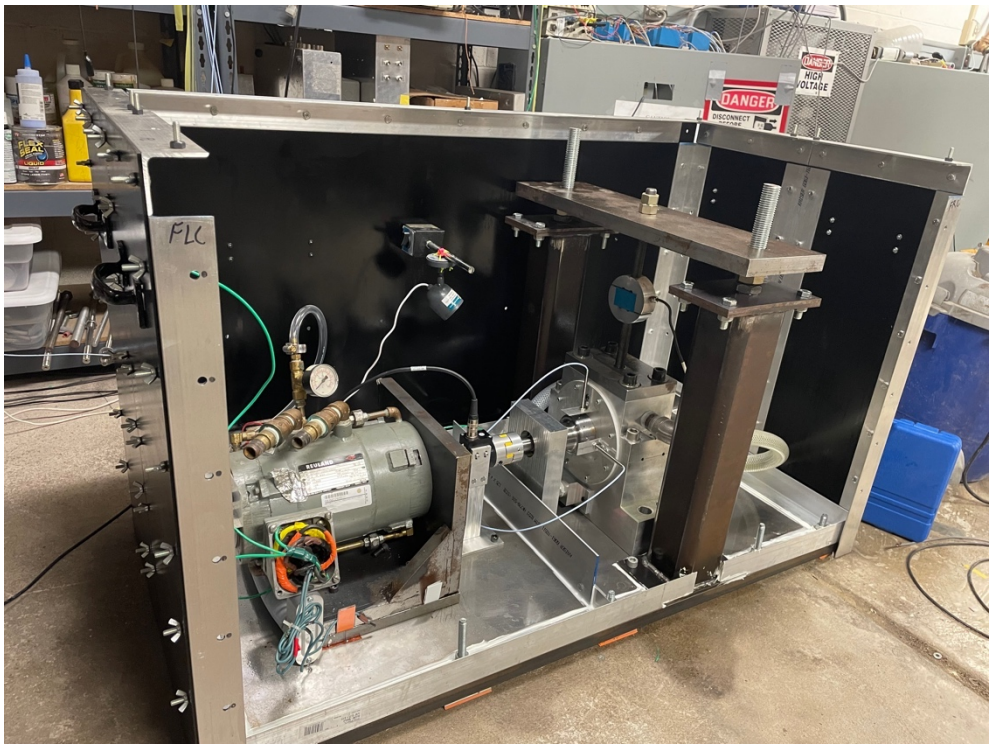

Figure 71: Completed Test Rig Left Side Angle

Figure 72: Completed Test Rig Right Side Angle

The completed test rig with all the previously discussed components installed is shown in Figure *70*, Figure *71*, and Figure *72*.

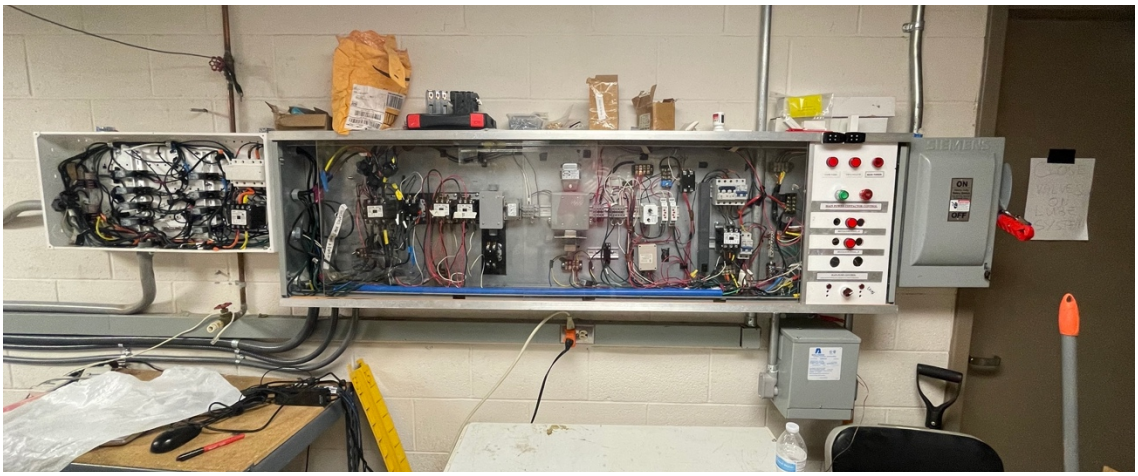

Figure 73: Test Rig Circuit Breaker and Electrical System

Figure 74: Test Rig VFD with Line Filter and Ferrites

Figure *73* and Figure *74* show the complete electrical system of the test rig. In Figure *73*, the main circuit breaker is shown which feeds power to the VFD and the oil system for the TPB. The panel allows for the timing of all systems to ensure that the motor is not run without oil being supplied. Similarly, the timing also ensures that scavenger pumps connected to the oil out flange on the TPB housing turn off last to keep from large amounts of oil from leaking out of the bearing seal plates and flooding the test rig base plate.

Figure *74* shows the electrical box which houses the VFD, line filter, and blue ferrites shown in the bottom left. The line filter ensures that no electrical noise is fed back into the main building power while the ferrites surround the wires running from the VFD to the motor to eliminate EMI from interfering with any sensors.

6.15. Test Rig Results

6.15.1. System Natural Frequency

The comparison between the test rig natural frequency and the predicted natural frequency from the VFD software is performed by first modeling the system in the VFD software using all the dimensions and physical properties shown in Figure *48*.

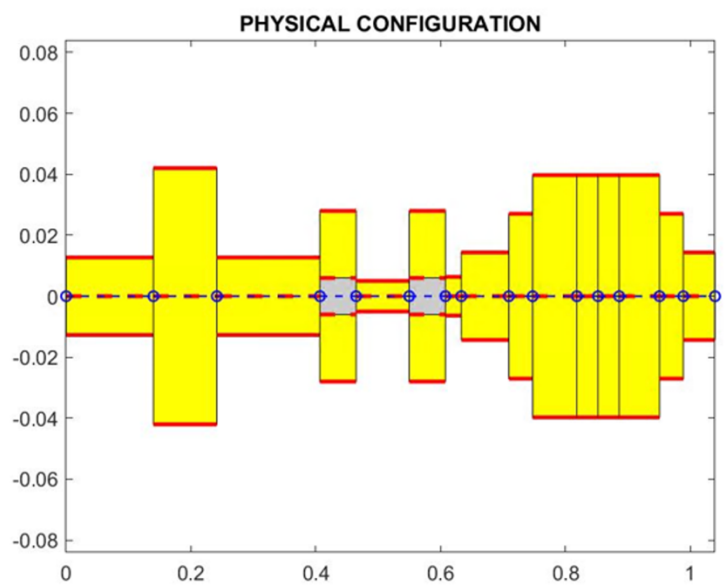

Figure 75: Physical Configuration of the Test Rig

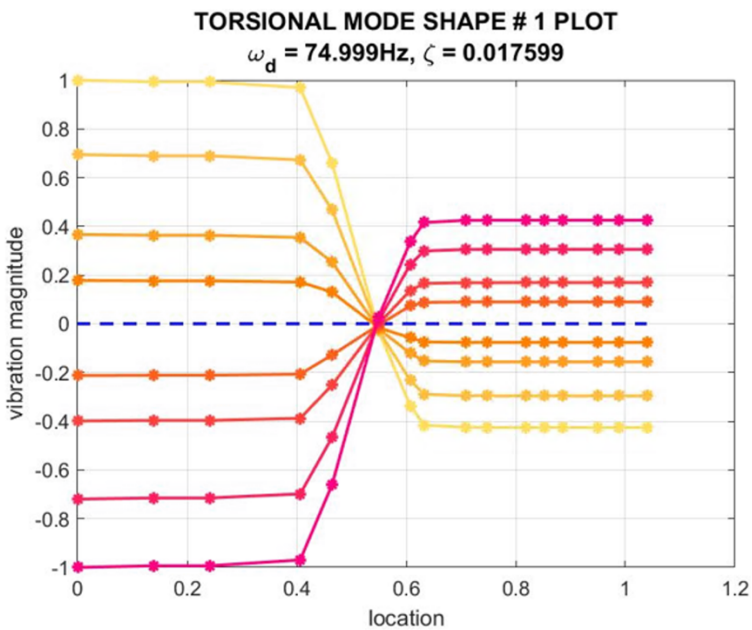

Figure 76: Natural Frequencies and Mode Shapes

The software solves the system model and returns the physical configuration and mode shape plots shown in Figure *75* and Figure *76*. The mode shape plot indicates that the expected torsional natural frequency should exists at 74.99 Hz.

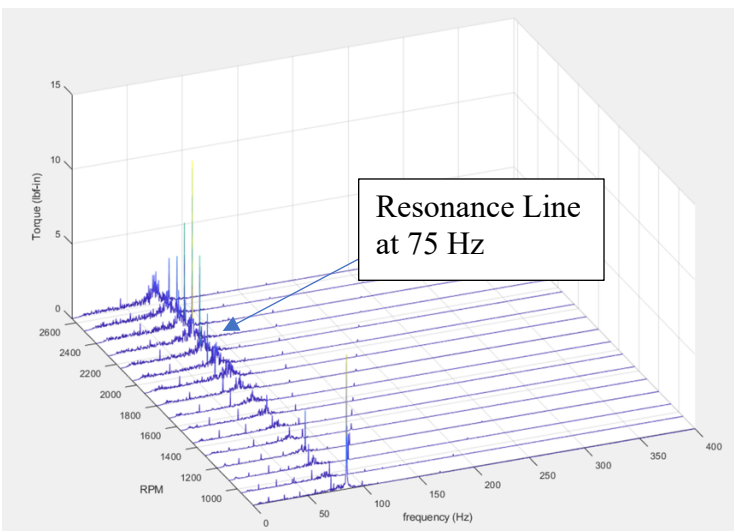

Figure 77: Waterfall Plot 7kHz PWM with 550lbs Side Load

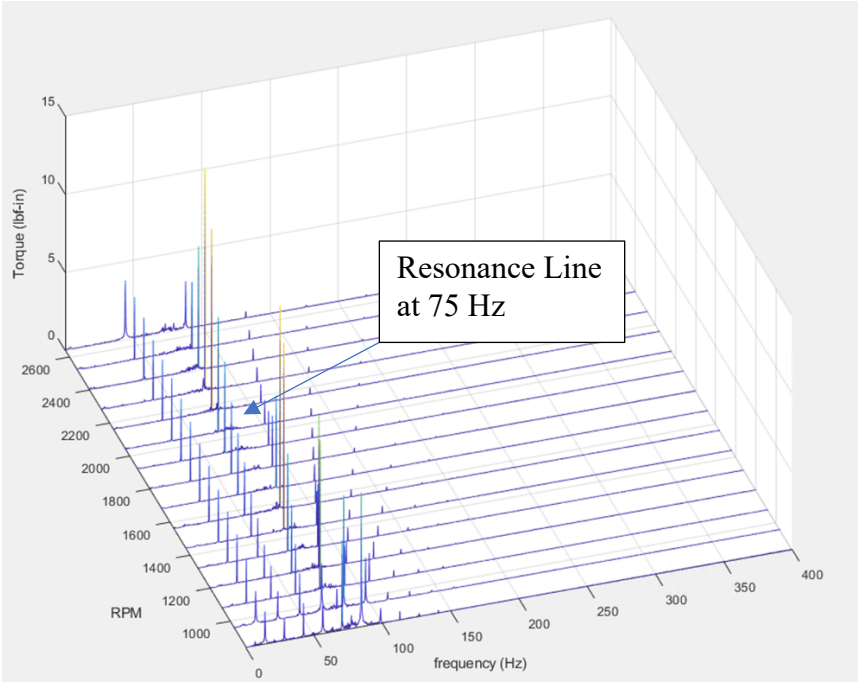

Figure 78: Waterfall Plot of 5kHz PWM with 550lbs Side Load

The predicted natural frequency of the system is experimentally validated using the waterfall plots in Figure *77* and Figure *78*. The two waterfall plots show the torque response of the motor running with a PWM frequency of 7kHz and 5kHz. Both plots show a constant frequency ridge at 75 Hz. When torque frequencies interact with the natural frequency, large torque amplitudes are experienced by the torque sensor, further indicating the presence of resonance at the natural frequency.

6.15.2. Measurement of Torque Harmonics

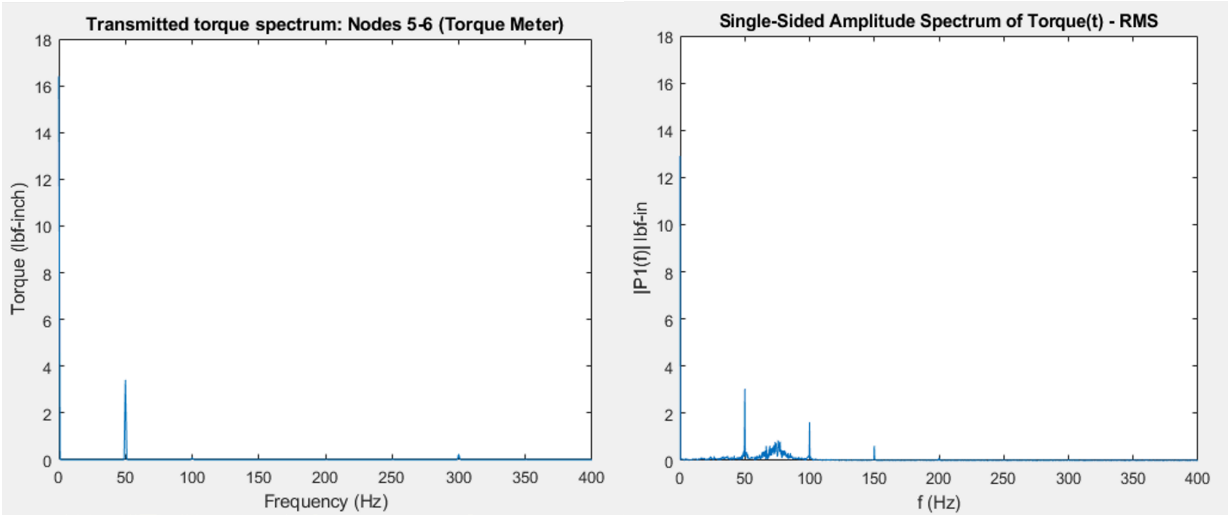

Figure 79: VFD Software Prediction (Left) Versus Test Rig (Right) for 10 kHz PWM at 3000 RPM

Table 4: Comparison of Software to Test Rig Data

	VFD Software	Test Rig	Error
Mean Torque (lbf.in)	16.4	12.9	21%
50 Hz Torque (lbf.in)	3.4	3.0	13%

$$f_T = |m.f_{PWM} \pm n.f_e|$$

THEORETICAL STEADY STATE TORQUE (SONG) HARMONICS FOR OPEN-LOOP V/HZ CONTROL		
Maximum m & n for Calculaton		
Max m		100
Max n		500
Possible Steady State Torque Harmonics		
m	n	Freq (Hz)
1	99	50
2	198	100
4	402	100
3	297	150
3	303	150
2	204	200

Figure 80: Potential Song Frequencies from VFD Software

A comparison between the software prediction and the test rig data is shown in Figure 79 with the error of the mean torque and 50 Hz torque shown in Table 4. This case is for a PWM switching frequency of 10 kHz and a running speed of 50 Hz (3000 RPM). The test rig results show a peak at 50 Hz which is comparable to the software prediction. However, the test rig also experiences other torque harmonics at 2x and 3x the line frequency. For the running speed of 3000 RPM and a PWM frequency of 10 kHz, the software shows that the experienced frequencies of 50 Hz 100 Hz and 150 Hz are potential torsional excitations as outlined by Song's formulas.

6.15.3. Waterfall Plots from the Software and Test Rig

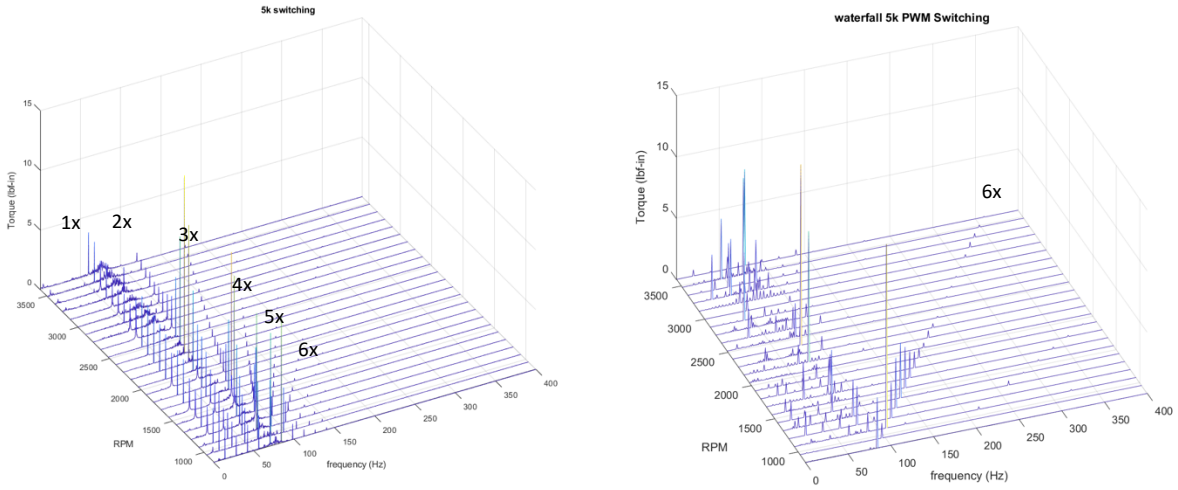

Figure 81: Waterfall 5kHz PWM Switching for Test Rig (Left) and Software (Right)

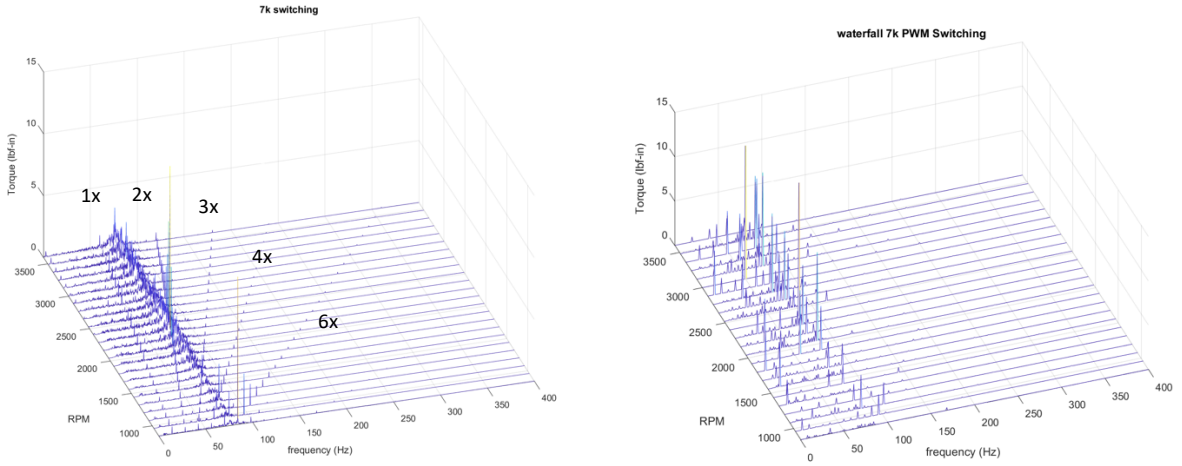

Figure 82: Waterfall 7kHz PWM Switching for Test Rig (Left) and Software (Right)

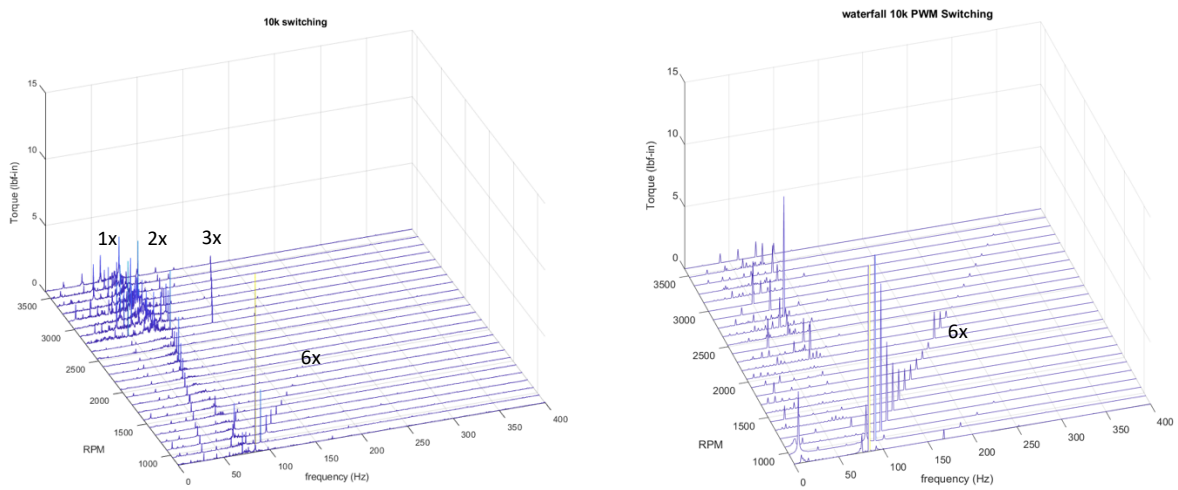

Figure 83: Waterfall 10kHz PWM Switching for Test Rig (Left) and Software (Right)

Waterfall plots are shown for both the test rig data and the VFD Software in Figure 81, Figure 82, and Figure 83. These plots are for PWM switching frequencies of 5kHz, 7kHz and 10kHz respectively. The test rig data for the 5kHz PWM switching frequency shows the largest amplitudes of torque harmonics at integer multiples of the running speed. Since the Reuland motor is a 2-pole machine this is the same frequency as the line frequency. The integer harmonics for the 7kHz and 10kHz PWM switching frequency are smaller yet still clearly present in the test rig data.

The VFD software shows a wider spectrum of torsional frequencies present in the test rig due to VFD control. An integer harmonic, however, is present at the baseband frequency of 6 times the line frequency as outlined by Song's formulas in [1]. This 6x frequency is most visible in both the 5kHz PWM waterfall plot and the 10kHz PWM waterfall plot. A strong 6x torque harmonic is also present in the experimental data from the test rig at 10kHz.

Initial guesses for the cause of the unexpected torque harmonics were that they were related to sensor noise, however, the harmonics clearly interact with the mechanical torsional natural frequency of the system, providing more evidence that these torques are truly present in the rig.

6.15.4. Torsional Vibration Measurements

The measurable torsional vibration amplitude will be greatest when the test rig has a torque harmonic occurring at the torsional natural frequency of the system. Because of the presence of integer harmonics in the test rig, this is achieved by setting the rotational speed to 37.5 Hz (2250 RPM). At this speed, the 2x torsional vibration will cause resonance.

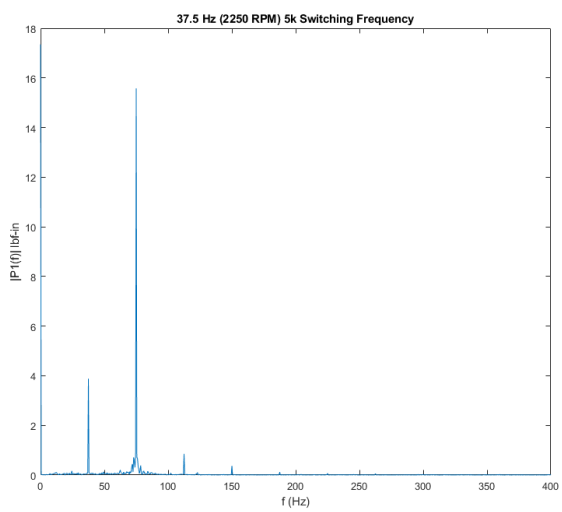

Figure 84: Test Rig Measured Torque at 2250 RPM 5kHz Switching Frequency

The measured torque spectrum at this speed is shown in Figure *84*. The largest torque amplitude is 15.58 lbf-in at the resonant frequency of 75 Hz.

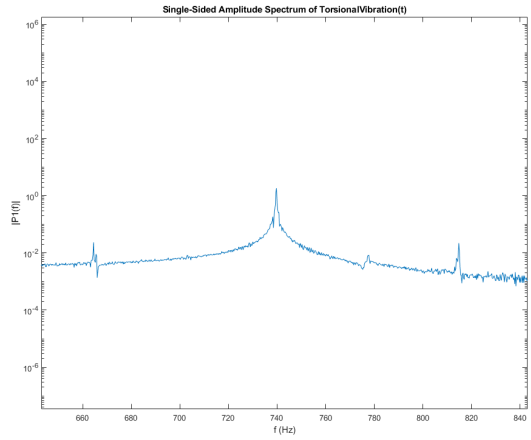

Figure 85: Torsional Vibration Bently Probe FFT

The FFT of the data from the torsional vibration sleeve is plotted and shown in Figure *85*. The FFT shows a main band at 739.8 Hz which is 20 times the rotational frequency of the shaft of 36.99 Hz. The side bands appear at 814.8Hz and 664.5 Hz with amplitudes of 0.0221 and 0.02339 respectively.

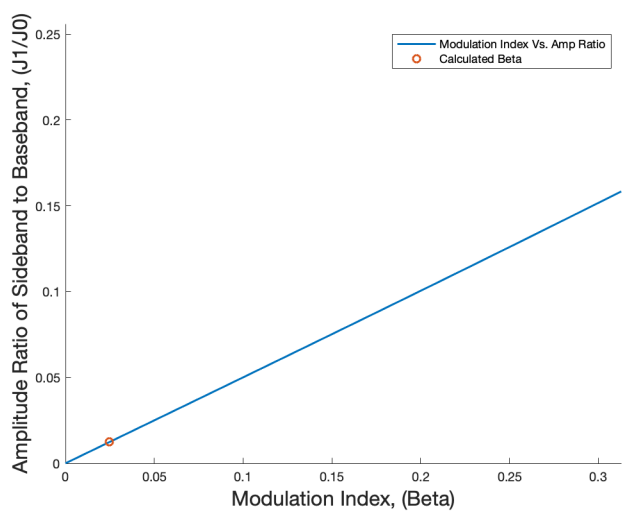

Figure 86: Beta Value for Bessel Function Analysis

The amplitude ratio of the average sideband amplitude to the main band amplitude is put into a MATLAB script which outputs the beta value plot and torsional vibration amplitude based on the number of teeth of the vibration sleeve. The measured torsional vibration was determined to have an amplitude of 1.2e-3 radians with a vibration frequency of 75 Hz.

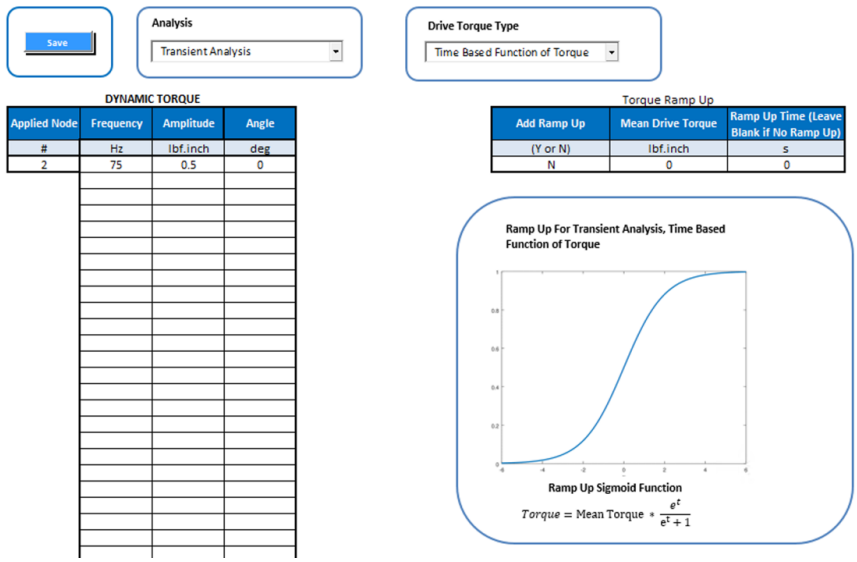

Figure 87: Time Based Function of Torque

Using several iterations of software simulations, the necessary excitation torque by the motor at 75 Hz to generate the measured 15.58 lbf-in torque at the torque transducer came out to be 0.5 lbf-in. The new transient analysis time-based function of torque option was then used to set the drive torque at 0.5 lbf-in at 75 Hz as shown by Figure *87*.

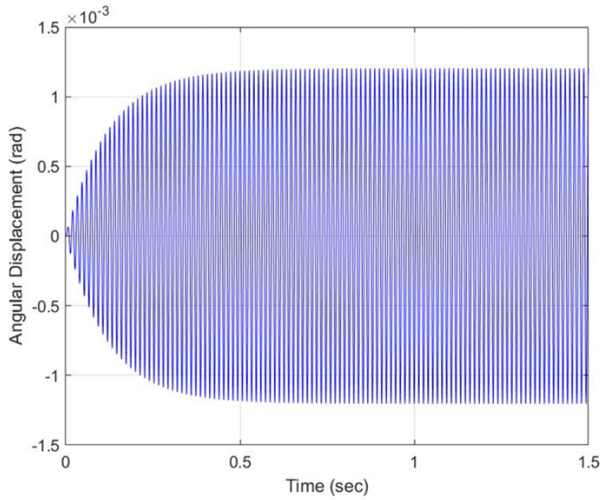

Figure 88: Software Predicted Torsional Vibration Amplitude

The resulting torsional vibration amplitude from the VFD Software is shown in Figure *88* with an amplitude of 1.204e-3 radians. This prediction aligns with the experimentally measured value from the torsional vibration sleeve data.

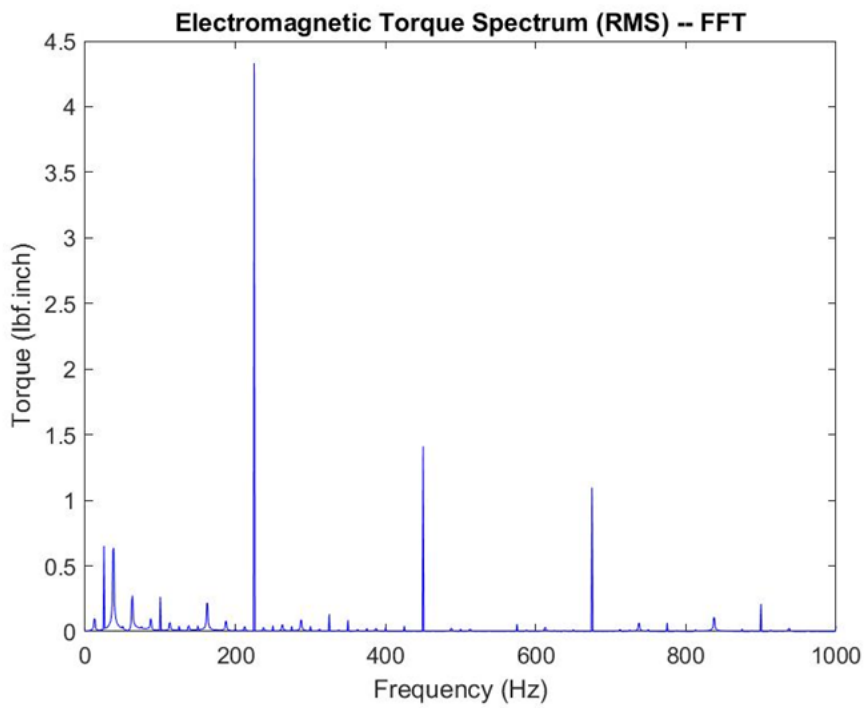

Figure 89: Predicted Electromagnetic Torque Spectrum 2250 RPM 5kHz PWM Switching

Table 5: Predicted Torque Spectrum Data

ACTUAL TORQUE HARMONICS IN TORQUE SIGNAL EXTRACTED FROM THE FFT	
Freq (Hz)	Torque Amplitude (lbf.inch)
225	4.33
450	1.41
675	1.1
25	0.65
38	0.64
63	0.27
100	0.26
162	0.22
900	0.21
325	0.13
838	0.11
12	0.1
87	0.1
288	0.09
350	0.09
187	0.08
113	0.07
775	0.07
737	0.06
575	0.06
263	0.05

The resonant frequency for the torsional vibration test was achieved by running the test rig at 2250 RPM (37.5 Hz). This allowed the 2x integer harmonic occur at the torsional natural frequency of 75 hz. When simulating the test rig's full electrical and mechanical system, no predicted torque harmonics occur at the 2x frequency of 75 Hz as shown by Figure *89* and Table *5*.

7. CONCLUSIONS AND FUTURE WORK

7.1. Conclusions

7.1.1. Strain-Based Life Prediction Method

The strain-based life prediction method is derived from the Coffin-Manson equation that utilizes the true stress and strain of the material at fracture along with the elastic and plastic strain constants. This equation is then converted into a form similar to the stress-based life prediction method in order to perform the life prediction from a S-N curve. Furthermore, the strain based life prediction method treats the life derating factors as functions of life instead of constants to produce even more accurate predictions. The strain-based life prediction method is considered to be an improvement of the stress-based method that is occasionally over conservative.

The strain-based life prediction method was added to the VFD Software package using MATLAB and an Excel UI. The results were compared to a manual calculation of the strain life method in Example 1. In another example, the strain life method was compared to a stress-based life prediction on a given system. This example illustrated the overconservativeness of the stress life method on certain elements while still identifying failure of other elements using both methods.

7.1.2. Transient Analysis with Time-Based Function of Torque

The new transient analysis user defined torque method allows for users to define the torque as a series of frequencies, amplitudes, and phase shifts. The user can select the node at which the torque is applied and can also decide to add a sigmoid ramp up to a specified mean torque value in a user defined rise time. This new feature is useful when the excitation torque is

known either from experimental data or previously performed analysis. An example of the usefulness of this new addition is presented by simulating the test rig with the torque excitations measured by the torque sensor. The torsional vibration amplitude is then calculated by the software and compared to experimental data from the torsional vibration sleeve in section 6.15.4

7.1.3. VFD Test Rig

The VFD experimental test rig is useful for both the present and future study of VFD induced torque harmonics and torsional vibrations. The test rig has the capability of measuring torque, torsional vibrations, lateral vibrations, rotational speed, and induced side load on a tilting pad bearing. The experimental results from the test rig show the presence of VFD induced torque harmonics. While some of the frequencies can be predicted by Song's formulas and the VFD code, a presence of integer harmonics at 1x, 2x, 3x, 4x, 5x, and 6x of the line frequency are found to dominate the torque harmonic spectrum. The cause of these harmonics is still unknown but several theories and ideas for improvement are discussed in the future work.

The results from the VFD test rig show a strong correlation between a measured torsional natural frequency and VFD Software predicted value. The experimentally measured natural frequency is seen as a constant frequency ridge at 75 Hz across all waterfall plots. The results from the torsional vibration measurement also show strong correlation to the values predicted by the software given a known torque excitation.

7.2. Future Work

7.2.1. VFD Software

The prediction of fatigue failure due to torsional vibrations is very important when implementing VFD control. The fatigue life and system failure analysis is also important when performing short circuit fault analyses on motor driven equipment. API standards 684 and 617 require that the torques generated by these faults are calculated for certain types of compressors to determine if failure will occur within the system. A clear improvement to the software is the performing of these required analyses along with the life prediction in the presence of these torque.

The VFD Software also has many useful abilities when it comes to the torsional analysis of rotordynamic systems. While the software also has the ability to perform basic lateral mode shape analyses, the lateral system analysis would be an extremely valuable feature. Some of the useful lateral features to be added include an unbalance response and system stability analysis.

7.2.2. VFD Test Rig

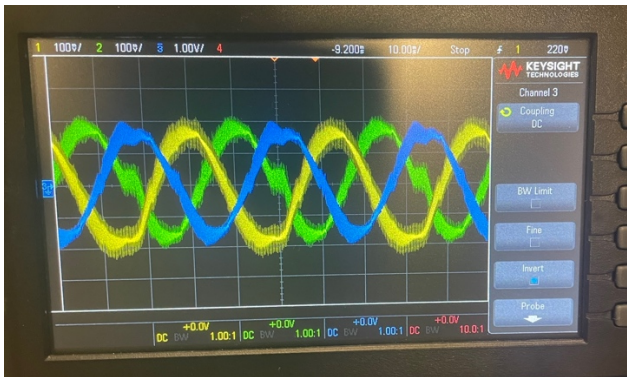

Figure 90: Phase Currents into the Motor

The experiments run with the VFD test rig show interesting results in the torque harmonic frequencies induced by VFD control. The integer harmonics present do not strongly align with Song's formulas or the frequencies predicted by the software. A future study needs to be run to determine the cause of these frequencies. A leading theory is that the phase currents shown in Figure 90 are resulting in the integer torque harmonics due to the flat region seen in the green channel. Studying the phase currents, using different VFDs to control the motor, and running experiments with a 4-pole motor would provide value to better understanding potential issues from VFDs.

The test rig can also be improved by running tests with different style couplings. The elastomer damping couplings in the rig were initially selected to protect the torque meter. These couplings may provide too much damping and nonlinear effects and better data may be seen with the use of other coupling styles.

Finally, higher loads above the tested 550 lbs. should be applied to the TPB housing and the rig should be run at higher speeds. These tests may prove to generate different torque spectra that align more with predicted values.

REFERENCES

[1] J. Song-Manguelle, S. Schroder, T. Geyer, G. Ekemb and J.-M. Nyobe-Yome, "Prediction of mechanical shaft failures due to pulsating torques of variable-frequency drives," *IEEE Transactions on Industry Applications,* vol. 46, no. 5, pp. 1979--1988, 2010.

[2] J. C. Wachel and F. R. Szenasi, "Analysis of torsional vibrations in rotating machinery.," in *Proceedings of the 22nd Turbomachinery Symposium*, Texas A&M University. Turbomachinery Laboratories, 1993.

[3] B. Howes, "Perplexing Variable Frequency Drive Vibration Problems," *CMVA, Edmonton, AB,* 2004.

[4] L. De la Roche and B. Howes, "Lateral and torsional vibration problems in systems equipped with variable frequency drive," *GMC, Covington, Ky,* 2005.

[5] R. J. Kerkman, J. Theisen and K. Shah, "PWM inverters producing torsional components in AC motors," in *2008 55th IEEE Petroleum and Chemical Industry Technical Conference*, 2008.

[6] M. Tsukakoshi, M. Al-Mamun, K. Hashimura, H. Hosoda, J. Sakaguchi and L. Ben-Brahim, "Novel torque ripple minimization control for 25 MW variable speed drive system fed by multilevel voltage source inverter," in *Proceedings of the 39th Turbomachinery Symposium*, Texas A&M University. Turbomachinery Laboratories, 2010.

[7] X. Han and A. B. Palazzolo, "VFD machinery vibration fatigue life and multilevel inverter effect," *IEEE Transactions on Industry Applications,* vol. 49, pp. 2562--2575, 2013.

[8] D. W. Novotny and T. A. Lipo, Vector control and dynamics of AC drives, vol. 1, Oxford university press, 1996.

[9] Vance, J. M. and French, R.S., "Measurement of Torsional Vibration in Rotating Macinery." ASME paper 84-DET-55 (1984).

[10] R. G. Budynas and J. K. Nisbett, Shigley's mechanical engineering design, McGraw-Hill Education, 2020.

[11] Corbo, Mark A.; Cook, Clifford P. (2000). "Torsional Vibration Analysis Of Synchronous Motor-Driven Turbomachinery,". *Proceedings of the Thirty-First Turbomachinery Symposium,* Turbomachinery Laboratory, Texas A&M University.

[12] E., Peterson R., and R. E. Peterson. *Stress Concentration Factors*. John Wiley and Sons.

[13] Juvinall, Robert C., and Kurt M. Marshek. *Fundamentals of Machine Component Design*. Wiley, 2020.

[14] Wang, Shyh-Jen. "Mean shear stress effect for a notch-free ductile material under pure cyclic torsional loads." (2006): 667-669.

[15] Shaft Alignment Procedures- Reverse Dial Method, RES Global. https://www.youtube.com/watch?v=9Ay5hcp9ybs

[16] Sandberg, Erik. "Torsional Vibrations." *Encyclopedia of Maritime and Offshore Engineering* (2017): 1-45.

APPENDIX

A.1. Drawings

A.1.1. Base Plate

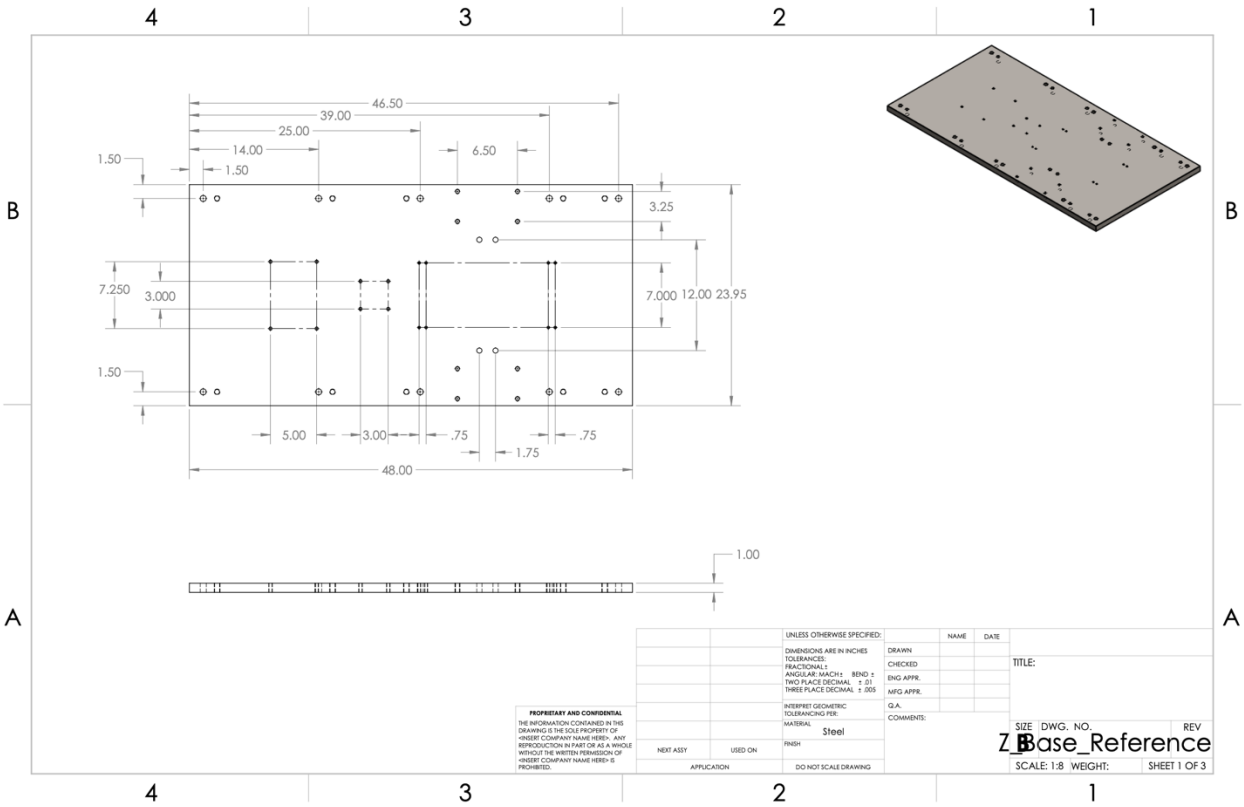

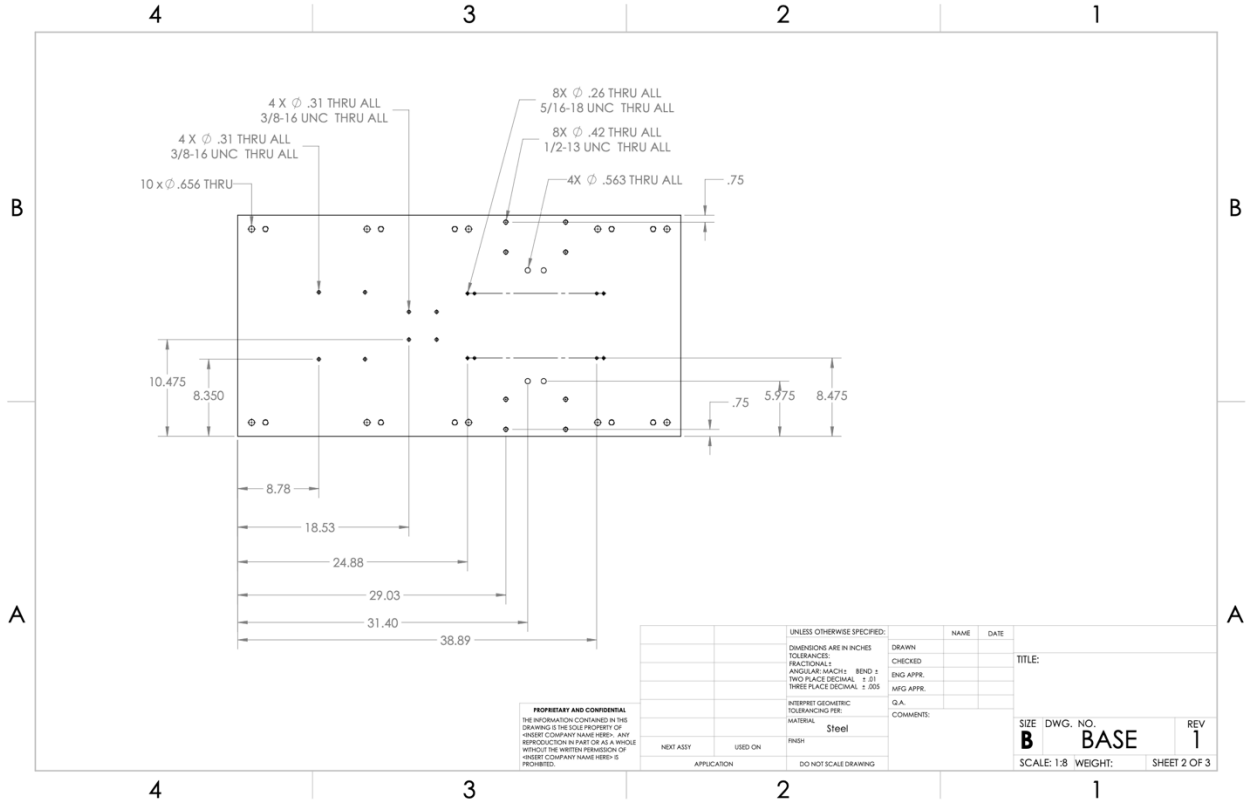
4 X ∅ .31 THRU ALL
3/8-16 UNC THRU ALL
4 X ∅ .31 THRU ALL
3/8-16 UNC THRU ALL
10 x ∅ .656 THRU
8X ∅ .26 THRU ALL
5/16-18 UNC THRU ALL
8X ∅ .42 THRU ALL
1/2-13 UNC THRU ALL
4X ∅ .563 THRU ALL
.75
10.475
8.350
.75
5.975
8.475
8.78
18.53
24.88
29.03
31.40
38.89
PROPRIETARY AND CONFIDENTIAL
THE INFORMATION CONTAINED IN THIS DRAWING IS THE SOLE PROPERTY OF <INSERT COMPANY NAME HERE>. ANY REPRODUCTION IN PART OR AS A WHOLE WITHOUT THE WRITTEN PERMISSION OF <INSERT COMPANY NAME HERE> IS PROHIBITED.
NEXT ASSY
USED ON
APPLICATION
UNLESS OTHERWISE SPECIFIED:
DIMENSIONS ARE IN INCHES
TOLERANCES:
FRACTIONAL ±
ANGULAR: MACH ± BEND ±
TWO PLACE DECIMAL ± .01
THREE PLACE DECIMAL ± .005
INTERPRET GEOMETRIC TOLERANCING PER:
MATERIAL
Steel
FINISH
DO NOT SCALE DRAWING
NAME
DATE
DRAWN
CHECKED
ENG APPR.
MFG APPR.
Q.A.
COMMENTS:
TITLE:
SIZE
B
DWG. NO.
BASE
REV
1
SCALE: 1:8
WEIGHT:
SHEET 2 OF 3

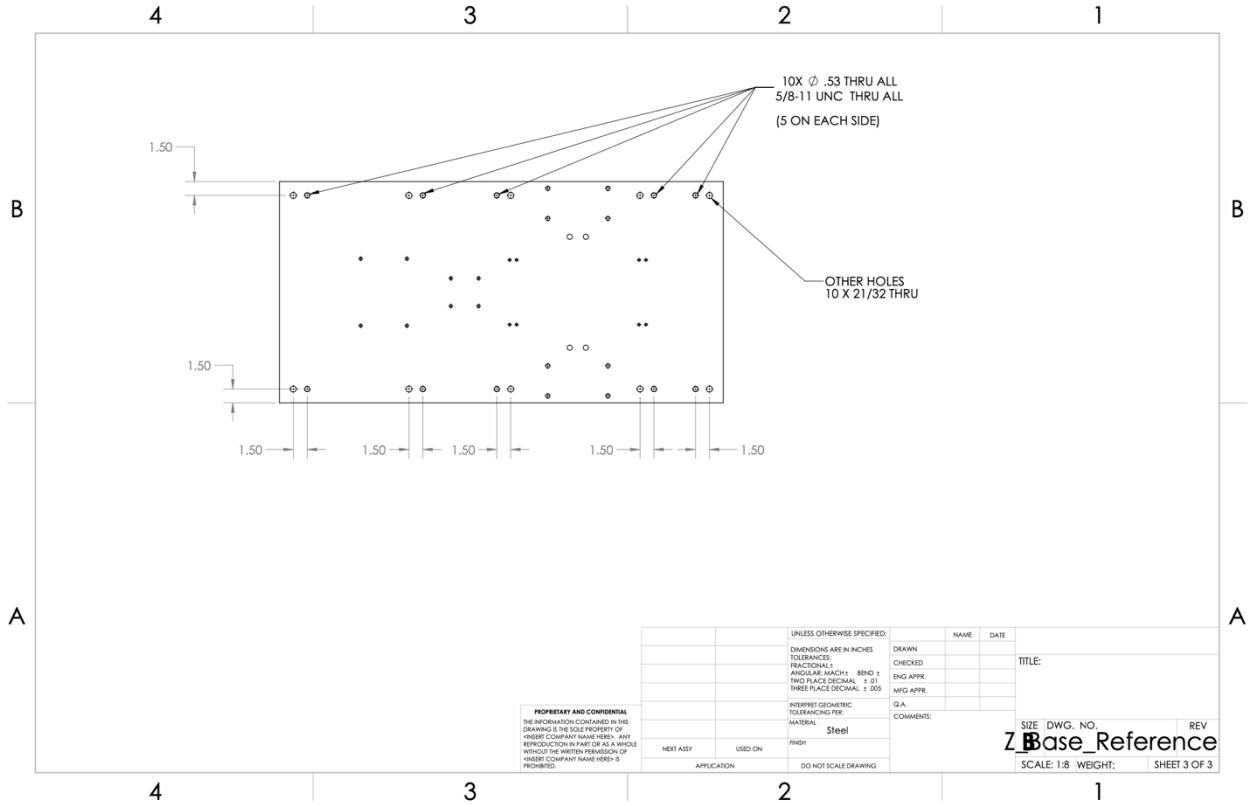
10X ∅ .53 THRU ALL
5/8-11 UNC THRU ALL
(5 ON EACH SIDE)
1.50
1.50
OTHER HOLES
10 X 21/32 THRU
1.50
1.50
1.50
1.50
1.50
PROPRIETARY AND CONFIDENTIAL
THE INFORMATION CONTAINED IN THIS DRAWING IS THE SOLE PROPERTY OF <INSERT COMPANY NAME HERE>. ANY REPRODUCTION IN PART OR AS A WHOLE WITHOUT THE WRITTEN PERMISSION OF <INSERT COMPANY NAME HERE> IS PROHIBITED.
NEXT ASSY
USED ON
APPLICATION
UNLESS OTHERWISE SPECIFIED:
DIMENSIONS ARE IN INCHES
TOLERANCES:
FRACTIONAL ±
ANGULAR: MACH ± BEND ±
TWO PLACE DECIMAL ± .01
THREE PLACE DECIMAL ± .005
INTERPRET GEOMETRIC TOLERANCING PER:
MATERIAL
Steel
FINISH
DO NOT SCALE DRAWING
NAME
DATE
DRAWN
CHECKED
ENG APPR.
MFG APPR.
Q.A.
COMMENTS:
TITLE:
SIZE
B
DWG. NO.
Z_Base_Reference
REV
SCALE: 1:8
WEIGHT:
SHEET 3 OF 3

A.1.2. TPB Housing

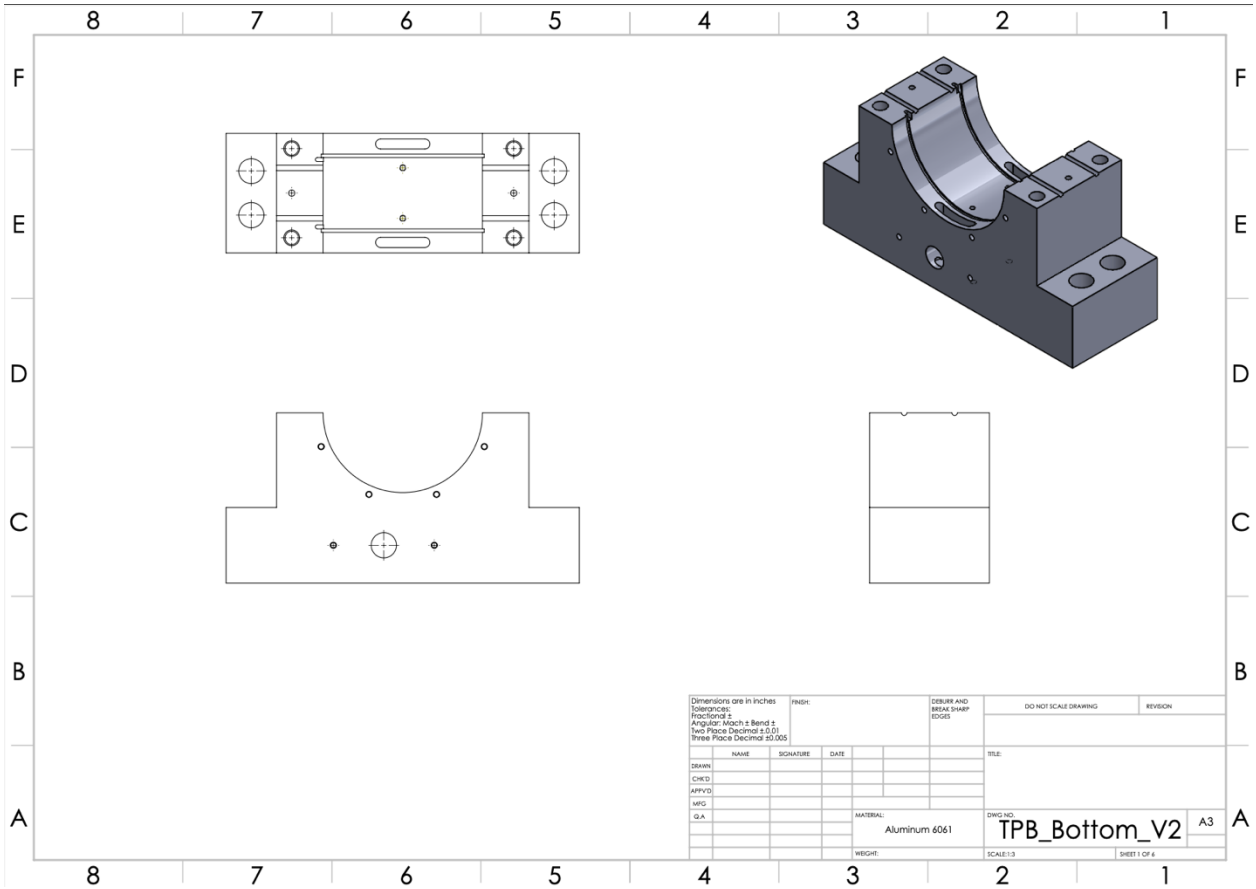

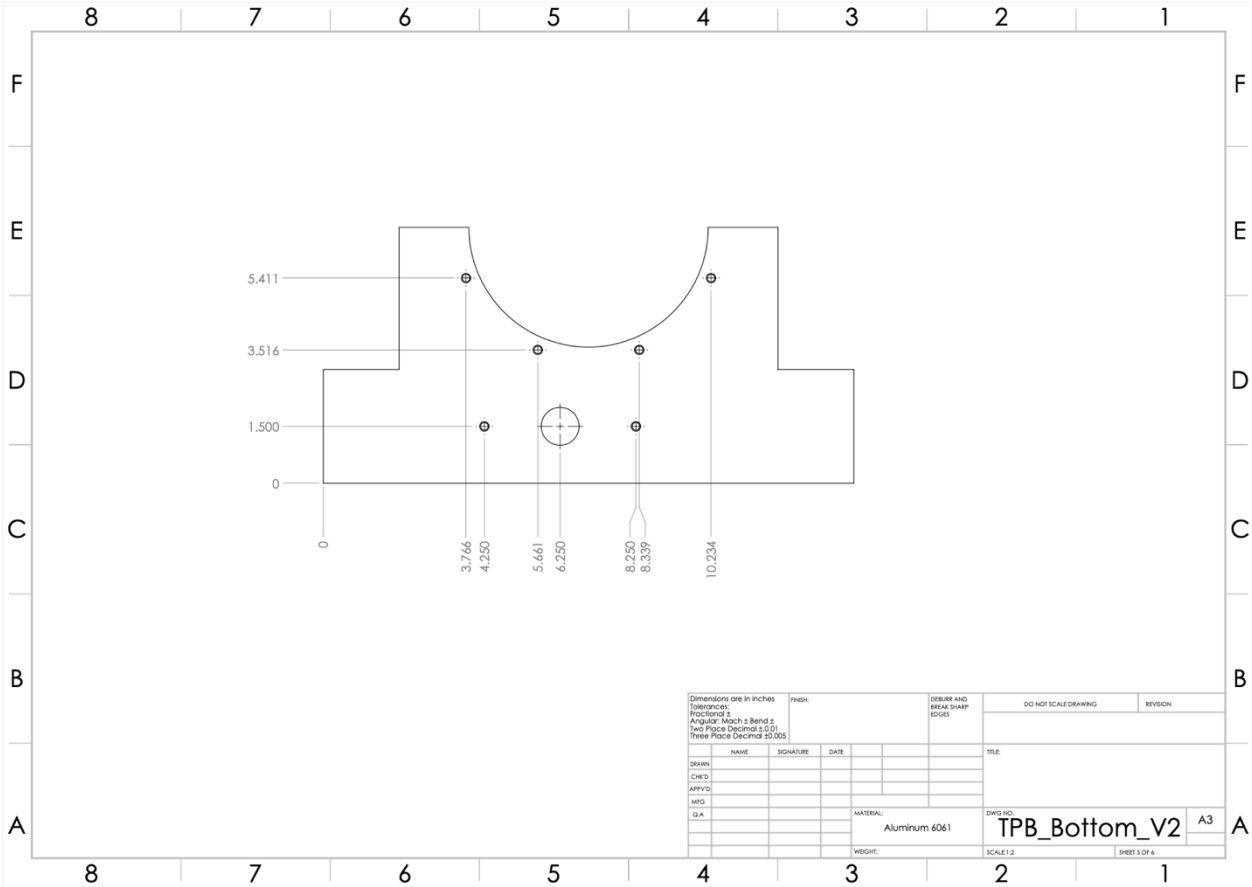
5.411
3.516
1.500
0
0
3.766
4.250
5.661
6.250
8.250
8.339
10.234
Dimensions are in inches
Tolerances:
Fractional ±
Angular: Mach ± Bend ±
Two Place Decimal ±0.01
Three Place Decimal ±0.005
FINISH:
DEBURR AND BREAK SHARP EDGES
DO NOT SCALE DRAWING
REVISION
NAME
SIGNATURE
DATE
DRAWN
CHK'D
APPV'D
MFG
Q.A
TITLE:
MATERIAL:
Aluminum 6061
WEIGHT:
DWG NO.
TPB_Bottom_V2
A3
SCALE:1:2
SHEET 3 OF 6

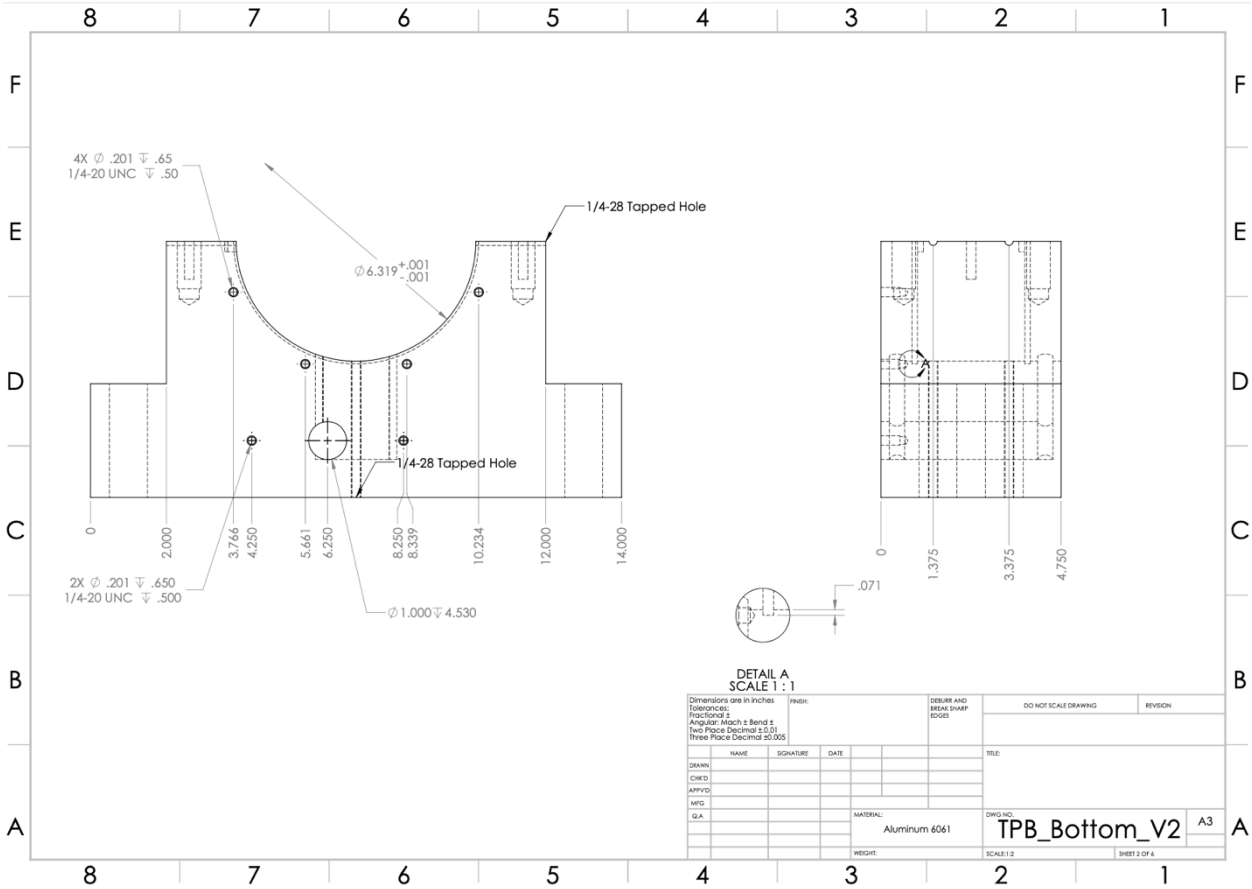
4X ∅ .201 ↧ .65
1/4-20 UNC ↧ .50
1/4-28 Tapped Hole
∅6.319 +.001 -.001
1/4-28 Tapped Hole
0
2.000
3.766
4.250
5.661
6.250
8.250
8.339
10.234
12.000
14.000
2X ∅ .201 ↧ .650
1/4-20 UNC ↧ .500
∅1.000 ↧ 4.530
0
1.375
3.375
4.750
.071
DETAIL A
SCALE 1 : 1
Dimensions are in inches
Tolerances:
Fractional ±
Angular: Mach ± Bend ±
Two Place Decimal ±0.01
Three Place Decimal ±0.005
FINISH:
DEBURR AND BREAK SHARP EDGES
DO NOT SCALE DRAWING
REVISION
NAME
SIGNATURE
DATE
DRAWN
CHK'D
APPV'D
MFG
Q.A
TITLE:
MATERIAL:
Aluminum 6061
WEIGHT:
DWG NO.
TPB_Bottom_V2
A3
SCALE:1:2
SHEET 2 OF 6

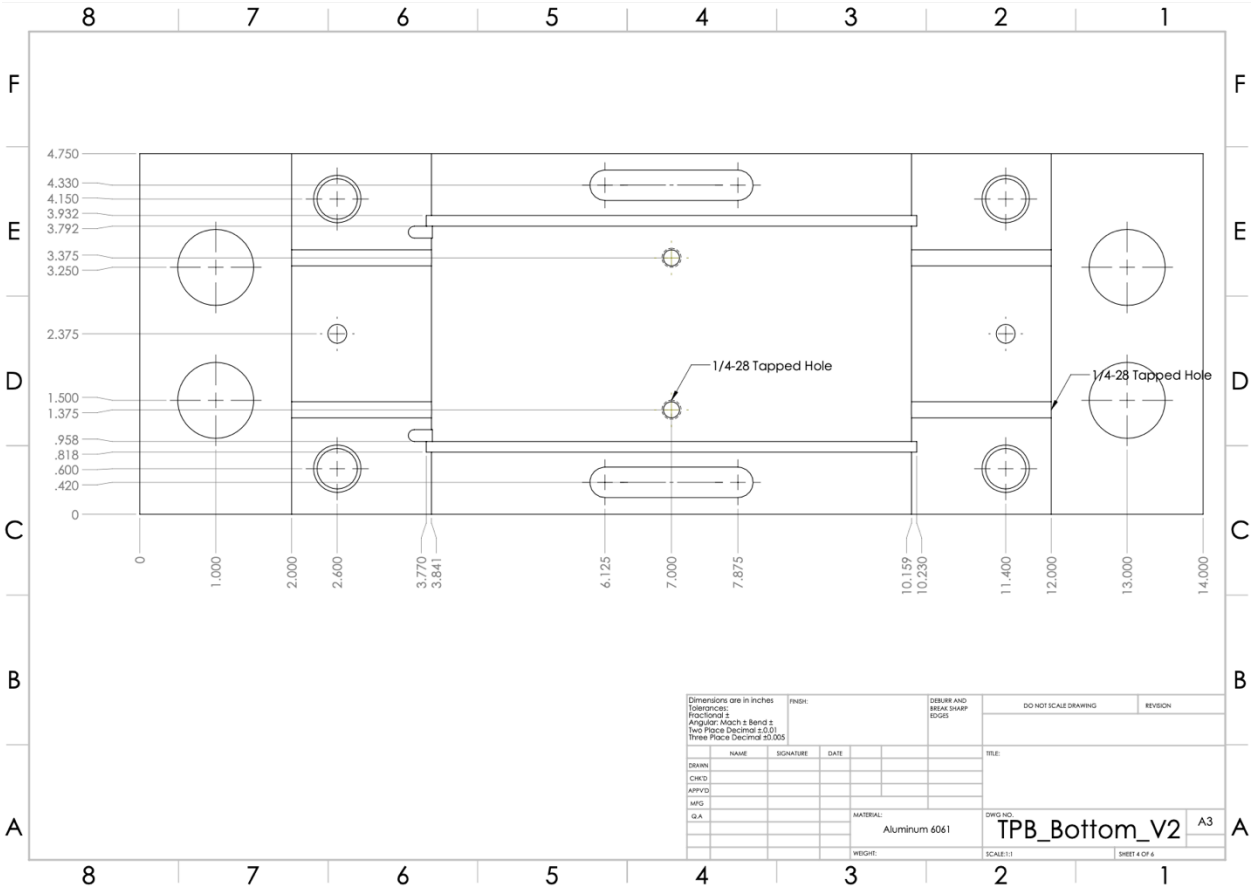
4.750
4.330
4.150
3.932
3.792
3.375
3.250
2.375
1.500
1.375
.958
.818
.600
.420
0
0
1.000
2.000
2.600
3.770
3.841
6.125
7.000
7.875
10.159
10.230
11.400
12.000
13.000
14.000
1/4-28 Tapped Hole
1/4-28 Tapped Hole
Dimensions are in inches
Tolerances:
Fractional ±
Angular: Mach ± Bend ±
Two Place Decimal ±0.01
Three Place Decimal ±0.005
FINISH:
DEBURR AND BREAK SHARP EDGES
DO NOT SCALE DRAWING
REVISION
NAME
SIGNATURE
DATE
DRAWN
CHK'D
APPV'D
MFG
Q.A
TITLE:
MATERIAL:
Aluminum 6061
WEIGHT:
DWG NO
TPB_Bottom_V2
A3
SCALE:1:1
SHEET 4 OF 6

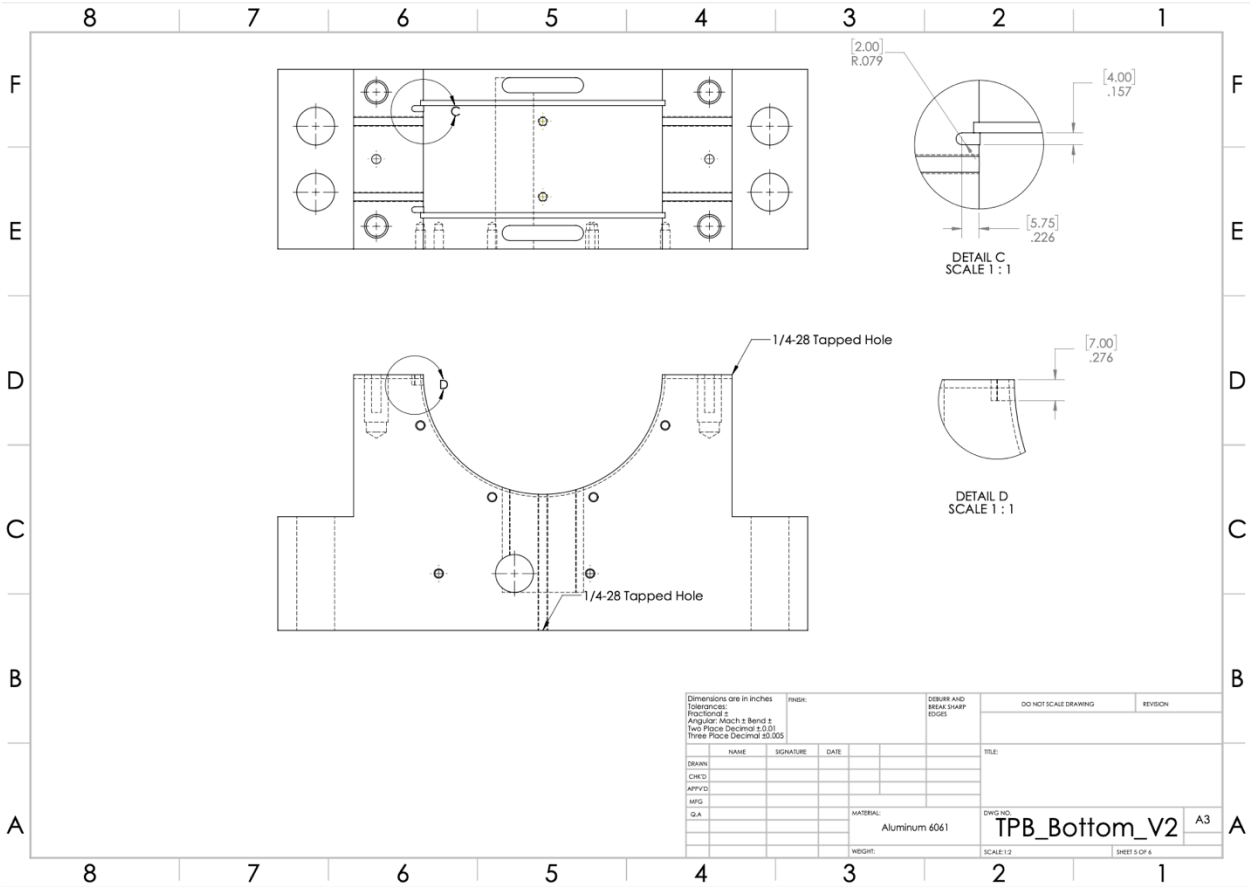
[2.00]
R.079
[4.00]
.157
[5.75]
.226
DETAIL C
SCALE 1 : 1
1/4-28 Tapped Hole
[7.00]
.276
DETAIL D
SCALE 1 : 1
1/4-28 Tapped Hole
Dimensions are in inches
Tolerances:
Fractional ±
Angular: Mach ± Bend ±
Two Place Decimal ±0.01
Three Place Decimal ±0.005
FINISH:
DEBURR AND BREAK SHARP EDGES
DO NOT SCALE DRAWING
REVISION
NAME
SIGNATURE
DATE
DRAWN
CHK'D
APPV'D
MFG
Q.A
TITLE:
MATERIAL:
Aluminum 6061
WEIGHT:
DWG NO.
TPB_Bottom_V2
A3
SCALE:1:2
SHEET 5 OF 6

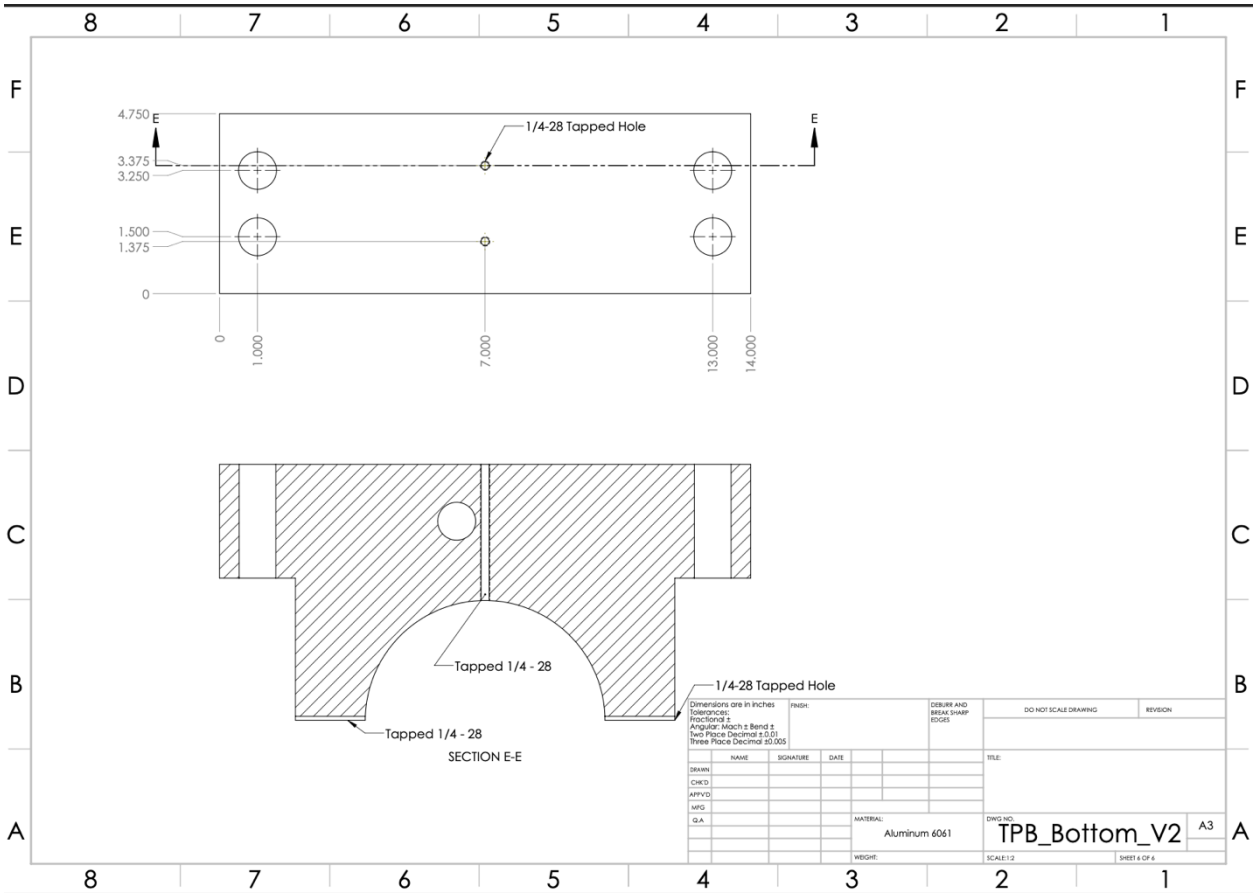
4.750
3.375
3.250
1.500
1.375
0
E
E
1/4-28 Tapped Hole
0
1.000
7.000
13.000
14.000
Tapped 1/4 - 28
1/4-28 Tapped Hole
Tapped 1/4 - 28
SECTION E-E
Dimensions are in inches
Tolerances:
Fractional ±
Angular: Mach ± Bend ±
Two Place Decimal ±0.01
Three Place Decimal ±0.005
FINISH:
DEBURR AND BREAK SHARP EDGES
DO NOT SCALE DRAWING
REVISION
NAME
SIGNATURE
DATE
DRAWN
CHK'D
APPV'D
MFG
Q.A
TITLE:
MATERIAL:
Aluminum 6061
WEIGHT:
DWG NO.
TPB_Bottom_V2
A3
SCALE:1:2
SHEET 6 OF 6

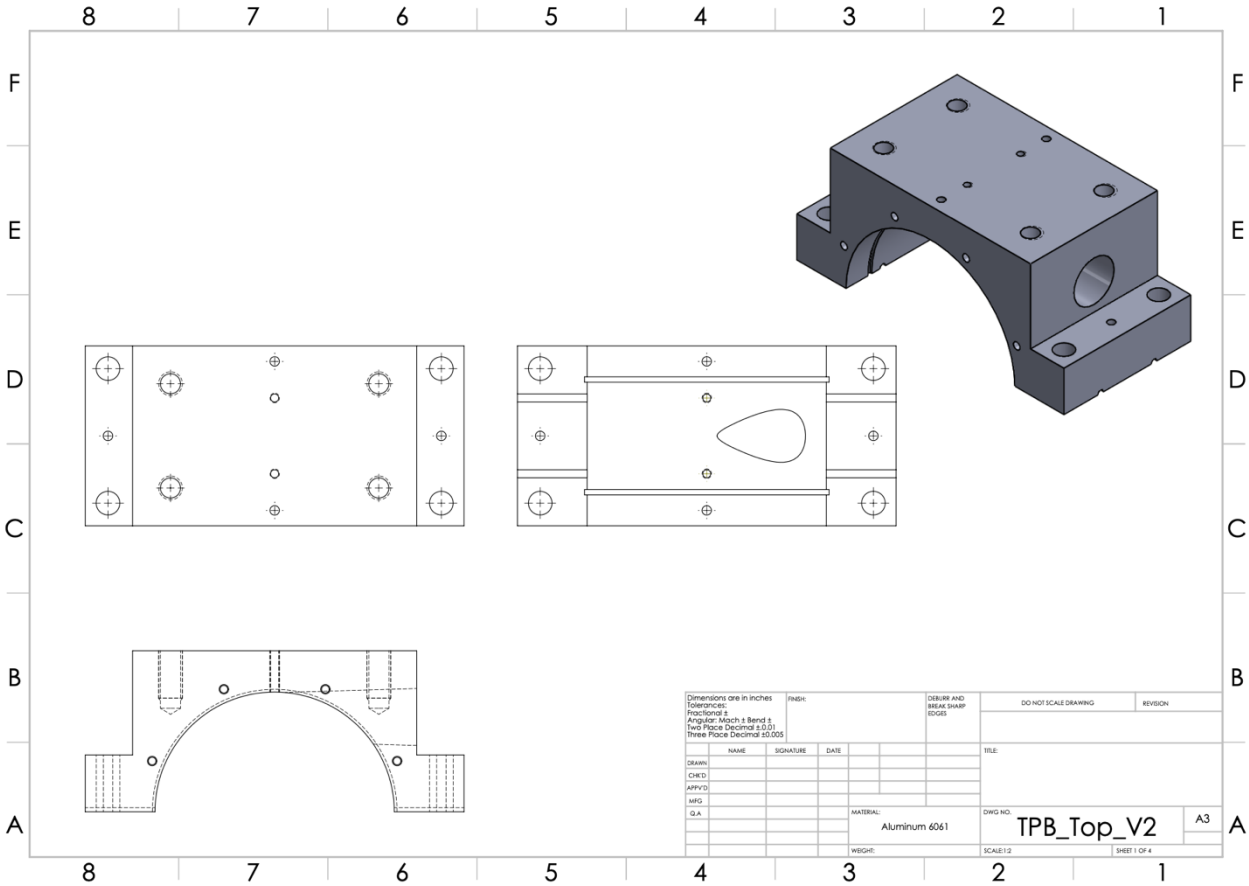
Dimensions are in inches
Tolerances:
Fractional ±
Angular: Mach ± Bend ±
Two Place Decimal ±0.01
Three Place Decimal ±0.005
FINISH:
DEBURR AND BREAK SHARP EDGES
DO NOT SCALE DRAWING
REVISION
NAME
SIGNATURE
DATE
DRAWN
CHK'D
APPV'D
MFG
Q.A.
TITLE:
MATERIAL:
Aluminum 6061
WEIGHT:
DWG NO.
TPB_Top_V2
A3
SCALE:1:2
SHEET 1 OF 4

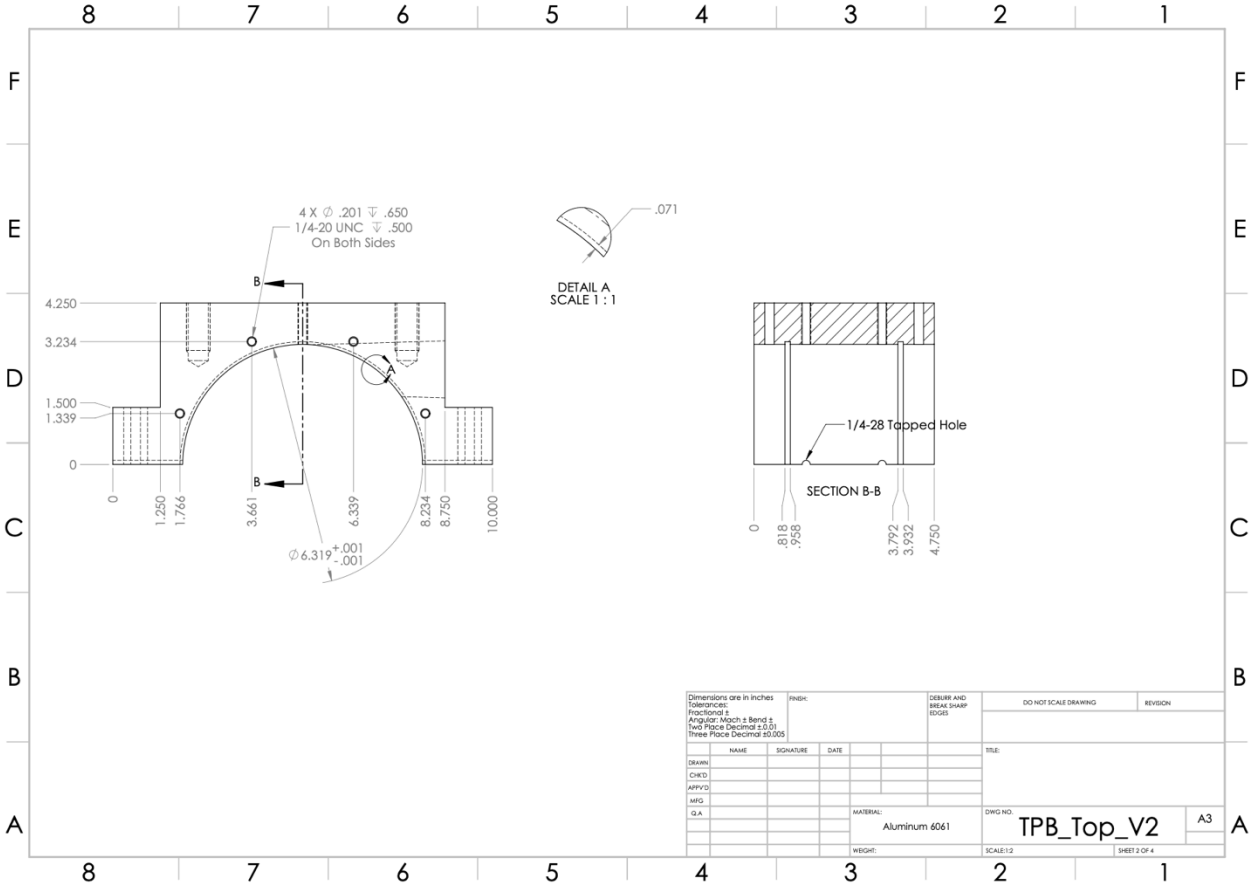
4 X ⌀ .201 ↧ .650
1/4-20 UNC ↧ .500
On Both Sides
4.250
3.234
1.500
1.339
0
B
0
1.250
1.766
3.661
6.339
8.234
8.750
10.000
⌀6.319 +.001 -.001
.071
DETAIL A
SCALE 1 : 1
1/4-28 Tapped Hole
SECTION B-B
0
.818
.958
3.792
3.932
4.750
Dimensions are in inches
Tolerances:
Fractional ±
Angular: Mach ± Bend ±
Two Place Decimal ±0.01
Three Place Decimal ±0.005
FINISH:
DEBURR AND BREAK SHARP EDGES
DO NOT SCALE DRAWING
REVISION
NAME
SIGNATURE
DATE
DRAWN
CHK'D
APPV'D
MFG
Q.A
TITLE:
MATERIAL:
Aluminum 6061
WEIGHT:
DWG NO.
TPB_Top_V2
A3
SCALE:1:2
SHEET 2 OF 4

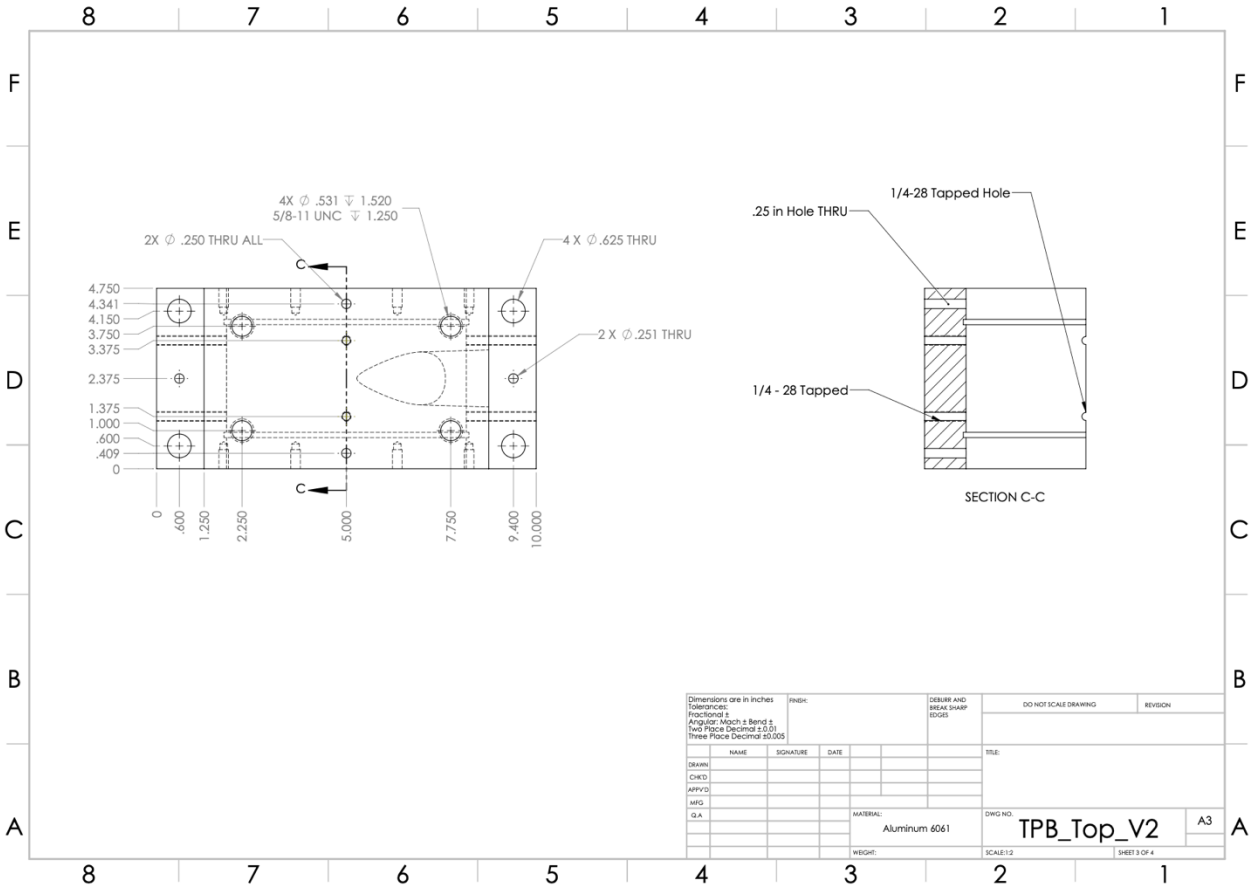
4X ∅ .531 ↧ 1.520
5/8-11 UNC ↧ 1.250
2X ∅ .250 THRU ALL
4 X ∅.625 THRU
2 X ∅.251 THRU
4.750
4.341
4.150
3.750
3.375
2.375
1.375
1.000
.600
.409
0
0
.600
1.250
2.250
5.000
7.750
9.400
10.000
C
C
1/4-28 Tapped Hole
.25 in Hole THRU
1/4 - 28 Tapped
SECTION C-C
Dimensions are in inches
Tolerances:
Fractional ±
Angular: Mach ± Bend ±
Two Place Decimal ±0.01
Three Place Decimal ±0.005
FINISH:
DEBURR AND BREAK SHARP EDGES
DO NOT SCALE DRAWING
REVISION
NAME
SIGNATURE
DATE
DRAWN
CHK'D
APPV'D
MFG
Q.A
TITLE:
MATERIAL:
Aluminum 6061
WEIGHT:
DWG NO.
TPB_Top_V2
A3
SCALE:1:2
SHEET 3 OF 4

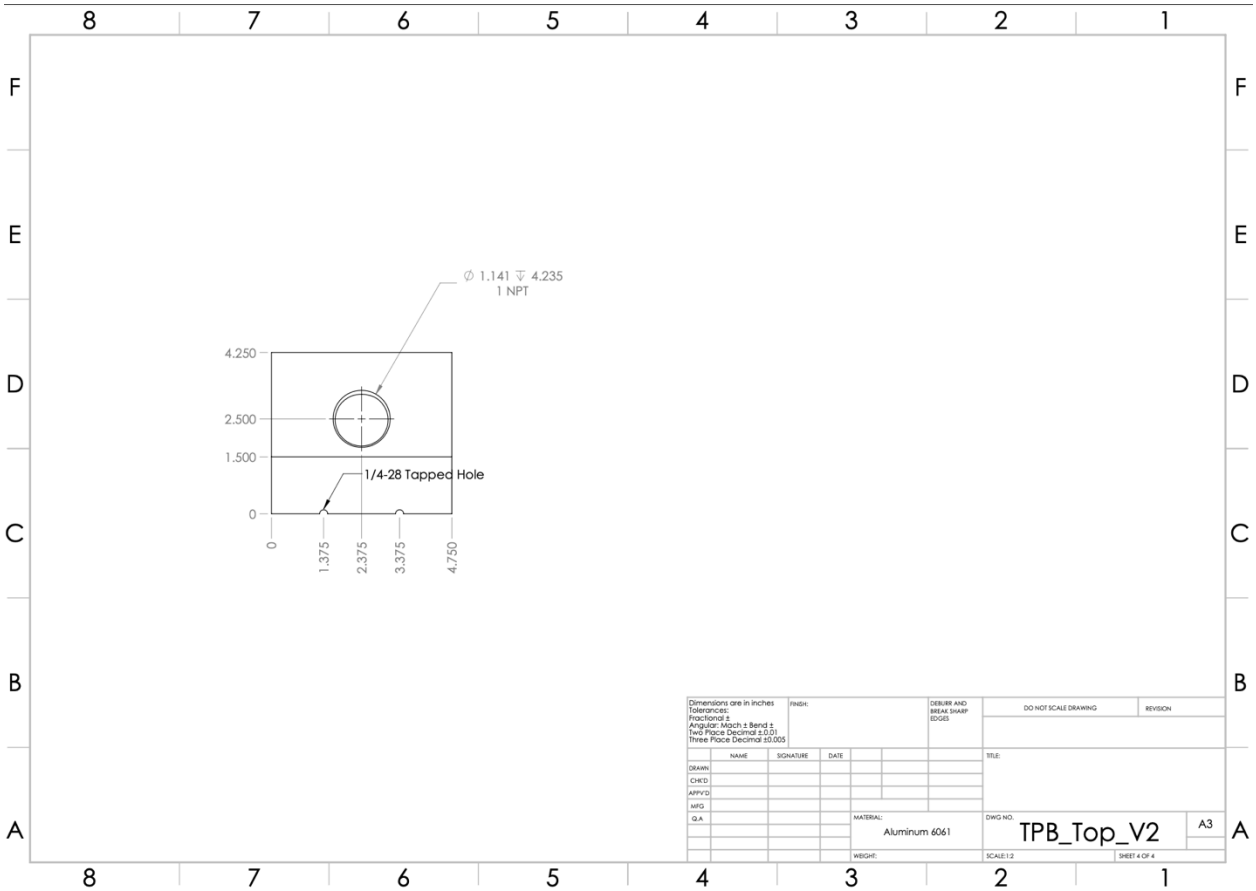
∅ 1.141 ↧ 4.235
1 NPT
4.250
2.500
1.500
0
1/4-28 Tapped Hole
0
1.375
2.375
3.375
4.750
Dimensions are in inches
Tolerances:
Fractional ±
Angular: Mach ± Bend ±
Two Place Decimal ±0.01
Three Place Decimal ±0.005
FINISH:
DEBURR AND BREAK SHARP EDGES
DO NOT SCALE DRAWING
REVISION
NAME
SIGNATURE
DATE
DRAWN
CHK'D
APPV'D
MFG
Q.A
TITLE:
MATERIAL:
Aluminum 6061
WEIGHT:
DWG NO.
TPB_Top_V2
A3
SCALE:1:2
SHEET 4 OF 4

A.1.3. TPB Top Force Plate

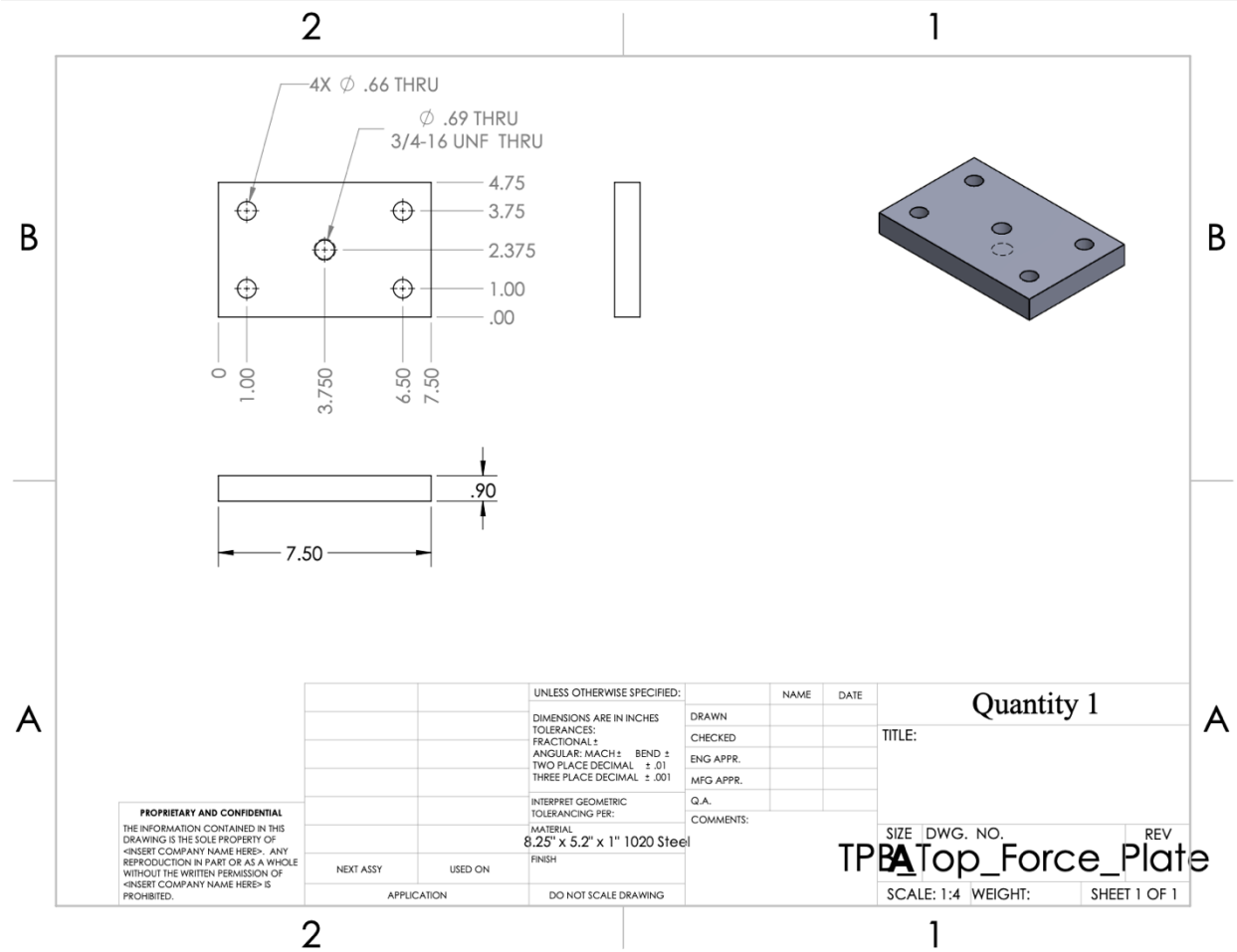

A.1.4. TPB Seal Plate

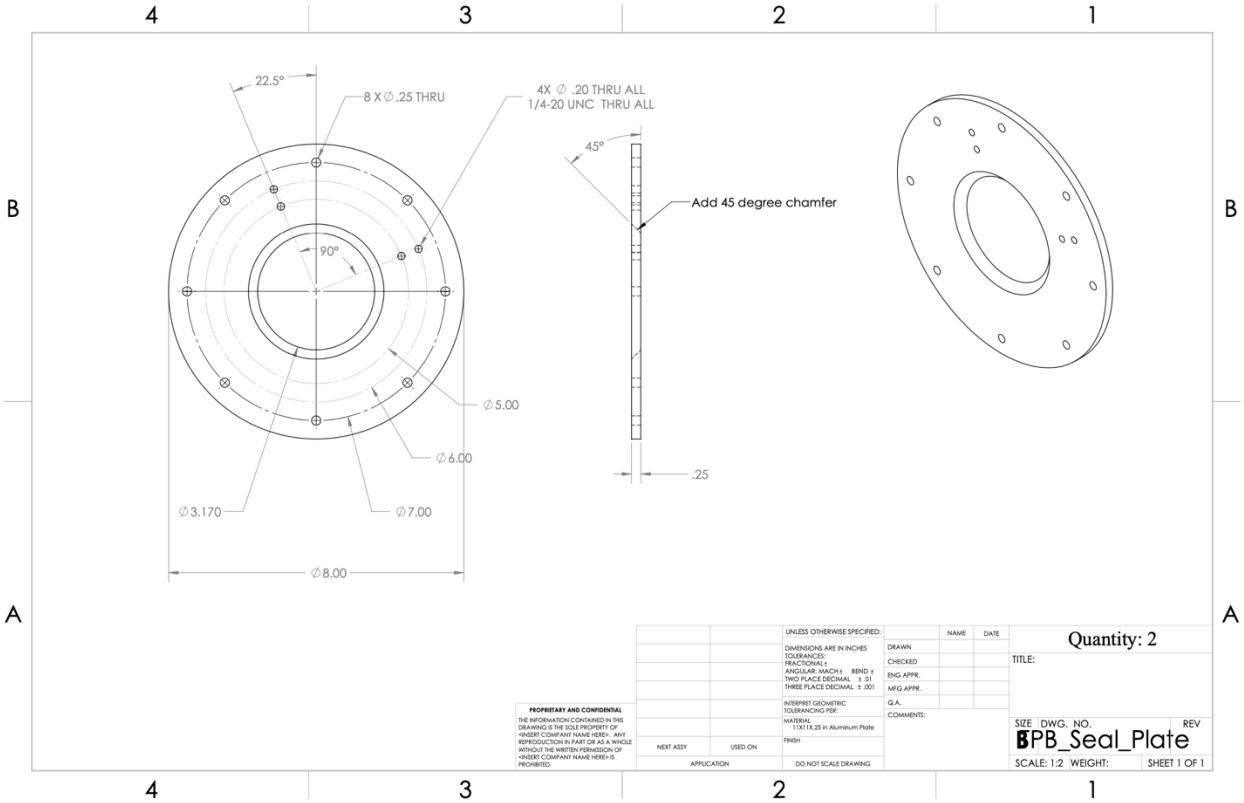

A.1.5. Torsional Vibration Sleeve

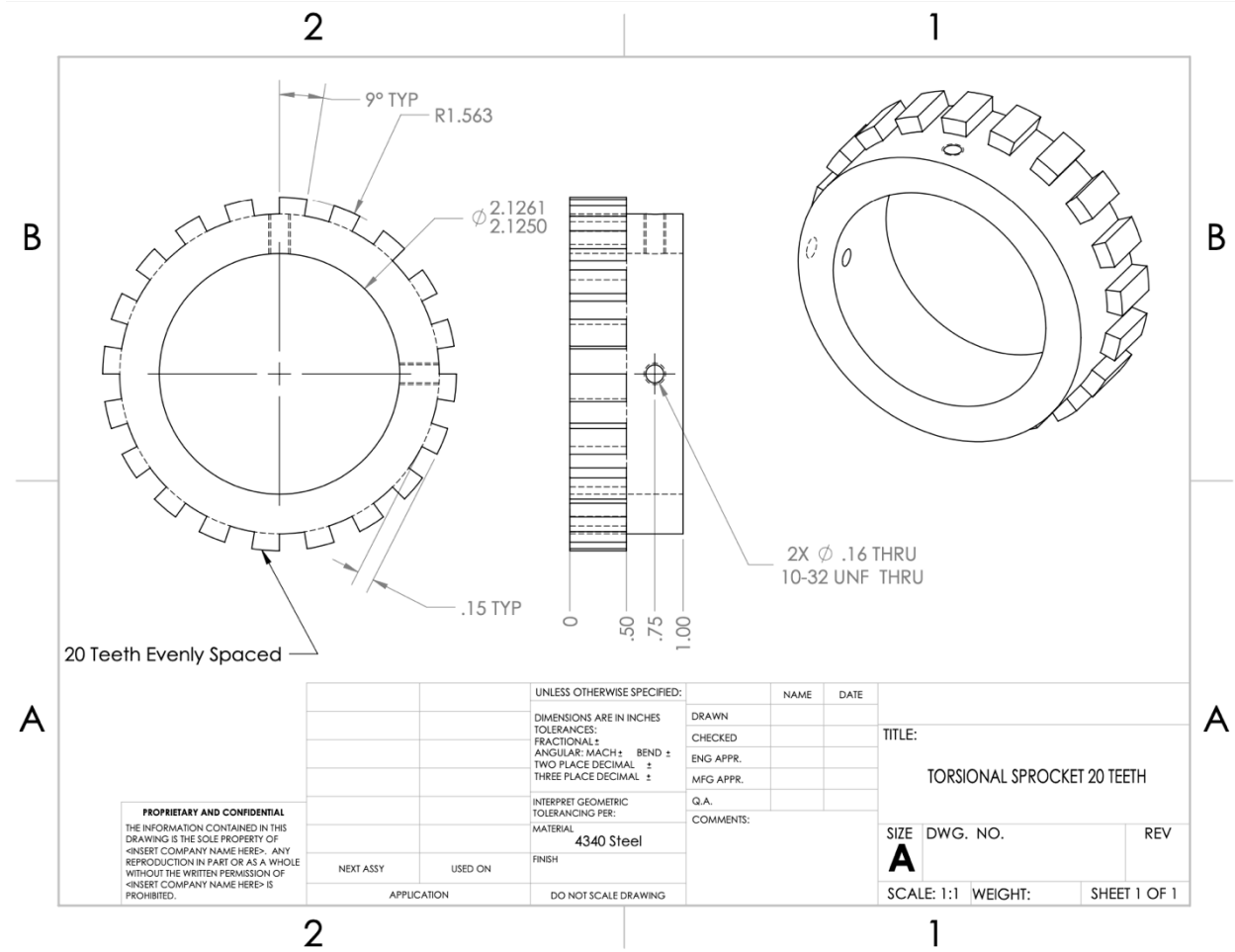

A.1.6. Shaft

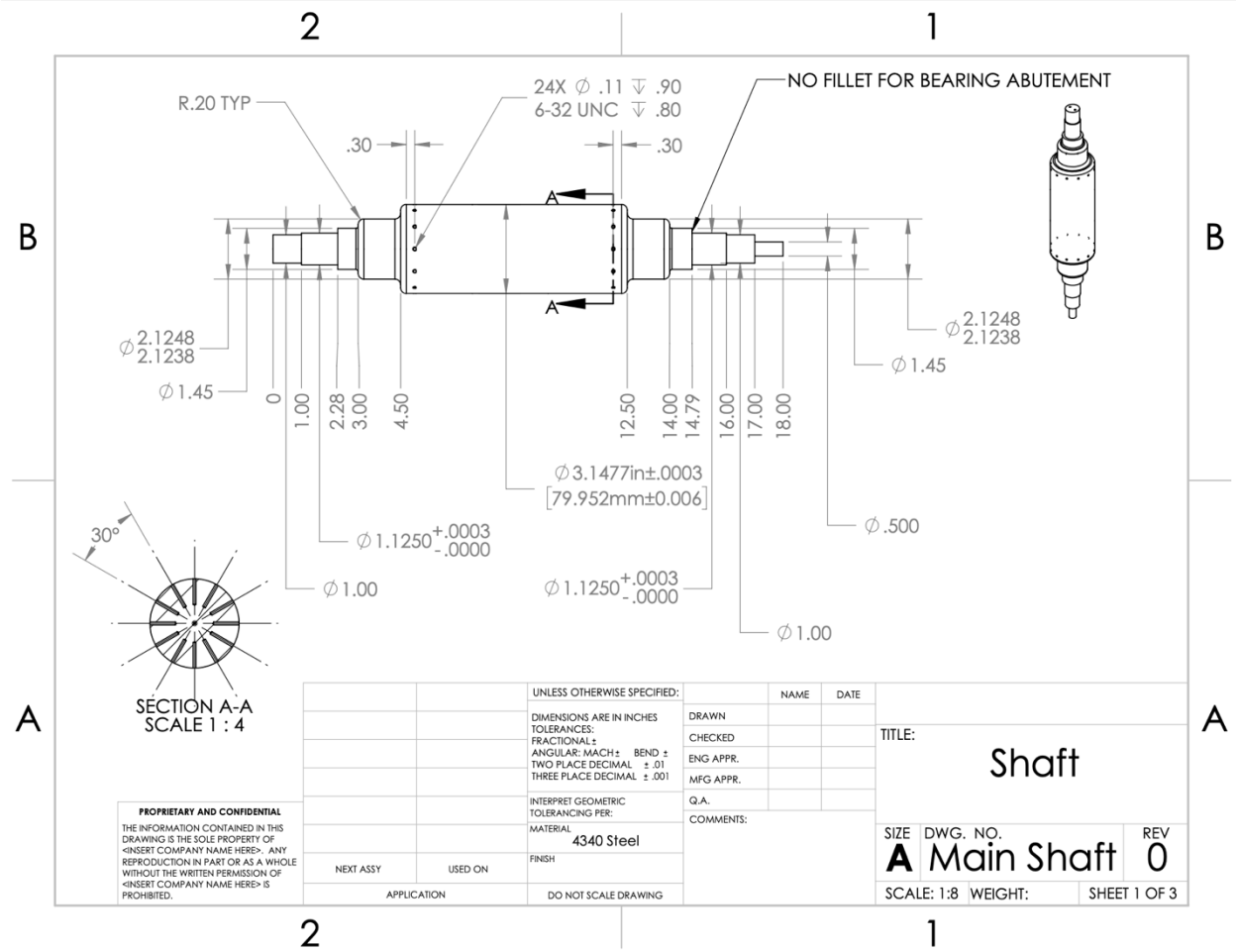
R.20 TYP
24X ∅ .11 ↧ .90
6-32 UNC ↧ .80
NO FILLET FOR BEARING ABUTEMENT
.30
.30
A
A
∅2.1248
2.1238
∅1.45
0
1.00
2.28
3.00
4.50
12.50
14.00
14.79
16.00
17.00
18.00
∅2.1248
2.1238
∅1.45
∅3.1477in±.0003
[79.952mm±0.006]
∅.500
∅1.1250+.0003 -.0000
∅1.00
∅1.1250+.0003 -.0000
∅1.00
30°
SECTION A-A
SCALE 1 : 4
UNLESS OTHERWISE SPECIFIED:
DIMENSIONS ARE IN INCHES
TOLERANCES:
FRACTIONAL ±
ANGULAR: MACH ± BEND ±
TWO PLACE DECIMAL ± .01
THREE PLACE DECIMAL ± .001
INTERPRET GEOMETRIC TOLERANCING PER:
MATERIAL
4340 Steel
FINISH
DO NOT SCALE DRAWING
NAME
DATE
DRAWN
CHECKED
ENG APPR.
MFG APPR.
Q.A.
COMMENTS:
TITLE:
Shaft
SIZE
A
DWG. NO.
Main Shaft
REV
0
SCALE: 1:8
WEIGHT:
SHEET 1 OF 3
PROPRIETARY AND CONFIDENTIAL
THE INFORMATION CONTAINED IN THIS DRAWING IS THE SOLE PROPERTY OF <INSERT COMPANY NAME HERE>. ANY REPRODUCTION IN PART OR AS A WHOLE WITHOUT THE WRITTEN PERMISSION OF <INSERT COMPANY NAME HERE> IS PROHIBITED.
NEXT ASSY
USED ON
APPLICATION

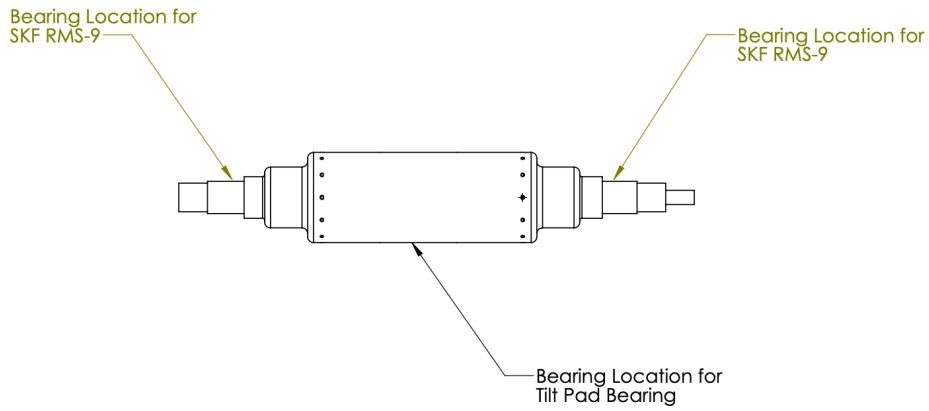

		UNLESS OTHERWISE SPECIFIED:		NAME	DATE
		DIMENSIONS ARE IN INCHES TOLERANCES: FRACTIONAL ± ANGULAR: MACH ± BEND ± TWO PLACE DECIMAL ± THREE PLACE DECIMAL ±	DRAWN		
			CHECKED		
			ENG APPR.		
			MFG APPR.		
		INTERPRET GEOMETRIC TOLERANCING PER:	Q.A.		
		MATERIAL	COMMENTS:		
NEXT ASSY	USED ON	FINISH			
APPLICATION		DO NOT SCALE DRAWING			

TITLE:

SIZE	DWG. NO.	REV
A	Main Shaft	
SCALE: 1:8	WEIGHT:	SHEET 2 OF 3

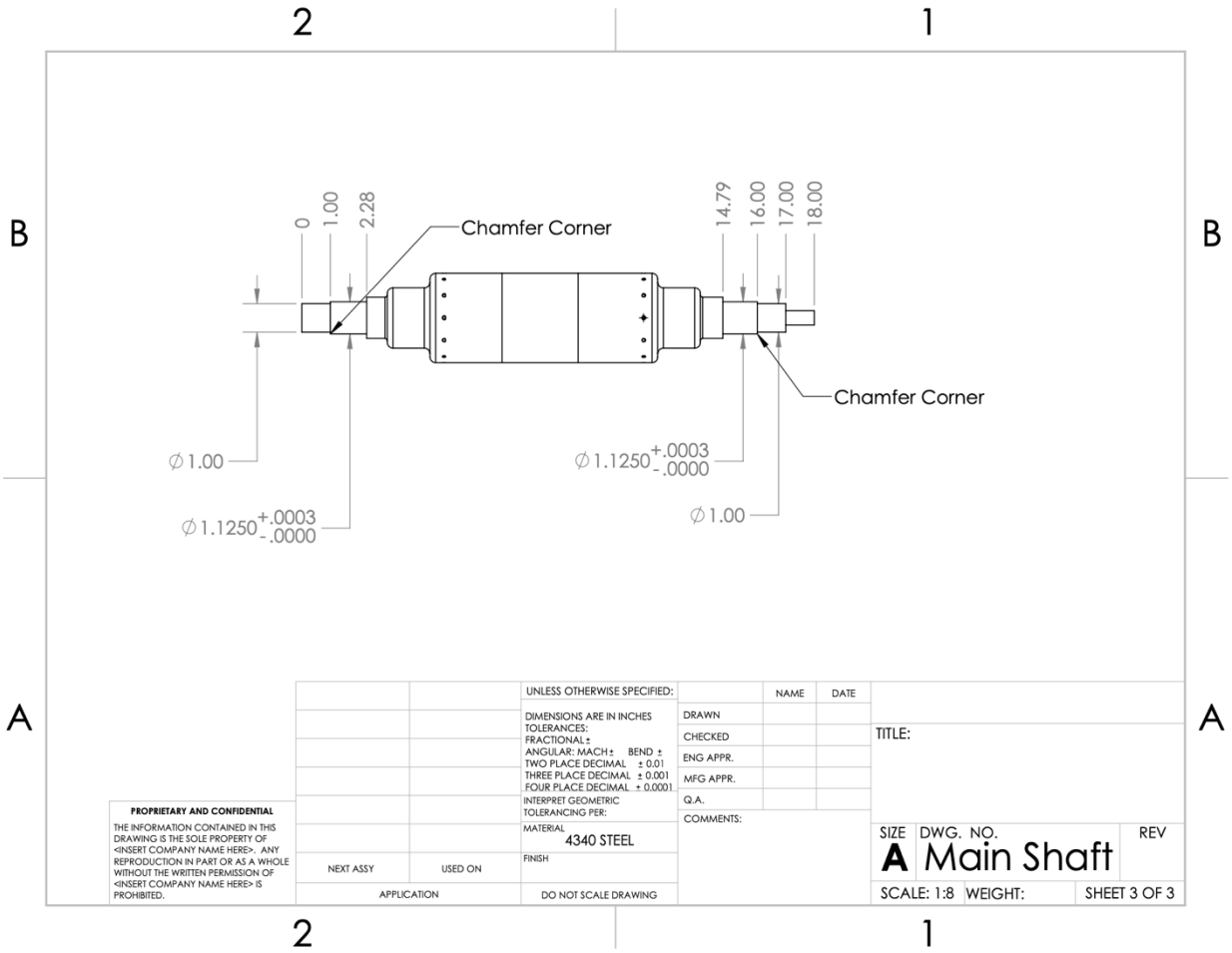
0
1.00
2.28
Chamfer Corner
14.79
16.00
17.00
18.00
Chamfer Corner
∅1.00
∅1.1250 +.0003 -.0000
∅1.1250 +.0003 -.0000
∅1.00
PROPRIETARY AND CONFIDENTIAL
THE INFORMATION CONTAINED IN THIS DRAWING IS THE SOLE PROPERTY OF <INSERT COMPANY NAME HERE>. ANY REPRODUCTION IN PART OR AS A WHOLE WITHOUT THE WRITTEN PERMISSION OF <INSERT COMPANY NAME HERE> IS PROHIBITED.
NEXT ASSY
USED ON
APPLICATION
UNLESS OTHERWISE SPECIFIED:
DIMENSIONS ARE IN INCHES
TOLERANCES:
FRACTIONAL ±
ANGULAR: MACH ± BEND ±
TWO PLACE DECIMAL ± 0.01
THREE PLACE DECIMAL ± 0.001
FOUR PLACE DECIMAL ± 0.0001
INTERPRET GEOMETRIC TOLERANCING PER:
MATERIAL
4340 STEEL
FINISH
DO NOT SCALE DRAWING
NAME
DATE
DRAWN
CHECKED
ENG APPR.
MFG APPR.
Q.A.
COMMENTS:
TITLE:
SIZE
A
DWG. NO.
Main Shaft
REV
SCALE: 1:8
WEIGHT:
SHEET 3 OF 3

A.1.7. Ball Bearing Housing

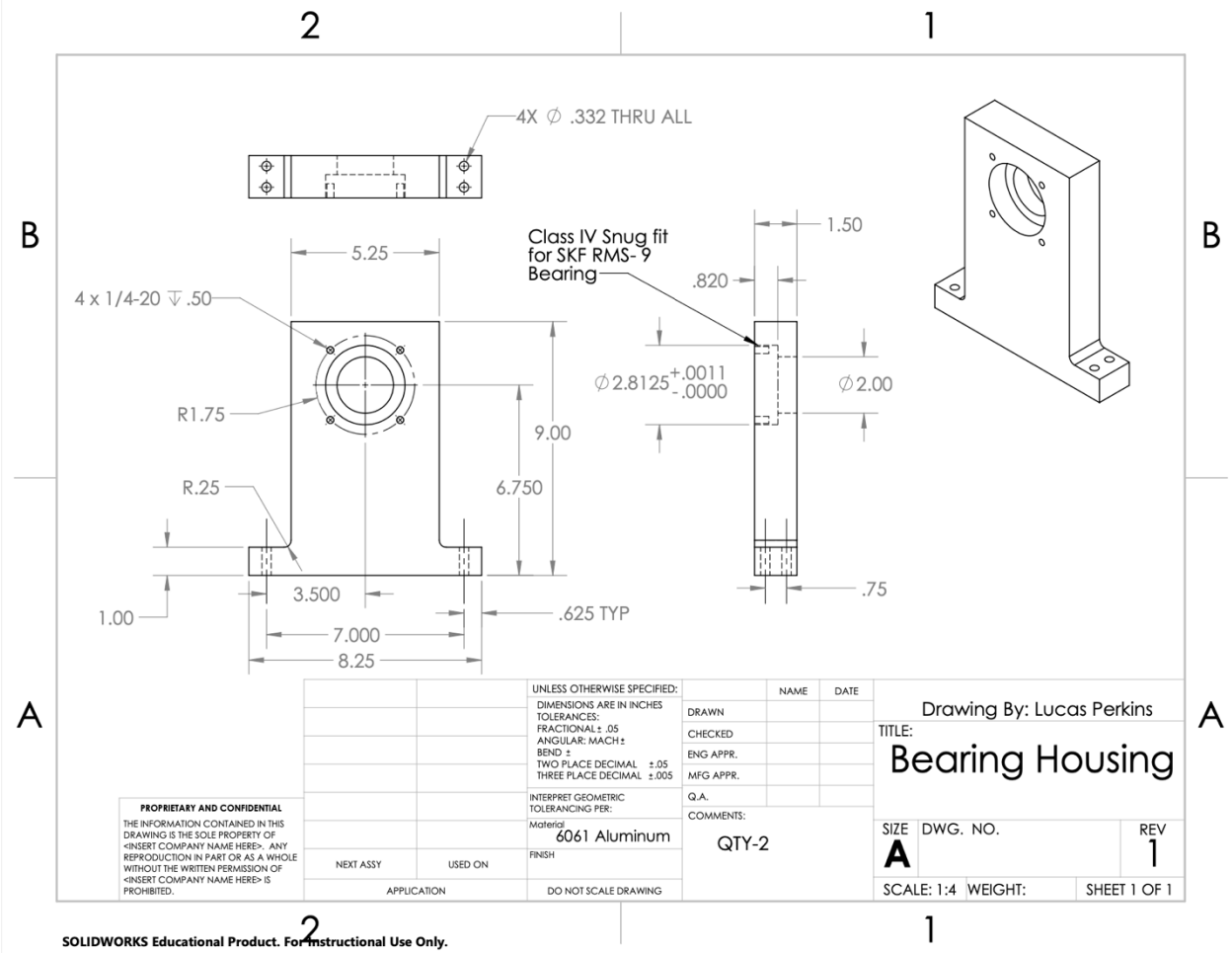

A.1.8. Oil Flange

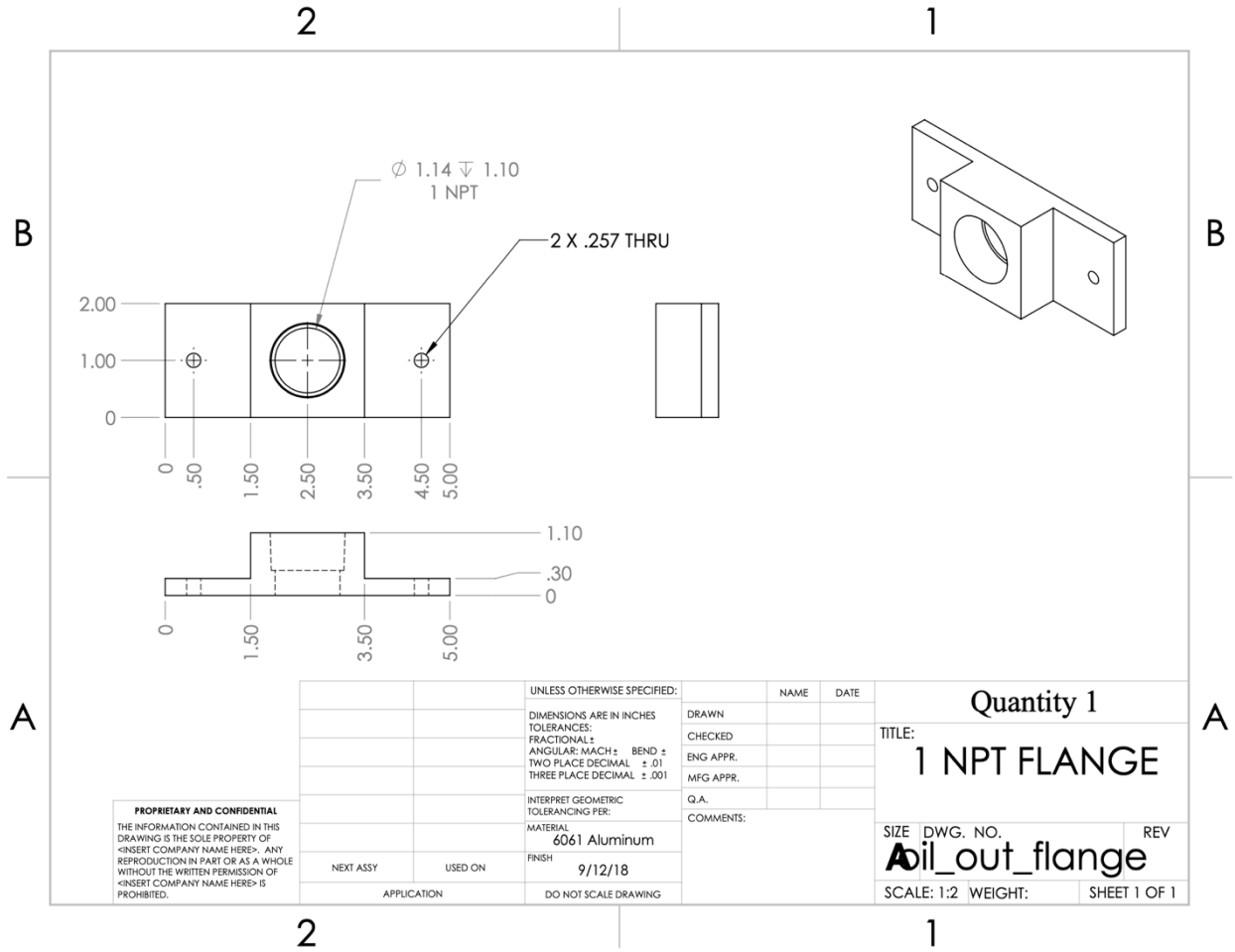

A.2. Coupling Damping

Type	Shore hardness	Color	Material	Relative damping (Ψ)	Temperature range	Features
C	80 Sh A	yellow	TPU	0.3 - 0.4	-30°C to +100°C	very high damping

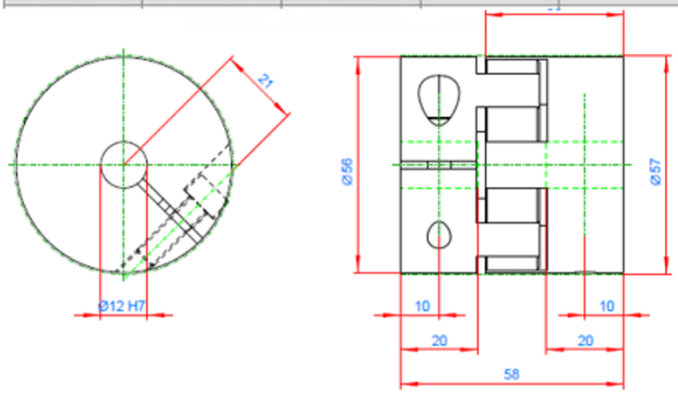

SIZE		60		
Type (Elastomer insert)		A	B	C
Static torsional stiffness (Nm/rad)	C_T	3290	9750	1400
Dynamic torsional stiffness (Nm/rad)	C_{Tdyn}	7940	11900	2072
Lateral (mm)	Max. values	0.12	0.1	0.25
Angular (Degree)	Max. values	1	0.8	1.2
Axial (mm)	Max. values	±2		

Figure 91: EKL-60C Data Sheet

From the data sheet values for the EKL-60C, the important coupling parameters are,

- Type: C
- Shore Hardness of Elastomer: 80 Sh A
- Relative Damping: ψ=0.4
- Dynamic Torsional Stiffness: 2072 Nm/rad

In [16], it is stated that the shaft damping or relative damping provided by the torsional coupling is rarely constant and is given by,

$$D = \frac{K}{M\omega}$$

Where,

D = shaft damping or relative damping (N-m-s/rad)

K = dynamic torsional stiffness (N-m/rad)

ω = excitation frequency, (natural frequency for impact vibration, and forcing frequency for forced vibration)

M =dynamic magnifier (dimensionless and can be assumed constant [16])

For highly damped couplings, M and ψ are related by,

$$M = \sqrt{\left(\frac{2\pi}{\psi}\right)^2 + 1}$$

For the EKL-60C coupling,

$$M = \sqrt{\left(\frac{2\pi}{\psi}\right)^2 + 1} = \sqrt{\left(\frac{2\pi}{0.4}\right)^2 + 1} = 15.74$$

Using the manufacturer provided dynamic torsional stiffness K = 2072 N-m/rad and natural frequency, ω=75 Hz = 471.2 rad/s, the shaft damping D is,

$$D = \frac{K}{M\omega} = \frac{2072}{15.74 * 471.2} = 0.279\frac{Nms}{rad} = 2.47 lbf.in\frac{s}{rad}$$